Deformation history of anorthosite massifs: a comparison of Sognefjord and Tafjord, south west Norway

Stijn W. Verhagen

Master-thesis
august 2011

Universiteit Utrecht

Faculty of Geosciences
Department of Earth Sciences
UtrechtUniversity

Abstract

Anorthosite massifs are a common feature in several geological provinces in Norway. In this paper the deformation history of the anorthosite massifs in Sognefjord and Tafjord, south west Norway, will be investigated. Relics of Precambrium deformation may be preserved in these anorthosite massifs. We want to find out if and where these relics are present. Furthermore deformation mechanisms of plagioclase under different metamorphic conditions will be examined and deformation mechanism maps for plagioclase will be constructed. Optical microscopy was used to study microstructures to determine recrystallization mechanisms. Grain size analysis is performed to infer the average recrystallized grain size, which are used to infer shear stress and strain rate. Three different paleopiezometers are used and compared. An estimate of the water content of the plagioclase was made using chemical reactions. Most of the anorthosites from Sognefjord have a composition which contains 20-35 percent mafic minerals. They were deformed during the Caledonian orogeny under retrograde amphibolite facies conditions, leading to mineral assemblages consisting of plagioclase, green hornblende, pyroxene and some residual garnet. Small scale shear zones are related to this deformation event. Recrystallization mechanisms obtained from microstructures associated with this event are bulging recrystallization and subgrain rotation recrystallization in partly to almost completely recrystallized fabrics. Three types of bands of recrystallized grains are found, monophase bands of plagioclase, with an average recrystallized grain size of 33 to 48 μm, multiphase bands of plagioclase-hornblende, or plagioclase-pyroxene, with an average recrystallized grain size of 23 to 41 μm, and monophase hornblende bands, which extend from hornblende porphroclasts, with a grain size that is too small to measure with optical microscopy. Also found in these anorthosites are predeformational, granulite facies conditions structures, like corona structures, which are probably post Sveconorwegian, and banded rocks with isoclinal folds, which are related to the Sveconorwegian orogeny. These granulite facies conditions structures have a composition consisting of plagioclase, pyroxene, mostly clinopyroxene, brown hornblende and garnet. The anorthosites from Tafjord are proper anorthosites, with only 5-10 percent mafic minerals. During the Caledonian orogeny these rocks were deformed under high grade metamorphic conditions. Microstructures are irregular shaped grains with subgrains, and interlobate grain boundaries, associated with high temperature grain boundary migration recrystallization and subgrain rotation recrystallization. The assemblages found in these anorthosites consist of plagioclase, biotite and hornblende, these are related to greenschist facies conditions, which is in contradiction with the high grade metamorphic conditions. Fast cooling after

deformation to greenschist facies conditions, with static recrystallization, could be a solution for this contradiction. Grain growth by grain boundary area reduction during static recrystallization would also explain the relatively large recrystallized grain sizes, of approximately 74 μm, found in the samples from Tafjord. Due to the complete recrystallization of the rocks during the Caledonian orogeny no relics of older deformation, during the Sveconorwegian orogeny, were found in the samples from Tafjord. The shear stress during the Caledonian orogen inferred for Sognefjord is approximately 37 MPa and an associated shear strain rate was inferred of approximately $1 \cdot 10^{-10}$. Due to static recrystallization after deformation, shear stresses inferred for Tafjord are an underestimate of the actual shear stress of deformation. Metamorphic conditions during the Caledonian orogeny were higher in Tafjord than in Sognefjord. Cooling after deformation was relatively fast at both locations. The rocks from Sognefjord and Tafjord have both undergone at least two deformation events after formation of the anorthosite massifs. First during the Sveconorwegian orogeny and later during the Caledonian orogeny. In Sognefjord relics of the Sveconorwegian orogeny are preserved, but in Tafjord the rocks have a completely recrystalized fabric, formed during the Caledonian orogeny. A water content of 0,3 weight percent seems accurate for the rocks in Sognefjord and Tafjord. After comparison of the three paleopiezometers, the one that gave the best fitting results was used to construct the deformation mechanism maps for plagioclase.

Contents

Photograph title page: Anorthositic rock along a road near Gudvangen.

1. Introduction

Anorthosite is an intrusive igneous rock characterized by a predominance of plagioclase, a solid solution series within feldspar, and a minimal mafic component. A proper anorthosite consists of 90-100 percent plagioclase, and only 0-10 percent mafic minerals. Pyroxene, ilmenite, magnetite, and olivine are the mafic minerals most commonly present (Wanvik, 2000). Anorthositic rocks are common in several geological provinces in Norway and occur at many areas in different parts of the country. See figure 1. Most of the bodies are of relatively small size, but some larger bodies occur. These are the Bergen Arc anorthosites, and more prominently, the 500 km^2 Rogaland anorthosite complex, and the 700 km^2 Inner Sogn-Voss anorthosite complex. These are the two largest anorthosite bodies in Norway, and western Europe (Wanvik, 2000).

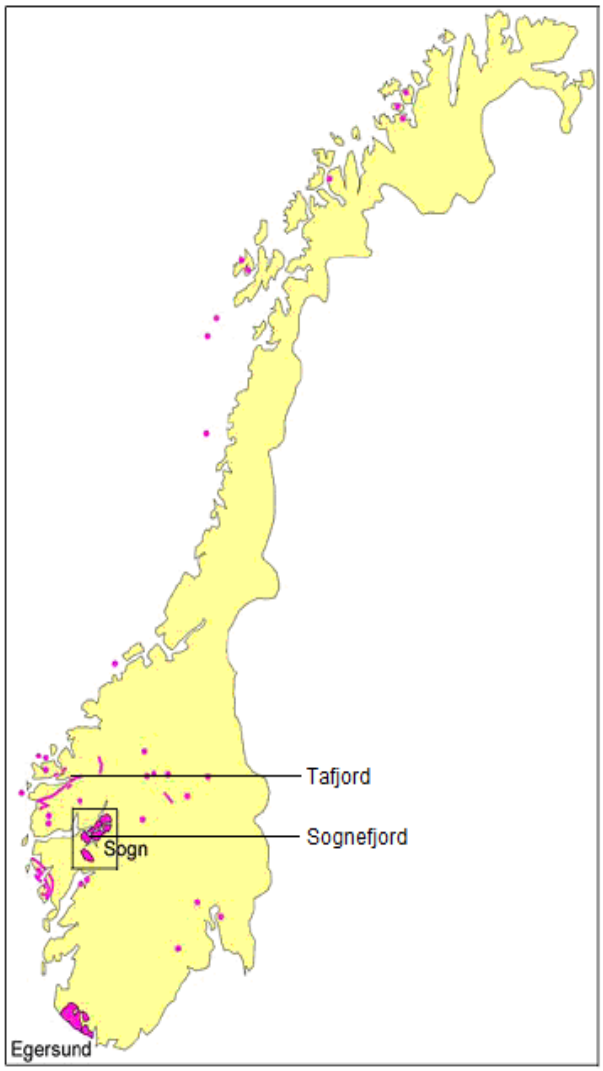

Figure 1: Distribution of anorthosites in Norway. Modified after Wanvik (2000).

Anorthosite has a great variety of industrial applications, anorthosite massifs are known to host important ore deposits, such as ilmenite, and can be excellent sources for high-quality rock aggregate and also for dimensionstone. The exploitation of anorthosite for industrial mineral products is growing, and the potential for future production of aluminium and other important constituents from anorthosites is considered to be quite considerable (Wanvik, 2000).

Figure 2: Exploitation of anorthosite in the quarry near Eide.

The anorthosites on Earth can be divided into two types, Proterozoic anorthosites and Archean anorthosites. These two types of anorthosite have different modes of occurrence, appear to be restricted to different time periods, and are thought to have had different origins. In this study we will concentrate on the Proterozoic anorthosites, which are also known as massifs or massif-type anorthosites, because the anorthosite bodies in the study areas of Sognefjord (Wanvik, 2000) and Tafjord (Brueckner, 1968) are of this type. See figure 1.

The objective of this study is to compare the deformation history of the anorthosite massif in the Sognefjord to the deformation history of the anorthosite massif in the Tafjord. Microstructures in thin sections were studied to infer recrystallization mechanisms. The compositions of the sampled rocks are also obtained from the thin sections, these are used to infer the metamorphic conditions during deformation of the rocks. The minimum water content, in weight percent, needed for the obtained compositions, was calculated using retrograde reaction formulas and atomic weights. After that a grain size analysis was performed. The recrystallized grain size obtained from the grain size analysis combined with the recrystallization mechanisms inferred from the microstructures were used in three different piezometers. The results of the piezometers were compared, and the best set of results was used to construct deformation mechanism maps for different plagioclase compositions and water contents.

2. Geological setting

Anorthosite massifs are a widespread component of Precambrian crust, but the mechanisms of their formation and their geological significance are still somewhat of a mystery (Lundmark and Corfu, 2007). The origin of massif type anorthosites will be discussed below, as well as the orogens that altered the anorthosites found at Sognefjord and Tafjord, the Sveconorwegian orogen and Caledonian orogen. After that consequences of these orogens for both locations will be discussed.

2.1 Origin of anorthosite massifs

The origin of Proterozoic (massif type) anorthosites has been a subject of theoretical debate for many decades. The problem for the formation of anothosite massifs begins with the generation of magma, the necessary precursor of any igneous rock. Magma generated by small amounts of partial melting of the mantle is generally of basaltic composition. Under normal conditions, the composition of basaltic magma requires it to crystallize between 50 and 70% plagioclase, with the bulk of the remainder of the magma crystallizing as mafic minerals. However, anorthosites are defined by a high plagioclase content (90–100% plagioclase), and are not found in association with contemporaneous ultramafic rocks. This problem is known as 'the anorthosite problem'. Proposed solutions to the anorthosite problem have been diverse, with many of the proposals drawing on different geological subdisciplines (Bédard, 2001). Emphasis has been placed on the association of massif anorthosites and collisional orogens. It has been proposed that the formation of anorthosites is a result of removal of overthickened lithosphere below a orogen, and upwelling of hot asthenosphere. The formation of large volumes of plagioclase, could result from either partial crystallization of a mantle-derived magma, which was situated in a chamber at or near the base of the continental crust, or melting of anhydrous lower crust, or mixes thereof, followed by diapiric emplacement at higher crustal levels (Lundmark and Corfu, 2007). Diapirism is a result of the buoyant upwelling of a light viscous liquid that is overlain by a heavier one. Such a state is metastable, therefore every disturbance of the system will lead to an overturning of the two liquid layers in order to reach the stable balanced state where the lighter liquid floats on top of the heavier one (Barnichon, 1999).

In the standard petrogenetic model after the two-stage model by Ashwal (1993), see figure 3, the formation of anorthosite massifs starts with a broadly basaltic magma, that is pounded and

differentiated in a large pancake-shaped chamber at or near the base of the crust. From this magma aggregates of plagioclase megacrysts, with rare interstitial high-alumina orthopyroxene megacrysts (HAOM) crystallize, these aggregates then float and accumulate at the roof of the chamber. The occurrence of these high-alimina orthopyroxene megacryst, that are interstitial to plagioclase megacrysts are a characteristic feature for massif type anorthosites (Barnichon et al. 1999). Due to density inversion with the surrounding, partially melted country rocks, masses of plagioclase, with some entrained high-alumina orthopyroxene megacrysts, formed by gravity instability rise through the crust as diapirs in anorogenic conditions. By the coalescence of several diapirs at mid-crustal depths anorthosite massifs start to form. During ascent, the plagioclase crystal mass is lubricated by gabbroic melts from which low aluminium and chromium orthopyroxene crystallize at the final stage of intrusion (Barnichon et al., 1999).

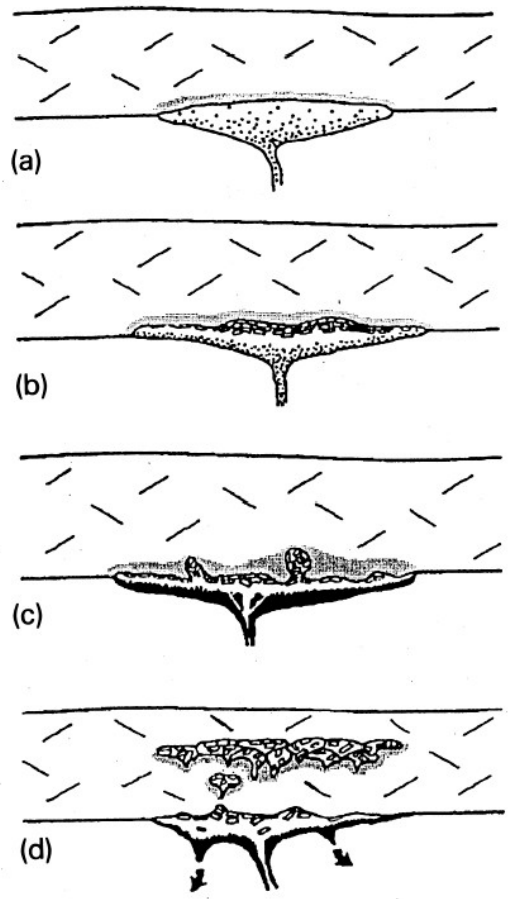

Figure 3: The two-stage model for the formation of anorthosite massifs after Ashwal (1993). (a) A magma chamber develops at the base of the crust in which a basic magma starts crystallizing mafic minerals. (b) Mafic minerals sink, while crystallized plagioclase floats and accumulates at the top of the magma chamber. (c) Plagioclase-rich lumps form and rise as diapirs through the lower crust. (d) Several diapirs coalesce at mid-crustal depth to make up anorthosite massifs. Stippled area: heat from the magma chamber causes partial melting of the crust (from Barnichon et al., 1999).

Barnichon et al. (1999) did a finite-element (FE) simulation on the diapiric emplacement of the Egersund-Ogna massif in south Norway. This anorthosite massif was chosen, because earlier studies have proven that a pristine post-collisional or anorogenic state was preserved here. The main objective of their study was to test the consistency of the petrological model by numerical modelling. A lagrangian FE code coupled with an automatic re-meshing algorithm and artificial passive markers were used for the modelling, and geochronological and petrological data were used to define a reasonable geometry and rheology of the model (Barnichon et al., 1999).

Results of the FE simulation show that buoyant rise of anorthositic material takes place in acceptable timings for a wide range of parameter values. The anorthositic material is displaced as a bulb shape, which rises through the viscous lower crust until it reaches the more rigid upper crust. After the vertical uprise, horizontal expansion takes place, which results in a mushroom shape. It was suggested to call diapirism the whole process, for uprise and expansion, because there is no reason to distinguish two different mechanisms, since the phenomenon is continuous and basically the same physical properties control the whole evolution (Barnichon et al., 1999). FE modelling indicates that anorthosite diapirism is correlated with a downward flow of lower crustal material along the flanks of the structure (Barnichon et al., 1999).

Numerical modelling of the Egersund-Ogna massif demonstrates that the diapirism suggested in the standard petrological model is an acceptable mechanism for the emplacement of anorthosite through an homogeneous lower crust in an anorogenic setting. It however does not imply that diapirism is the only possible mechanism (Barnichon et al., 1999).

Lafrance et al. (1996) distinct three structural types of anorthosite within individual massifs: layered, diapiric, and massive. Layered anorthosites contain sequences of well developed compositional layering commonly associated with a strong plagioclase lamination, diapiric anorthosites have a strong, planar deformation fabric along their margins formed during the emplacement of the intrusion, and massive anorthosites lack any planar or linear fabrics, which have been attributed to static recrystallization, or to the emplacement of the intrusive bodies as crystal mushes. Lafrance et al. (1996) investigated the Poe Mountain anorthosite, Wyoming. They suggest that syn-emplacement, pervasive recrystallization is an important factor in the formation of all massive and diapir anorthosite massifs. This syn-emplacement, pervasive recrystallization creates shear zones. Lafrance et al. (1998) did research after shear zones in the Poe Mountain anorthosite, Wyoming, they distinguish two different types of shear zones, ultra high-temperature shear zones, which form with an interstitial melt present, and subsolidus shear zones. The ultra high-temperature shear zones formed during emplacement of the anorthositic rocks, with minor deformation and recrystallization continuing during cooling of the body to temperatures of 865-

940°C, that is 110-185°C below the solidus temperature, of 1050°C, of anorthosite, while the subsolidus shear zones formed at granulite facies conditions (Lafrance et al., 1998).

2.2 Sveconorwegian orogeny

The Sveconorwegian orogenic belt, a well-exposed Grenvillian orogenic belt, is situated at the southwestern margin of Fennoscandia, the exposed portion of the Baltic Shield. The Sveconorwegian orogeny was active between 1140 and 900 Ma (Bingen et al., 2008). The Sveconorwegian orogenic belt resulted from collision between Fennoscandia and another major plate, it is unsure which plate, but Amazonia is the most likely, at the end of the Mesoproterozoic. The belt can be divided from east to west, into a Paleoproterozoic Eastern Segment, and four mainly Mesoproterozoic terranes, that were transported relative to Fennoscandia. These are the Idefjorden, Kongsberg, Bamble and Telemarkia or Telemark Terranes (Bingen et al., 2008). See figure 4. The Eastern Segment is lithologically related to the Transcandinavian Igneous Belt, in the Fennoscandian foreland of the belt. The terranes are thought to be native to Fennoscandia, though an exotic origin for the Telemark Terrane is possible. It might have accreted during the Sveconorwegian orogeny by closure of an oceanic basin, here a suture zone, the area where two continental plates have joined together through continental collision, might have formed between the Telemark and Idefjorden Terranes. (Bingen et al., 2008). Bingen et al. (2008) proposed a four-phase model for Sveconorwegian orogeny, a review of existing geological and geochronological data supports this model for the assembly of these lithotectonic units. The division of the Sveconorwegian orogeny into four genetic orogenic phases is a step towards improved correlation of the Sveconorwegian belt with other Grenvillian belts, which can help to improve paleogeographic reconstructions for the Mesoproterozoic and Neoproterozoic (Bingen et al., 2008). The four Sveconorwegian orogenic phases have distinct tectonometamorphic significance.

1) The Arendal phase, at 1140-1080 Ma, represents the collision between the Idefjorden and Telemark Terranes, which produced the Bamble and Kongsberg orogenic wedges. This phase involved closure of an oceanic basin, and possibly accretion of the Telemark Terrane, accretion of a volcanic arc, high-grade metamorphism and deformation in the Bamble and Kongsberg Terranes peaking in granulite-facies conditions at 1140-1125 Ma, and thrusting of the Bamble Terrane onto the Telemark Terrane at 1090-1080 Ma (Bingen et al., 2008).
2) The Agder phase, at 1050-980Ma, corresponds to crustal thickening and imbrication in the

central part of the orogen, probably as a result of the main event of oblique continent-continent collision. Towards the foreland of the belt it resulted in underthrusing and burial of the Idefjorden Terrane to high-pressure conditions at 1050 Ma, followed by exhumation. Towards the hinterland of the belt, in the Telemark Terrane, crustal thickening led to protracted granite magmatism starting at 1050 Ma and to high-grade metamorphism starting at 1035 Ma. Metamorphism peaked in granulite facies conditions in the Rogaland-Agder sector (Bingen et al., 2008).

3) The Falkenberg phase, at 980-970 Ma, reflects the final convergence in the belt, shortly followed by divergence. This last step of foreland propagation of the orogeny is indicated by underthrusting of the Eastern Segment to eclogites facies conditions at 970 Ma (Bingen et al., 2008).

4) The Dalane phase, at 970-900 Ma, corresponds to gravitational collapse of the belt. It is associated with post-collisional magmatism increasing in volume westwards, exhumation of the southern part of the Eastern Segment as a core complex, and exhumation of the Rogaland-Agder sector as a wide gneiss dome. Formation of the gneiss dome peaked at 930-920 Ma with low-pressure high-temperature granulite-facies metamorphism and intrusion of an anorthosite-mangerite-charnockite complex (Bingen et al., 2008). The Rogaland anorthosite complex, is the second largest anorthosite massif in Norway and Western Eurpe (Wanvik, 2000).

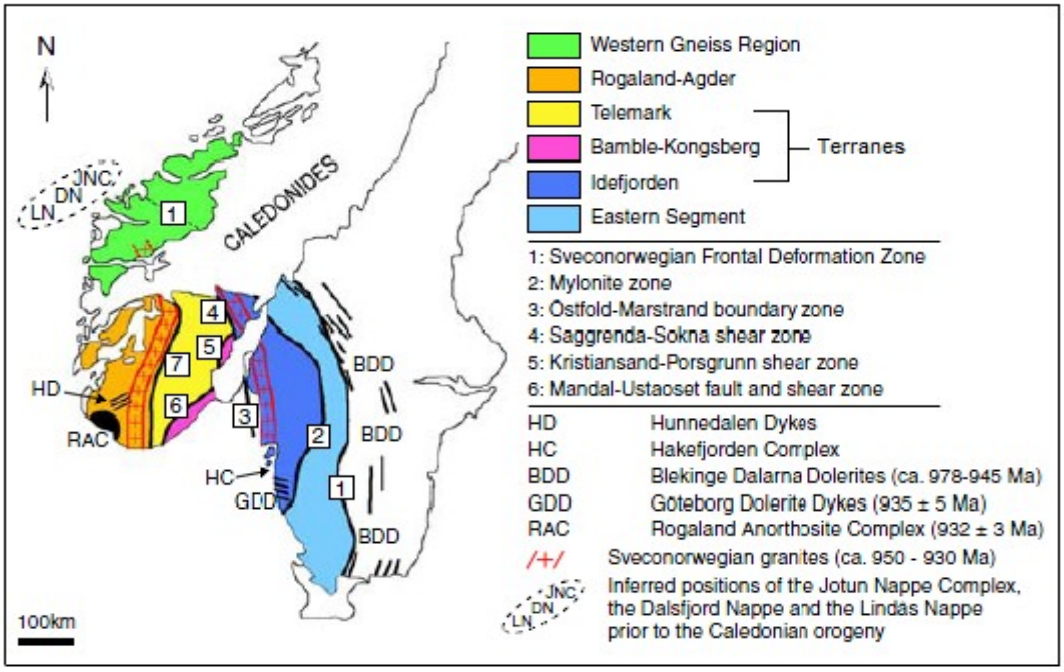

Figure 4: Simplified map of southwestern Scandinavia (modified after Lundmark and Corfu, 2007).

3.3 Caledonian orogeny

The Scandinavian Caledonides cover a large portion of the surface of Norway, they consist of innumerable thrust sheets composed of diverse rock complexes with distinct origins and wide ranging metamorphic grade. See figure 5. The Caledonides were formed by a series of tectonic events in the Early Paleozoic, at 520-400 Ma. Gradual oblique convergence of the plates Baltica and Laurentia, led to closure of the Iapetus Ocean, and a collision involving subduction of the margin of Baltica beneath Laurentia in Silurian to Early Devonian time, at 420-400 Ma. Sediments of the Baltoscandian passive margin and shelf successions, as well as exotic, oceanic and arc terranes derived from the Iapetus Ocean were transported eastward, progressively shoved into each other, and deposited onto Archaean and Proterozoic crystalline rocks of the Fennoscandian Shield. A distinctive tectonostratigraphy can be recognised as a result (Roberts, 2003).

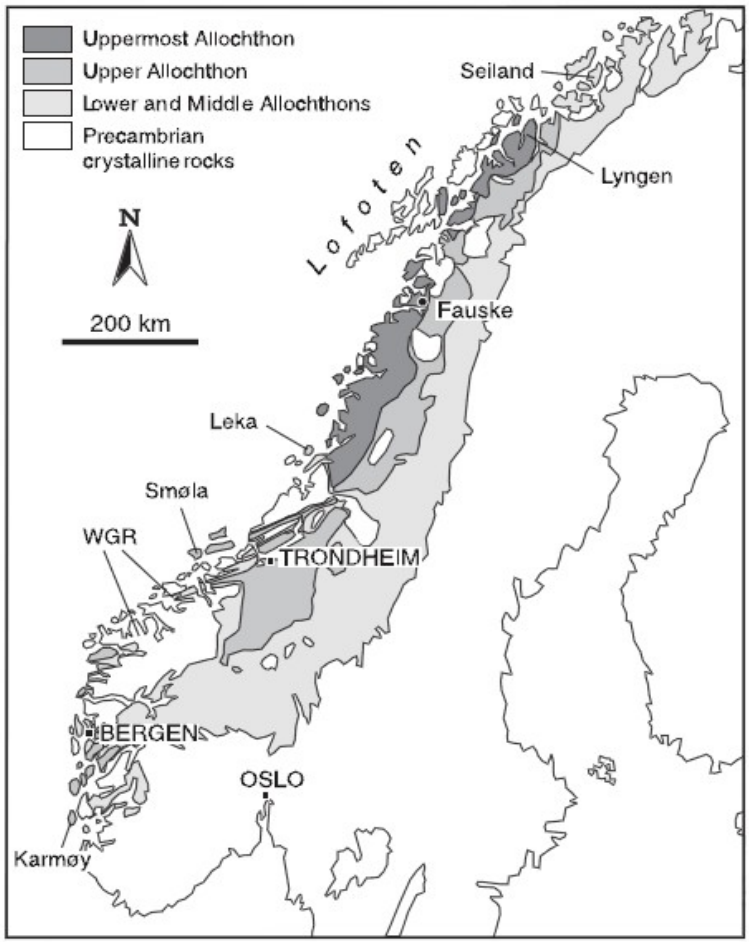

Figure 5: Simplified tectonostratigraphical subdivisions of the Scandinavian Caledonides (from Roberts, 2003). WGR stands for Western Gneiss Region. Here ultra high pressure (UHP) metamorphic conditions are found. Temperature and pressure are gradually decreasing from the WGR to the interior of Norway, eastward (Walsh and Hacker, 2004).

The Caledonian orogen in Scandinavia has been divided into a series of major allochthons; the Lower, Middle and Upper allochthons, with arautochthonous and autochthonous units in the foreland to the east, along the Baltoscandian margin of the palaeocontinent Baltica. The Lower Allochthon, as well as the thin foreland units are characterised by platform and shelf successions. The Middle and Upper Allochthon consist of the thick, late Neoproterozoic, continental rise accumulations, with mafic dyke intrusions, of the Baltoscandian margin, where the bulk of the Upper Allochthon consist of diverse, oceanic terranes, that are situated outboard of these accumulations, and on top of that the more exotic carbonate shelf, slope/rise and evolved magmatic arc assemblages of Laurentian orogin (Roberts, 2003). Next to these major allochthons, there are parautochthonous units and an autochthonous sedimentary cover that can be followed along the entire front of the exposed orogen. Also, slices of Precambrian crystalline basement have been found in many thrust sheets (Roberts, 2003).

Four tectonothermal events are distinguished for the for the formation of the Scandinavian Caledonides, based on the above tectonostratigraphy and palaeogeography, that followed a major period of extension or transtension, with rifting along the Baltoscandian margin leading to Iapetus sea-floor spreading.

1) Finnmarkian event, at 520-500 Ma. During this event the contraction or the Iapetus Ocean starts. The event is characterised by the collision of the Baltoscandian margin with a magmatic arc, above a seaward-facing subduction zone. The magmatic arc may have been largely oceanic, positioned in the Iapetus Ocean between Baltica and Siberia, or partly developed on a micro-continental block that had earlier rifted away from Baltica. Metamorphism locally reached eclogite facies conditions, at 505 Ma. The effects of this event appear to diminish gradually on moving south along the Baltoscandian margin (Roberts, 2003).
2) Trondheim event, at 480-475 Ma. During this event oceanward subduction continues, to depths of blueschist facies metamorphic conditions. This is followed by ophiolite obduction. Baltica rotates anticlockwise away from Siberia, slowly approaching Laurentia in a gradually contracting Iapetus seaway (Roberts, 2003).
3) Taconian event, at 470-450 Ma. This event is characterised by arc accretion, and it involved some ophiolite obduction, along the Laurentian margin. Metamorhpic conditions were of amphibolite to locally eclogite facies (Roberts, 2003).
4) Scandian event, at 420-400 Ma. The collision of Baltica with Laurentia characterises the Scandian orogeny. It involves major thrusting, and the subduction of the Baltican margin to

ultra high pressure depths, exceeding 100 km. Both subduction and exhumation occurred very rapidly. The timing of the Scandian event varies widely, both transversely and laterally (Roberts, 2003).

5) Late- to post-Scandian events. During and after the Scandian event an important phases, of extensional deformation took place, including sinistral, transpressive shear, with upright folding in some areas. Two main phases can be distinguished, first a phase of initial orogenic collapse and backsliding, with sedimentation and contractional deformation at depth and to the east in the platformal domain, second a crustal collapse phase with shear zones cutting earlier, extensional detachments, and with continuing deposition. Some minor contraction continued in the eastern parts of the foreland domain. This last phase of extension continued into Late Devonian and possibly Early Carboniferous (Roberts, 2003).

2.4 Sognefjord

The anorthosite samples from the Sognefjord are part of the Inner Sogn-Voss anorthosite complex, with 700 km^2 the largest anorthosite occurrence in Norway and West-Europe (Wanvik, 2000). The anorthositic rocks of the Inner Sogn-Voss region belong to the Jotun Nappe, which is part of the Middle Allochthon of the Caledonides (Wanvik, 2000). The Jotun Nappe Complex consists of polymetamorphosed and polydeformed rocks, with numerous shear zones cutting through. The shear zones are of Sveconorwegian or Caledonian origin, including late- to post-Caledonian extensional shear zones (Lundmark and Corfu, 2007). The Jotun Nappe Complex is separated from the basement by a layer of early Palaeozoic phyllitic and quartzitic rocks. This layer is part of the Lower Allochthon, and forms the detachment along which the nappes were displaced. The nappe complex is divided into two units, The Lower Jotun Nappe and the Upper Jotun Nappe. The Lower Jotun Nappe can be found along the margins of the complex, while the overlying Upper Jotun Nappe is situated in the central part of the nappe complex, they are separated by mylonitic shear zones (Lundmark and Corfu, 2007). The Lower Jotun Nappe mainly consists of syenitic to monzonitic and gabbroic rocks, that were metamorphosed to amphibolite facies conditions, at 909 ± 16 Ma. It can locally be associated with a Neoproterozoic sedimentary rock, that was deposited along the Baltoscandian margin (Lundmark and Corfu, 2007). The upper Jotun Nappe is geographically divided into two area's. The north-eastern part is dominated by partially retrograded gneisses of granitic, syenitic, monzonitic, dioritic, and gabbroic compositions, in this area

anorthositic rocks are rare. The central and south-western parts of the Upper Jotun Nappe are dominated by high-grade metamorphosed anorthositic to gabbric rocks and subsidiary metatroctolite. The anorthosites are separated form other highgrade gneisses by tectonic contacts, forming thrust sheets. Locally quartz-rich layers can be found along the contacts that are highly deformed (Lundmark and Corfu, 2007). If anorthosite is present in the contacts, the primary rock has been saussuritised, resulting in the formation of albitic plagioclase and epidote minerals (Wanvik, 2000). The rocks of the Upper Jotun Nappe have undergone retrograde granulite-facies metamorphism, at 941 ± 10 Ma (Lundmark and Corfu, 2007).

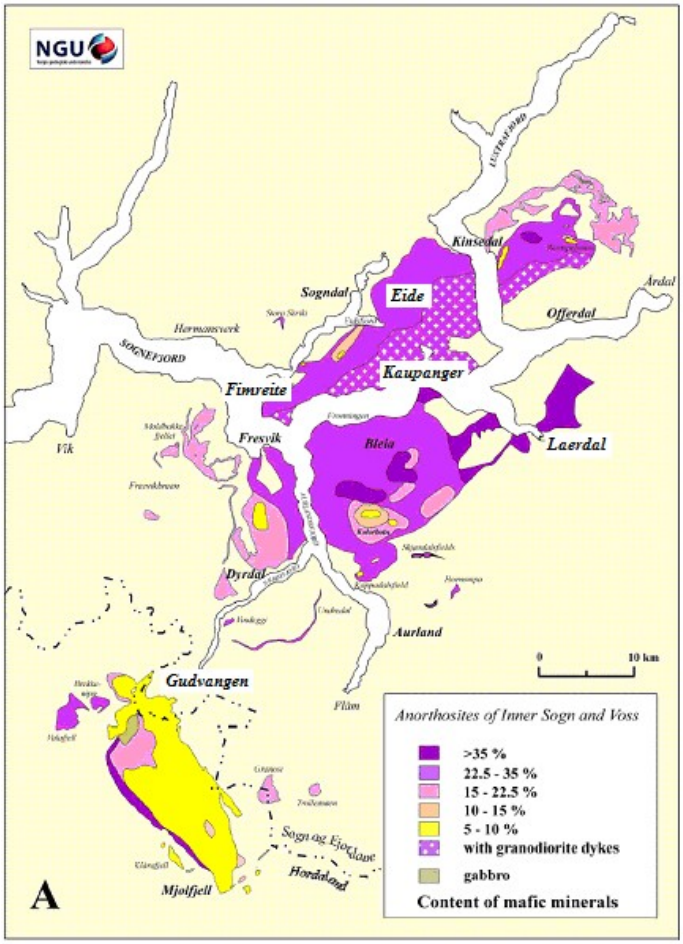

Figure 6: Variation in content of mafic minerals of the anorthosites of the Inner Sogn-Voss anorthosite complex, with locations of the samples. (from Wanvik, 2000).

The anorthositic rocks mainly occur in two distinct geographical areas. See figure 6. The southern area, between Gudvangen and Mjølfjell, consists of a single large massif and several smaller satellite bodies. The northern area, which extends from Dyrdal in outer Nærøyfjord to Kinsedal in

Lustrafjord, is consists of one large massif, that is separated into 4-5 separate bodies by the Sognefjord, and several satellite bodies. In the Fresvik area, one of the separated bodies of the northern area, the Upper Jotun Nappe displays a primary intrusive layering seen on a regional scale. In here alternating anorthosite and gabbro layers with a thickness from tens to hundreds of metres can be found. The total thickness of the massifs can be as much as 2000 metre, because the anorthosites are internally isoclinally folded (Wanvik, 2000). The mafic mineral content of the anorthositic massifs varies widely. Proper anorthosite (< 10 % mafic minerals) is dominant in the southern Nærøydal-Mjølfjell area, while anorthositic leucogabbro (10-35% mafic minerals) and anorthosite-gabbro (22.5-35 % mafics) are dominant in the northern areas, with proper anorthosite being restricted to only minor local occurrences (Wanvik, 2000). In the proper anorthosites the mafic minerals consist of epidote and brown amphibole, with minor amounts of garnet, biotite and sericite. The leucogabbro and anorthosite-gabbro contains less epidote, but clinopyroxene, that is locally altered to green amphibole, as well as some garnet are present. The mafic minerals in anorthositic leucogabbro and anorthosite-gabbro form patches, spots and bands, depending on the type and generation of the anorthositic rock (Wanvik, 2000). The Sogn anorthosite is characterised by a high anorthite content of the plagioclase, An55-80. Especially the southern Gudvangen-Mjølfjell Massif has a high An content, An65-78, while the northern regions are less calcic, An40-60. The high An content of the Sogn anorthosite is a common feature of Archaean anorthosites, however the Sogn anorthosite is considered to be of Proterozoic age, circa 1700 Ma (Wanvik, 2000).

Figure 7: Photograph of the Sognefjord. The milky white rocks are anorthosites.

2.5 Tafjord

The anorthosite samples from Tafjord are part of a smaller anorthosite occurrence, situated in an offshoot of the Middle Allochthon of the Scandinavian Caledonides, within the Western Gneiss Region. See figure 8. The Middle Allochthon, in the east of the map, is composed of the Risberget and Saetra Nappes. The Risberget Nappe is dominated by megacrystic, K-feldspar augen gneiss with a fine-grained, biotite-rich matrix that grades with increasing deformation into variably mylonitic, fine-grained, laminated biotite–quartz–plagioclase gneiss in which the feldspar augen have been destroyed. Smaller bodies of metagabbro, anorthosite, amphibolite, equigranular orthogneiss and local eclogite are also present, in association with the augen gneiss (Walsh and Hacker, 2004). Structurally overlying the Risberget Nappe is the Saetra Nappe, which consist of strongly laminated, feldspathic and micaceous quartzite associated with amphibolite. To the west, in the central part of the map, in the offshoot of the Middle Allochthon, which lies within the Western Gneiss Region, the Risberget Nappe is less abundant, and epidote–biotite gneiss, muscovite gneiss, garnet–muscovite–quartz gneiss and anorthosite are the typical Middle Allochthon rocks (Walsh and Hacker, 2004). This is where the Tafjord anorthosite is situated. The majority, about 95 percent, of the anorthosites found at Tafjord are creamy to chalky white to dark grey bodies, consisting of 75 to 95 percent plagioclase, An45 to An65, with hornblende, actinolite, biotite, epidote, chlorite and muscovite as the major accessories (Brueckner, 1968).

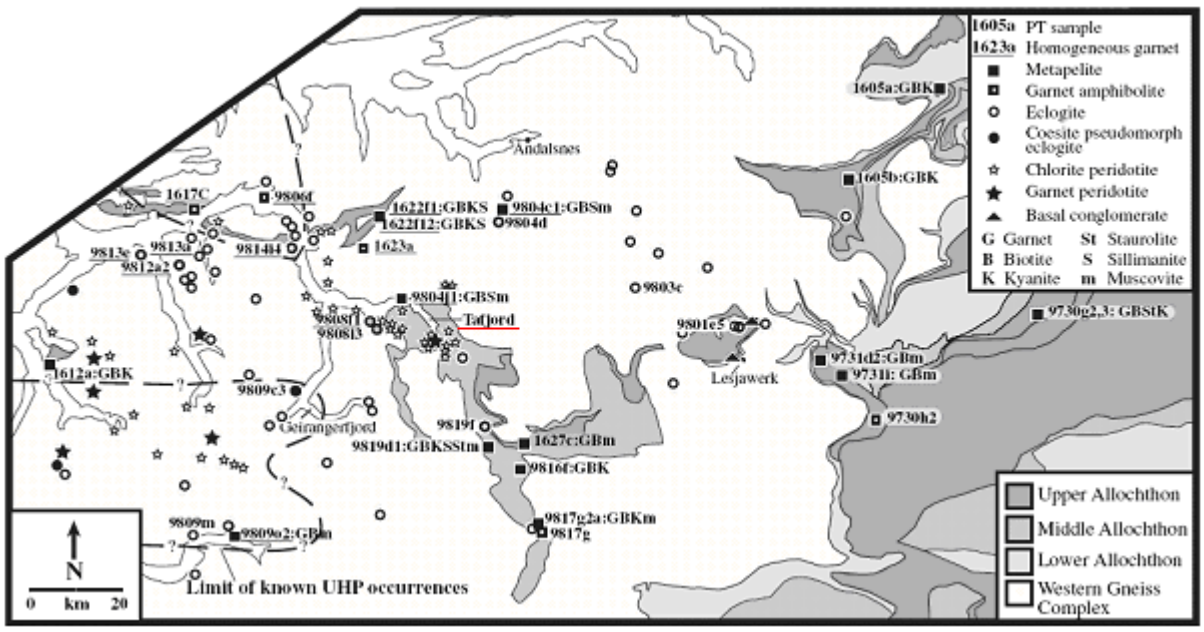

Figure 8: Geological map of Tafjord (from Walsh and Hacker, 2004).

The Upper Allochthon in this area is represented by the Blåhø and Gula Nappes. The Blåhø Nappe is dominated by garnet ± kyanite ± staurolite mica schist and coarse-grained garnet amphibolite with plagioclase-rich laminae, biotite schist, feldspathic gneiss, muscovite–quartz gneiss, retrogressed eclogite pods and rare carbonate layers are also present. The Blåhø Nappe is spatially associated with the Risberget Nappe across the whole area shown in the map. The Gula Nappe, exposed at the eastern edge of the transect, consists of fine-grained slate and garnet–staurolite phyllite (Walsh and Hacker, 2004).

Figure 9: Photograph taken at the top of Kallskaret. The rocks in the front are weathered anorthosites.

3. Method

In this section the methods used in this study will be discussed. Starting with the fieldwork, followed by microstructures, grain size analysis, and paleopiezometry.

3.1 Fieldwork

The samples from Sognefjord are taken from several locations within the Inner Sogn-Voss region. See figure 6. The main location is near Fimreite, along the road from Kaupanger to Fimreite. Another location is along the same road, near Kaupanger. See figure 10. The other locations are in Gudvangen, Lærdal, and a quarry near Eide. All of these locations are easy to reach, this in contrast to the sampless from Tafjord. The samples from Tafjord are taken from one location at Kallskaret, this is at the top of a mountain. A one hour climb along a dirt path is followed by a one hour climb over boulders to reach this location. The samples from Sognefjord show more diversity, therefore more samples from this area, than from Tafjord, were used and compared in this study.
For most samples at all locations foliation and lineation were measured. Thin section from the samples from these locations were taken parallel to the lineation. The thin sections have a thickness of 30 µm.

Figure 10: Left: Overview of part of the road section near Fimreite. Right: Close-up of the rocks, at sample location NFAS08 15.10b.

Composition

The composition of the sampled rocks is obtained from the field and from the thin sections. With the obtained compositions it is possible to infer the metamorphic conditions that were present during deformation of the rocks.

With increasing hydration and retrogression, pyroxene is replaced by hornblende and later biotite, accompanied by a decrease in the amount of garnet (Lundmark and Corfu, 2007).

Kruse and Stünitz (1999) have investigated Precambrian shear zones and mylonites in anorthositic to gabbroic rocks of the Jotun Nappe Complex. They found that the predeformational granulite facies mineral assemblage consists of orthopyroxene, clinopyroxene, brown (Ti-rich) hornblende, plagioclase, and garnet. At some places corona structures of hornblende, pyroxene and garnet, that formed due to reactions between plagioclase and primary olivine, can be found, here some olivine may be present as well. The predeformational granulite facies mineral assemblage is preserved in some of the mylonitic layers (Kruse and Stünitz, 1999). From microstructural observations it is inferred, that an assemblage of clinopyroxene, hornblende, garnet, and plagioclase is stable during most of the mylonitization history of the Precambrian shear zones, however orthopyroxene-bearing assemblages have only been stable during the early, granulite facies parts of the deformation history. In some areas the predeformational granulite facies mineral assemblage is partly replaced by retrograde assemblages during deformation under amphibolite facies conditions. There can be found two amphibolite facies mineral assemblages. The first one consists of clinopyroxene, green hornblende, and plagioclase, with possibly small amounts of orthopyroxene and garnet, while the second assemblage contains brown hornblende, and plagioclase, with possibly small amounts of garnet (Kruse and Stünitz, 1999).

Water content

The minimum amount of water, in weight percent, needed for the retrograde reaction can be calculated using the atomic weights for the minerals and the reaction formulas given below. First we need the chemical formulas of the minerals involved, plagioclase = $(Na,Ca)(Si, Al)_4O_8$, pyroxene = $XY(Si,Al)_2O_6$, a more specific chemical formula for augite = $(Ca,Na)(Mg,Fe,Al)(Si,Al)_2O_6$, hornblende = $Ca_2(Mg,Fe,Al)_5(Al,Si)_8O_{22}(OH)_2$, biotite = $K(Mg,Fe)_3AlSi_3O_{10}(F,OH)_2$. The first retrograde reaction is from pyroxene to hornblende:

$$15\mathrm{XY}(Si, Al)_2O_6 + 4\mathrm{H}_2O + O_2 \rightarrow 4\mathrm{Ca}_2(Mg, Fe, Al)_5(Al, Si)_8O_{22}(OH)_2 \quad (1)$$

The second retrograde reaction is from hornblende to biotite:

$$2\mathrm{Ca}_2(Mg, Fe, Al)_5(Al, Si)_8O_{22}(OH)_2 + 2\mathrm{H}_2O \rightarrow 4\mathrm{K}(Mg, Fe)_3AlSi_3O_{10}(OH)_2 + O_2 \quad (2)$$

It is assumed that reaction (2) will not take place until reaction (1) has taken place for 100%, thus replacing all pyroxene, therefore pyroxene and biotite will not be present in the same rock samples. With the atomic weights we can calculate the weight percent of water for the above formulas, by dividing the weight of the water by the total weight. The total weight is determined by adding the weight of plagioclase to the weight of the left hand of one of the two reactions. For example: in a rock sample that consists of 80% plagioclase and 20% pyroxene the amount of water needed to convert 100% of the pyroxene to hornblende is calculated as follows: the total weight of the left hand of reaction (1) is 15 times the (average) weight of pyroxene added to four times the weight of water and one oxygen. The 15 pyroxenes make up 20% of the rock, assuming that the pyroxene and plagioclase grains are about the same size there are 60 plagioclases needed to make up 80% of the rock. The weight of these 60 plagioclases is added to the weight of the left hand of the reaction. The weight percentage of water is obtained by dividing the weight of the water by the total weight. Using variable amounts of mafic minerals and variable amounts of retrograded minerals we can get a geological correct water content for the rocks. Both the amount of mafic minerals and the amount of retrograded minerals will be estimated from the thin sections also and will be compared to the results of the water content estimation.

3.2 Microstructures

Microstructures of the rocks are needed to determine the recrystallization mechanisms. Which are needed in order to apply the correct piezometric relations, see below. The microstructures are obtained from the thin sections using optical microscopy. In this study we concentrate on the deformation in plagioclase, because it is the most abundant mineral in anorthosites. The deformation of plagioclase is strongly dependent on metamorphic conditions. Deformation mechanisms associated with increasing temperature and decreasing strain rate will be given below. The indicated temperatures are for average crustal strain rates, and will vary with chemical

composition and water content (Passchier and Trouw, 2005, Pryer, 1993, Rybacki and Dresen, 2000, Tullis and Yund, 1987, 1991, Tullis et al., 1990).

At low metamorphic grade conditions (below 400ºC) brittle fracturing and cataclastic flow are the main deformation mechanisms in plagioclase. Associated structures in the resulting cataclasite are angular grain fragments with grain sizes ranging widely. Strong intracrystalline deformation is abundant within these grain fragments, leading to grain scale faults, and bent cleavage plains and twins. Deformation twinning on albite and pericline law plains is also an important mechanism, where albite twins may form at the tips of microfaults and vice versa (McLaren and Pryer, 2001). Also normally present are patchy undulose extinction and subgrains with vague boundaries. It was pointed out with TEM studies that these structures are not due to dislocations, but to very small scale brittle fractures (Tullis and Yund, 1987).

At low to medium grade metamorphic conditions (400ºC-500ºC) internal fracturing is still the dominant deformation mechanism in plagioclase, assisted by minor dislocation glide. Tapering deformation twins, bent twins, undulose extinction, deformation bands, and kink bands with sharp boundaries can all occur. Clearly seperable augen and matrix, as well as core-and-mantle structures are absent. Bulging (BLG) recrystallization may be present (Pryer, 1993).

At medium metamorphic grade conditions (450ºC-600ºC) dislocation climb becomes possible in plagioclase and recrystallization starts to be an important process, predominantly along grain edges. Most recrystallization is BLG recrystallization by nucleation and growth of new grains (Tullis and Yund, 1991). This can be recognized in thin sections by the development of fine grained plagioclase mantles with sharp boundaries along the cores of the old grains, without the presence of transition zones with subgrain structures. Typical core-and-mantle structures, and micro shear zones of recrystallized grains within the plagioclase cores can develop under these conditions (Passchier and Trouw, 2005). Fracturing becomes less promenent, but microkinking is abundant (Tullis and Yund, 1987). The fine grained recrystallized material has a uniform grain size and polygonal grains, therefore it can be distinguished from the cataclasite formed at lower temperature. Grain boundary sliding may be the deformation mechanism in this fine grained recrystallized plagioclase, but this is very difficult to assess by optical microscopy or TEM (Tullis et al., 1990). Useful optical criteria are lack of lattice preferred-orientation and unusual homogenous mixing of the plagioclase grains and other minerals in the fine grained aggregates (Passchier and Trouw, 2005). It it proposed that at these conditions microscopic gouge zones can be recrystallized and develop into small ductile shear zones, thereby destroying the evidence for the brittle faulting that occurred at an earlier stage (Tullis et al., 1990). Towards higher temperature deformation twinning becomes less abundant (Passchier and Trouw, 2005).

At high grade metamorphic conditions (above 600ºC) subgrain structures are formed, because dislocation climb and recovery become relatively easy in plagioclase (Kruse and Stünitz, 1999, Pryer, 1993). Both BLG recrystallization and subgrain rotation (SGR) recrystallization occur at these conditions. Core-and-mantle structures can still occur, but the boundary between core and mantle is less pronounced than at lower temperatures (Passchier and Trouw, 2005). Isolated micro-kink bands occur in strain free plagioclase grains at low and intermediate pressures. There can still be abundant fracturing of grains at these pressures (Kruse and Stünitz, 1999). At high pressures microfractures, kinkbands, deformation bands, undulose extinction have been observed, with recrystallization by SGR recrystallization, or by BLG recrystallization at high strain rate (Passchier and Trouw, 2005).

At ultra high grade metamorphic conditions (>850ºC) high temperature grain boundary migration (GBM) recrystallization has been observed for plagioclase, in the presence of a melt phase (Lafrance et al., 1996, 1998). This was concluded from strain-free grains with interlobate grain boundaries and left-over grains (Passchier and Trouw, 2005).

At high grade metamorphic conditions diffusion creep may be important in plagioclase (Passchier and Trouw, 2005).

Undulose extinction, deformation bands, and the formation of subgrain boundaries are all due to recovery processes. Recovery processes reduce the dislocation density in the crystal lattice until it reaches equilibrium, which is at the lowest possible dislocation density (Passchier and Trouw, 2005). A crystal has a certain amount of internal strain energy, which is lowest when the crystal lattice is free of dislocations. If a crystal is deformed, dislocations are formed as a response to the imposed differential stress, and the internal strain energy increases. Dislocations cannot be observed by optical microscopy, only by TEM (Passchier and Trouw, 2005).

Another process to reduce the dislocation density is grain boundary mobility (Drury and Urai, 1990). Atoms along the grain boundary of a crystal with a high dislocation density can be displaced slightly to fit to the lattice of a neighboring grain with a low dislocation density. Resulting in local displacement of the grain boundary, and growth of the less deformed grain, the one with the low dislocation density, at the expense of the more deformed grain (Passchier and Trouw, 2005). This process may increase the total length of grain boundaries, and thus the internal free energy of the crystal aggregate, however the removal of dislocations leads to a greater decrease of the internal free energy, thus new small grains with low dislocation densities may replace old grains with high dislocation densities. The process of the reorganization of matter with a change in grain size, shape, and orientation within the same mineral is know as recrystallization (Hirth and Tullis, 1992). In

solid solution minerals, like plagioclase, recrystallization can be associated with a change in composition. This change in composition may be an additional driving force (Passchier and Trouw, 2005). recrystallization that is active during deformation is called dynamic recrystallization. There are three form of dynamic recrystallization; bulging recrystallization, subgrain rotation recrystallization, and high temperature grain boundary migration recrystallization. Bulging recrystallization operates at low temperature, at which grain boundary mobility may be local, and cause a grain boundary to bulge into the crystal with high dislocation density, forming small new grains (Stipp et al., 2002). If dislocations are relatively free to climb lattice planes, climb accommodated dislocation creep can occur, where dislocations are continuously added to subgrain boundaries, increasing the angle between the crystal lattice on both sides of the subgrain boundary, until the subgrain becomes a new grain. This process is called subgrain rotation recrystallization (Passchier and Trouw, 2005). At relatively high temperatures grain boundary mobility increases, so that grain boundaries can sweep through crystals to remove dislocations. This process is known as high temperature grain boundary migration recrystallization (Stipp et al., 2002).

As mentioned above an increase in the grain boundary length means an increase in the internal free energy of a crystal, therefore a decrease in the grain boundary length will lead to a decrease in the internal free energy of a crystal (Evans et al., 2001). Straight grain boundaries and large crystals are therefore favoured, and a process called grain boundary area reduction (GBAR) will take place, a process of grain boundary migration resulting in grain growth and straightening of grain boundaries. The reduction of free energy caused by grain boundary area reduction is much less than the reduction of free energy caused by dynamic recrystallization. Although grain boundary area reduction is active during deformation its effect becomes more dominant after deformation ceases, especially at high temperature (Passchier and Trouw, 2005).

When the deformation on a rock decelerates or stops the crystals will not be in a state of minimum free energy. If deformation took place at relatively low temperatures or if little free water was present in the rock, the deformed fabric may be preserved, but if the temperature of deformation was high or there was excess water present along grain boundaries processes like recovery, recrystallization, and grain boundary area reduction can continue in absence of deformation, to decrease the internal free energy. These processes that take place after deformation are known as static recrystallization (Evans et al., 2001). The term annealing is also used to indicate processes of recovery and static recrystallization induced by passive heating on a previously deformed material. During static recrystallization unstable minerals are replaced by stable ones, dislocation tangles are removed, grain boundaries are straightened, and grains grow due to grain boundary area reduction, modifying the geometry of grain and subgrain boundaries (Passchier and Trouw, 2005).

If the temperature of deformation in a deforming rock is relatively high with respect to the melting temperature of the rock forming minerals, the crystals in the rock will deform by migration of vacancies through the lattice. This process is called grain scale diffusive mass transfer, which has two basic types; Coble creep, and Nabarro-Herring creep. Coble creep operates by the diffusion of vacancies in the crystal lattice along grain boundaries, while Nabarro-Herring creep operates by the diffusion of vacancies throughout the crystal lattice (Wheeler, 1992). The term diffusion creep is often used as a collective term for these two processes (Passchier and Trouw, 2005). In fine grained aggregates, grain boundary sliding takes place, this is a process where crystals can slide past each other, while the development of voids between the crystals is prevented by solid state diffusive mass transfer, locally enhanced crystalplastic deformation, or solution and precipitation through a grain boundary fluid. This deformation process is known as granular flow (Kruse and Stünitz, 1999). The strain rate of granular flow is determined by grain boundary sliding, since this is a fast accommodation mechanism (Passchier and Trouw, 2005).

Identification of microstructures in thin sections

Most arguments for the identification of microstructures in thin sections presented in this section are obtainable with optical microscopy.

In plagioclase both growth twins and deformation twins can occur. These twins can be distinguished by shape, growth twins are straight and may be stepped, while deformation twins are tapered, in plagioclase deformation twins taper towards the grain centre. Twins often form in specific part of a crystal, growth twins are commonly bound by zoning, while deformation twins occur at high strain sites, such as the rim of the crystal or sites where two crystals touch each other. See figure 11. Twinning can only accommodate a small amount of strain, additional processes are needed to accommodate large strains (Passchier and Trouw, 2005).

A process that is often found that can accommodate the larger strains is dynamic recrystallization. For dynamic recrystallization two types of microstructures can be distinguished, partially and completely recrystallized fabrics. A bimodal grain size distribution is characteristic in partly recrystallized fabrics, with aggregates of small new grains of approximately uniform grain size between larger old grains with undulose extinction. In completely recrystallized fabrics the grains have internal deformation, a lattice preferred orientation, and the grain size is relatively uniform, therefore it can be distinguished from a non recrystallized equigranular fabric. The uniform grain size of the new grains is due to deformation and recrystallization at a specific differential stress

(Passchier and Trouw, 2005). There are three mechanisms of dynamic recrystallization, bulging recrystallization, subgrain rotation recrystallization, and high temperature grain boundary migration recrystallization. Also see figure 12.

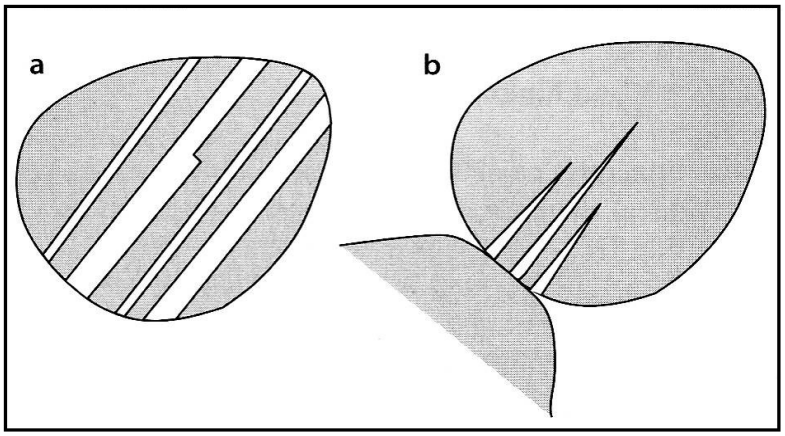

Figure 11: a) Growth twins with steps in plagioclase. b) Deformation twins in plagioclase, with tapering edges nucleated on a high stress site at the edge of the crystal (from Passchier and Trouw, 2005).

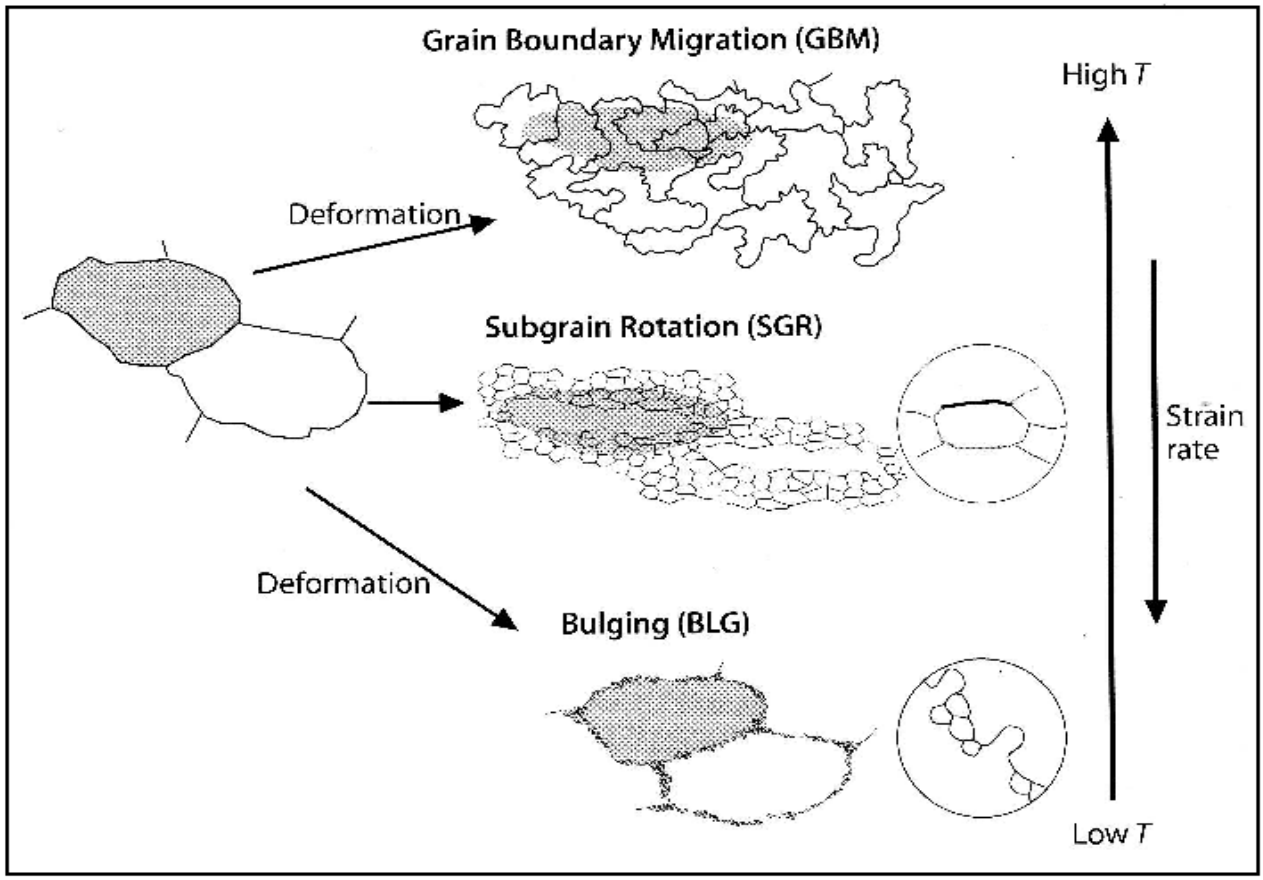

Figure 12: The three mechanisms of dynamic recrystallization. The substance of one of two large grains that are recrystallized is indicated by shading (from Passchier and Trouw, 2005).

In the case of bulging recrystallization the old grains can have patchy undulose extinction, kinks, deformation lamellae, and evidence for brittle fracturing. The grain boundaries are irregular and loboid, where the lobes are on the scale of the new grains. These new grains form at the expense of old grains along grain boundaries. Aggregates of small uniform sized grains are formed between the old grains (Passchier and Trouw, 2005). An aggregate of small, dynamically recrystallized grains around a crystal core with the same mineral composition is called a core-and-mantle structure (Passchier and Trouw, 2005).

In the case of subgrain rotation recrystallization the old grains are flattened, and can have sweeping undulose extinction. The old grains contain subgrains, with the size of new grains, gradual transition in orientation from subgrains to new grains occurs. In the recrystallized aggregates a lattice preferred orientation can occur (Passchier and Trouw, 2005).

In the case of high temperature grain boundary migration recrystallization the distinction between old and new grains is rather difficult. Large grains with interlobate grain boundaries, which are subdivided in smaller subgrains, are typical for GBM recrystallization. Grain boundaries can be pinned by a second phase. Left over grains can occur if a grain is almost completely replaced by a neighbouring grain. If the neighbouring grains have an identical orientation this may indicate the presence of a larger original grain (Passchier and Trouw, 2005).

In samples from naturally deformed rocks the characteristic features of the different recrystallization mechanisms are often found together, because temperature can change during deformation (Passchier and Trouw, 2005).

If the temperature of deformation was high or if much excess water was present in the grain boundaries static recrystallization will take place after deformation in naturally deformed rocks. The microstructures in the rock will be altered. Crystals with straight or smoothly curved grain boundaries, without undulose extinction or subgrains, that are found in a rock that was strongly deformed, shown by the presence of folds, or a lattice preferred orientation, are evidence for static recrystallization and its principal mechanism, grain boundary area reduction. See figure 13. Another indicator for static recrystallization are small grains of a second phase with a preferred orientation, that are included in the grains of the main mineral. Relics of a destroyed older structure are often found in statically recrystallized fabrics (Passchier and Trouw, 2005).

Diffusion creep is hard to find in thin sections, because a processes like solid state diffusion creep and grain boundary sliding leave few traces. Possible indications for solid state diffusion creep are strongly curved and lobate grain boundaries between two different minerals, the erasure or modification of chemical zoning in grains, and the modification of fluid inclusion density and

content in grains. Solid state diffusion creep combined with grain boundary sliding may prevent the development of or destroy a lattice preferred orientation (Passchier and Trouw, 2005).

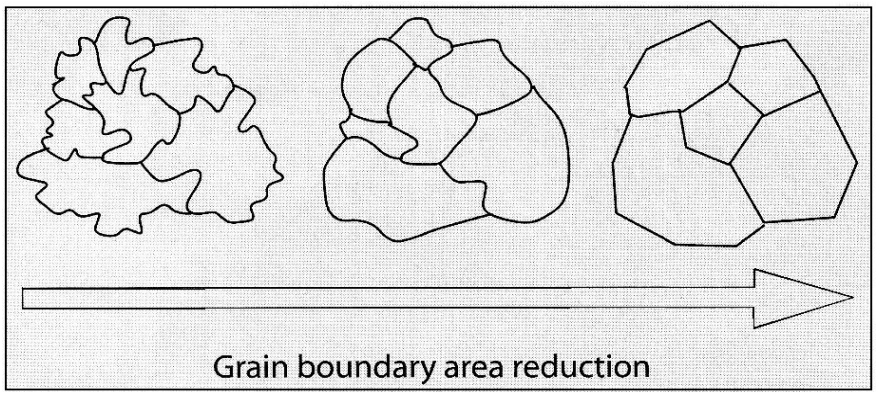

Figure 13: The process of grain boundary area reduction by grain boundary adjustment and grain growth, resulting in a decrease of grain boundary length and energy. Irregular grain boundaries are straightened, and some small grains are eliminated (from Passchier and Trouw, 2005).

Sognefjord

Kruse and Stünitz (1999) did research after the microstructures of the anorthosites of the Jotun Nappe Complex. They found that at the onset of retrograde amphibolite facies deformation, plagioclase grains show undulose extinction and begin to recrystallize dynamically by bulging recrystallization, forming core–mantle structures. At this stage of the deformation, only a weak shape fabric of elongated porphyroclasts of plagioclase is developed. With increasing deformation, the amount of recrystallized plagioclase grains increases and a proto-mylonitic foliation and lineation develops when the fraction of recrystallized plagioclase grains exceeds approximately 30 percent of the rock volume. Plagioclase porphyroclasts become strongly elongated parallel to the stretching lineation during subsequent stages of deformation. The highest-strain mylonites consist of an almost completely recrystallized plagioclase matrix with few porphyroclasts of clinopyroxene, orthopyroxene and hornblende (Kruse and Stünitz, 1999).

The mafic minerals, orthopyroxene, clinopyroxene and brown (Ti-rich) hornblende are partly recrystallized as well. They are mechanically stronger than plagioclase and always show much less elongation of the porphyroclasts (Kruse and Stünitz, 1999). Ortho- and clinopyroxene porphyroclasts form tails of either recrystallized fine-grained pyroxene or of mixtures consisting of pyroxene and green hornblende. In addition to the formation of monomineralic tails, there also

occurs a mixing of pyroxene and plagioclase in certain layers of the strongly deformed rock, here dispersed pyroxene–plagioclase mixtures, which extend from the porphyroclasts of pyroxene, are formed. Some of the recrystallized pyroxenes are replaced by green hornblende. The replacement appears to be synkinematic in most cases, because the new grains of green hornblende occur only between small pyroxene grains in the tails, not rimming pyroxene porphyroclasts (Kruse and Stünitz, 1999). Brown hornblende recrystallizes dynamically into monophase layers, other hornblende grains form tails of two-phase mixtures of hornblende and plagioclase. Garnet is fractured or remains undeformed (Kruse and Stünitz, 1999).
The predeformational granulite facies assemblage of the Upper Jotun Nappe anorthosites is locally preserved, it contains corona structures of pyroxene, which is commonly partially replaced by hornblende, and garnet due to reactions between plagioclase and primary olivine (Kruse and Stünitz, 1999, Lundmark et al., 2007). Studies of the coronas suggest that corona formation resulted from two stages of subsolidus reaction during magmatic cooling, followed by a flattening of the coronas that define a granulite facies foliation (Lundmark and Corfu, 2007).

Tafjord

The microstructures found within the anorthosites from Tafjord were investigated by Brueckner (1968). The microstructers found are fine- to medium-sized, interlocking, anhedral plagioclase grains, with at least 50 percent of the grains having twins, and many grains show zoning. The mafic minerals may be concentrated into thin laminae and show very strong preferred orientations, giving some anorthosites a banded appearance. Cataclastic features, including microfractures, microfaults, banded or irregular extinction, bent twins and cleavage plains and granulated margins may occur (Brueckner, 1968).

3.3 Grain size analysis

All constants needed in the piezometer equations can be obtained from the literature. However we also need to obtain the recrystallized grain size to estimate the stress with the piezometers. The recrystallized grain sizes are obtained from the thin sections. For this the thin sections where digitised. The photographs were taken under cross polarised light, because single plagioclase grains can not be determined under plain polarised light. The digital versions of the thin sections were then

copied into photoshop to draw the grain boundaries. The grain boundaries where drawn in a new layer, placed on top of the photograph. See figure 14. This layer, consisting only of lines representing the grain boundaries was copied into ImageJ to calculate the grain size. See figure 14. In ImageJ a binary was made of the layer. See figure 14. ImageJ measures the grain size on the basis of pixels, therefore a line-section, with the size of the scale bar, was used to set the scale to mm. The output of the ImageJ calculations were copied to a spreadsheet to analyse the grain size. Area, perimeter, major and minor axis and angle with the north were measured. The diameter of the grains was calculated using these measurements. The major and minor axis are measured by applying the best fit ellipsoid to the grains. From this the shape of the grains (major axis/minor axis) can be calculated. Plots were made of major versus minor axis, grain shape versus grain size, grain orientation (angle with north) versus grain shape, and grain orientation versus grain size. Also histograms were made of grain size distribution and grain orientation.

The lines that represent the grain boundaries are relatively thick compared to the grain boundaries. To compensate for this the diameter of the grain was calculated using the following formula:

$$d = 2\sqrt{\frac{V+p}{\pi}} \tag{3}$$

where d is the diameter in mm, V is the area in mm^2, and p is the perimeter. Normally the perimeter would be left out of the equation. The addition of the perimeter in the equation makes more of a difference for the small grains than for the large grains, because the area increases as a square function. The thickness of the line is small compared to the thickness of the thin section, which is 30μm. Therefore the thickness of the thin section is the most important limitation to the measured grain size. Many of the grains are smaller than 30μm, the thickness of the thin section. This might make the measurements less accurate. The major and minor axis are measured by fitting an ellipsoid to the grains. This works best for (sub) rounded grains, this is another limitation to the measuring technique. Some of the grains have very irregular grain boundaries. For these grains the boundaries were smoothed a little by a magnitude of one to two times the thickness of the line.

Kruse and Stünitz (1999) investigated the dynamically recrystallized grain size of the anorthosites from the Jotun Nappe Complex. They found that plagioclase porphyroclasts recrystallize dynamically to a fine-grained pure plagioclase matrix. The recrystallized grain size of pure plagioclase layers ranges between 50 and 70 μm. The recrystallized grain size in the polyphase

layers, mixtures of plagioclase and pyroxene or plagioclase and hornblende, is smaller, it ranges between 10 and 70 µm, than in monophase layers or tails (Kruse and Stünitz, 1999).

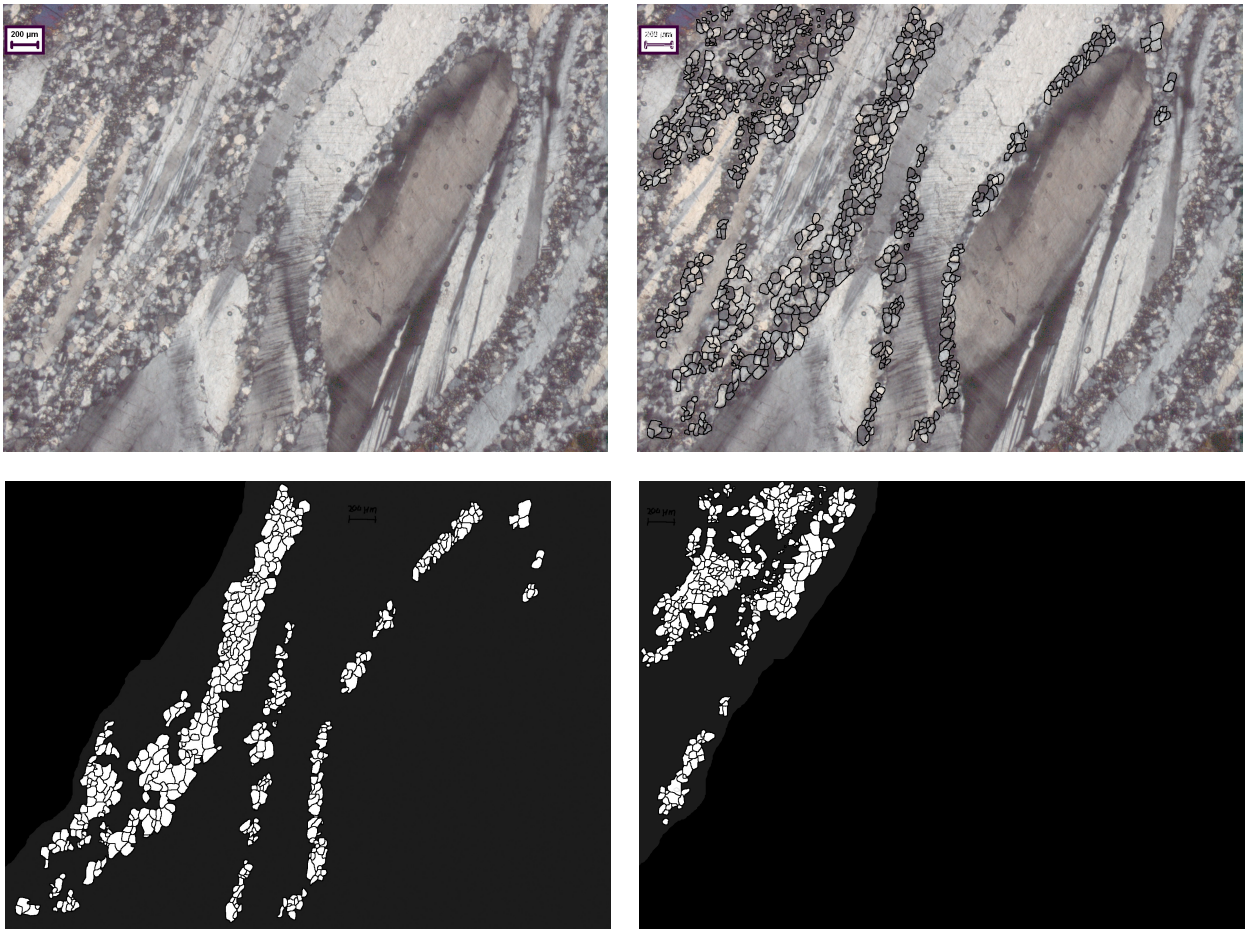

Figure 14: Top left: Digitised photograph of thin section 15-8-05. Top right: Digitised photograph with grain boundaries in a new layer. Bottom left: Binary of layer with grain boundaries for monophase layer of plagioclase. Bottom right: Binary of layer with grain boundaries for multiphase layer, containing plagioclase, and hornblende or pyroxene. The scale bar in the top left corner indicates a length of 200µm.

3.4 Paleopiezometry

Paleopiezometers are used to infer stress from microstructures preserved in naturally deformed rocks. If callibrated experimentally, a piezometer based on the recrystallized grain size can be used on naturally deformed rocks without the use of Transmitting Electron Microscopy (TEM), because the recrystallized grain size can be obtained from thin sections using optical microscopy.

A piezometer uses the relation between the steady-state flow stress for dislocation creep and the

subgrain size or the recrystallized grain size. This piezometric relation was obtained from numerous experiments on metals, ceramics and minerals. The relation for a recrystallized grain size piezometer is given by an equation of the type:

$$d = A \cdot \sigma^m \qquad \text{(Post and Tullis, 1998)} \qquad (4)$$

where d is the recrystallized grain size, σ is the steady state flow stress, m is refered to as the piezometer exponent. Both A and m are material and mechanism specific constants (Post and Tullis, 1998, de Bresser et al.,2000). In this study the stress is estimated from the measured recrystallized grainsize, obtained by grain size analysis, therefore the equation should be rewritten as:

$$\sigma = \left(\frac{d}{A}\right)^{1/m} \qquad (5)$$

Three different recrystallized grain size paleopiezometers of this form are used and compared in this study.

Post and Tullis recrystallized grain size piezometer for feldspar

The recrystallized grain size piezometer for low-temperature migration recrystallization in feldspar was calibrated experimentally. The experiments were performed on fine grained (grain size 1-10μm) samples of hot-pressed albite powder and a natural albitic feldspar aggregate (grain size 150μm). Fine-grained synthetic aggregates were chosen because the sample strain needed for total recrystallization of the sample is less for fine-grained aggregates than for a coarse-grained aggregate. An albite composition feldspar (Ab98An1Or1) was chosen because it does not form zoisite under experimental conditions and similar dislocation creep regimes have been observed in feldspars of different composition. The samples were hot-pressed in situ at a temperature of 900ºC and a confining pressure of 1500 MPa for 10 hours prior to deformation (Post and Tullis, 1998).
The experiments were performed in a Tullis-modified Griggs apparatus using an all-NaCl confining medium. All samples were deformed in simple shear and axial compression at 900ºC, 1500 MPa confining pressure and different axial shortening rates, ranging from 0.008 to 0.02 mm/s, corresponding to shear strain rates between $3 \cdot 10^{-4}\ s^{-1}$ and $2 \cdot 10^{-5}\ s^{-1}$ (Post and Tullis, 1998).
Transmitting Electron Microscopy was used to determine the deformation mechanism. TEM

microstructures indicated that deformation occurred by dislocation creep, accommodated by low-temperature migration recrystallization. With the flow stresses ranging from 100 to 450 MPa, and the geometric mean intercept lengths ranging from 0.9 to 2.5 μm, the following recrystallized grain size piezometer relation was obtained:

$$d = 55 \pm 5 \cdot \sigma^{-0.66 \pm 0.07} \qquad \text{(Post and Tullis, 1998)} \qquad (6)$$

The piezometer exponent in this relation differs from the ones calibrated in earlier studies for rotation recrystallization and high-temperature migration recrystallization. The exponents for these earlier studies are lower (-1 to -1.5) than the value for low-temperature migration recrystallization given here. Identification of the recrystallization mechanism is crucial for the application of recrystallized grain size piezometers to naturally deformed rocks, because it seems that all three recrystallization mechanisms have a different grain size-stress relation (Post and Tullis, 1998). After alteration equation (5) for stress estimates the following equation is obtained:

$$\sigma = \left(\frac{55}{d} \right)^{1.515} \qquad (7)$$

where d is the recrystallized grain size in μm, and σ is the steady state flow stress in MPa.

Applications of this experimental recrystallized grain size piezometer to naturally deformed rocks requires extrapolation to lower temperatures and slower strain rates. The experiments were performed at a temperature of 900ºC whereas in naturally deformed feldspar the tested low-temperature migration recrystallization mechanism takes place at lower temperatures of 400º to 600ºC (Post and Tullis, 1998). The shear strain rates used in the experiment are of a factor 10^{-4}-10^{-5} s^{-1}. Geologically correct strain rates for naturally deformed rocks are of a factor 10^{-10}-10^{-14} s^{-1}.
The use of this piezometer can be complicated by post-deformational static annealing and grain boundary pinning by other phases. If static grain growth would have taken place after deformation, the recrystallized grain size would be larger than the equilibrium size, and the stress inferred from the piezometer would be an underestimate of the actual shear stress at which the rock was deformed. If the grains where pinned by a second phase, the recrystallized grains would be smaller than the equilibrium size, and the stress would be overestimated by using the piezometer (Post and Tullis., 2000). Furthermore this the use of the piezometer can be complicated by the effect of water content (Post and Tullis 1998). It is of great importance that the recrystallization mechanism that

deformed the rock is identified correctly, because only a piezometer that was calibrated for the same mechanism can be applied to this rock (Post and Tullis, 1998).

Twiss theoretical paleopiezometer

This piezometer accounts for both subgrains and recrystallized grains. The theory for this theoretical paleopiezometer is based on the fundamental assumption that the formation of subgrains and recrystallized grains must be the energetically favourable processes. This means that the total strain energy of dislocations ordered into a closed surface, which can be either a subgrain or a recrystallized grain boundary, must be less than or equal to the total energy of a steady state density of dislocations within the enclosed volume (Twiss, 1977). Assuming then that the energies are equal gives us a grain dimension d for any given state. As the grain size changes, the total volume energy varies as the volume of this grain dimension, as d^3. Where the total grain boundary energy varies as the surface area of d, as d^2. There is a grain size at which the energies are equal. The condition for this specific grain size is expressed for an ideal cubic subgrain or recrystallized grain by:

$$6\gamma d^2 = w\rho d^3 \qquad \text{(Twiss, 1977)} \qquad (8)$$

where γ is the dislocation strain energy per unit area in the grain boundary, w is the dislocation strain energy per unit length in the grain volume, d is the grain dimension and ρ is the steady state dislocation density in the grain volume. The stress is introduced into the relation through the equation relating differential stress σ to the dislocation density:

$$\sigma = \alpha \Gamma b \rho^{1/2} \quad \text{, with} \quad \Gamma \equiv \frac{\mu}{1-\nu} \qquad \text{(Twiss, 1977)} \qquad (9)$$

where b is the Burgers vector, μ the shear modulus, ν the Poisson ratio, and α an empirical parameter of order 1. The assumption was made that at steady state creep, the back stress on a dislocation, caused by its interaction with other nearby dislocations, must equal the applied stress. The parameter α corrects for the complexity of the dislocation interactions (Twiss, 1977).
Further, to simplify the equation, it is assumed that all dislocations are edge dislocations, that all boundaries are simple tilt boundaries, and that crystals are elastically isotropic. With these assumptions relatively simple equations can be found for the volume and boundary energy

densities. These assumptions are adequate for a first order approximation, because the self energy of edge and screw dislocations differs only by a factor (1 - ν), and tilt boundaries are very common among subgrain boundaries. The low angle tilt boundary theory is good for misorientations up to 10°-15°. This includes subgrain boundaries, which commonly have misorientations of 1° or less, and it is considered adequate for the initial stages of recrystallization before grain rotation has proceeded too far (Twiss, 1977). After some manipulation equation (8) can be reduced to the forms:

$$\frac{\sigma}{\Gamma} = K\left(\frac{d}{b}\right)^{-p} \quad \text{or} \qquad \log\frac{\sigma}{\Gamma} = \log K - p\log\frac{d}{b} \qquad \text{(Twiss, 1977)} \qquad (10)$$

where $$p \equiv \frac{\phi}{2\phi - 1} \qquad \text{(Twiss, 1977)} \qquad (11)$$

and where ϕ is the ratio of total dislocation length in the boundary to that in the enclosed volume. The value of the parameter ϕ is the only difference between subgrains and recrystallized grains in this theory. Theoretical values of ϕ_s for subgrains and ϕ_r for recrystallized grains where obtained with the assumtion that the subgrain volume contains a steady state density of dislocations. From the assumption that the subgrain size that forms is the smallest stable size, it was inferred that $\phi_s = 1$. For a dislocation free recrystallized grain, again with the assumption that the smallest stable grain size is favoured to develop, it was inferred that $1.4 \leq \phi_r \leq 2$. Using these values for ϕ in equation (11) gives $p_s = 1$ and $0.78 \geq p_r \geq 0.67$. The theory was tested by plotting data sets on the variation of stress with subgrain size and recrystallized grain size on non-dimensional coordinates for olivine, quartz and several metals. The best fit slopes and best fit intercepts to the data sets give:

$$p_s = 1 \pm 0.03 \quad , \qquad \log K_s = 0.91 \pm 0.01 + 3.85\,\Delta p_s \qquad \text{(Twiss, 1977)} \qquad (12)$$

$$p_r = 0.68 \pm 0.02 \quad , \qquad \log K_r = 0.38 \pm 0.01 + 5.30\,\Delta p_r \qquad \text{(Twiss, 1977)} \qquad (13)$$

Applying these values for p in equation (10) gives for subgrains:

$$\log\frac{\sigma}{\Gamma} = 0.91 - \log\frac{d}{b} \qquad \text{(Twiss, 1977)} \qquad (14)$$

and for recrystallized grains:

$$\log\frac{\sigma}{\Gamma}=0.38-0.68\log\frac{d}{b}$$ (Twiss, 1977) (15)

If the value of the Burgers vector and the effective isotropic elastic moduli for a mineral are known, a relation can be obtained, that allows the steady state recrystallized grain size to be used as a paleopiezometer. Equation (15) can be rewritten:

$$\sigma = Bd^{-0.68}$$, with $$B \equiv K\,\Gamma\, b^{p}$$ (Twiss, 1977) (16)

where σ is the steady state flow stress in MPa, and d is recrystallized grain size in mm (Twiss, 1977). Values for the constants are given by Twiss (1977), for anorthosite $\mu = 3.8\cdot10^{-4}$ MPa, $\nu = 0.31$, applying these values to equation (9) gives $\Gamma = 5.51\cdot10^{-4}$ MPa, and the value for the Burgers vector $b = 7\cdot10^{-7}$ mm. With K_r from equation (13), we can now calculate B by applying the values to equation (16), $B = 8.63$ MPa·mm for anorthosite.

The most important requirement for the paleopiezometer to work is that the measured grain size equals the steady state size of syntectonically recrystallized mineral grains. The steady state grain size that is formed during steady state dynamic (syntectonic) recrystallization is a balance of two processes: recrystallization, which diminishes the grain size, and grain growth, which increases the grain size (Twiss, 1977).

If the temperature remains high after deformation, annealing and grain growth can proceed, while dynamic recrystallization ceases, because the stress is removed. The measured grain size will be larger than the steady state grain size, and the stress estimated with the piezometer will be too low. Rocks with high dislocation density and small grain size, associated with high stress, are most subjected to this process of annealing and grain growth, thus the textures obtained from high stresses are more difficult to preserve and will tend to give stress estimates that are too low. In naturally deformed rocks post-deformational annealing is common, which limits the use of this paleopiezometer (Twiss, 1977). The dynamically recrystallized grain size must be preserved for the piezometer to be useful. This can be the case for a naturally deformed rock that was cooled rapidly after deformation at high temperature, or if the temperature during deformation didn't reach high temperatures, because here the kinetics of grain growth can become very slow, preventing a significant increase in grain size after deformation. If the stress would remain constant during cooling, the dynamically recrystallized grain size will not change, because for this piezometer it was assumed that the recrystallized grain size is independent of temperature. The dynamically

recrystallized grain size may also be preserved if the grains are enclosed by grains of another phase (Twiss, 1977). For a coarse grained rock, in which the rate of grain growth is small and the dislocation density is low, there can be a different problem. If the stress is low the grains might not reach the steady state grain size during deformation, because the driving forces for grain growth are small in these rocks. In this case the stresses obtained with the paleopiezometer will be an overestimate of the shear stress during deformation (Twiss, 1977).

The theoretical paleopiezometer from Twiss has been criticized, because the application of equilibrium thermodynamics is incorrect. During syntectonic recrystallization, subgrains and recrystallized grains are cyclically formed and removed, this is a non-equilibrium, dynamic process. Furthermore, the stable grain size predicted by Twiss is the smallest grain size possible, however the system can always lower it energy by allowing these small grains to grow (de Bresser et al., 2000).

De Bresser et al. temperature dependent paleopiezometer

The temparature dependent paleopiezometer is linked to the field boundary model. This model is based on an earlier theory of de Bresser et al. (1998), which suggests that, for materials in which grain size reduction is sufficiently effective, dynamic recrystallization should lead to a steady state balance between grain size reduction and grain growth processes set up in the boundary region between the dislocation, grain size insensitive (GSI), and diffusion, grain size sensitive (GSS), creep field. The boundary can be found using the equation for dislocation creep combined with the equation for diffusion creep. The equation for dislocation creep is obtained from a study by Edward et al. (1982). They present a model for steady state dislocation creep. The relation is given by a power law or Dorn equation:

$$\dot{\varepsilon}_r = B\sigma^n \exp\left(\frac{-Q_r}{RT}\right) \qquad \text{(de Bresser et al., 2000)} \qquad (17)$$

where B and n (the power law exponent) are constants, Q_r is the activation energy for the process controlling the rate of dislocation creep ε_r, R is the gas constant, and T is the absolute temperature. This model for dislocation creep uses the subgrain size, d_s instead of the recrystallized grain size, d. The stress-grain size relation obtained by Edward et al. is:

$$d_s = K_1 \sigma^{-n/4} \exp\left(\frac{Q_r - Q_{cl}}{4RT}\right) \qquad \text{(de Bresser et al., 2000)} \qquad (18)$$

where, K_1 is a constant, and Q_{cl} is the activation energy for the diffusion process controlling dislocation climb in the boundary (de Bresser et al., 2000). The model of Edward et al. (1982) is based on the arrival and annihilation of dislocations at subboundaries, and therefore overcomes the problems with the Twiss piezometer. Furthermore the stress exponent *m* is dependent on the creep behaviour of the respective material, and the stress-subgrain size relation includes the activation energy. This stress-subgrain size relation will be dependent on temperature for all cases in which Q_{cl} is not equal to Q_r. One of those cases is if dislocation climb in the subgrain wall is controlled by pipe diffusion, for which $Q_{cl}<Q_v$, while creep is controlled by lattice diffusion, where $Q_r=Q_v$. Here the steady state subgrain size will be larger at lower temperature than at higher temperature at the same stress. Another case is if dislocation climb in the sub-boundary is controlled by lattice diffusion, $Q_{cl}=Q_v$, while creep is controlled by dislocation cross slip, $Q_r<Q_v$. Here the steady state subgrain size will increase with increasing temperature (de Bresser et al., 2000).

Since dislocation creep is grain size insensitive we won't use the relation from equation (18) for the piezometer. The piezometer is based on the recrystallized grain size, which occurs in the relation for diffusion creep, which is grain size sensitive. The relation for diffusion creep is given by the equation:

$$\dot{\varepsilon}_d = A\left(\frac{\sigma}{d^p}\right)\exp\left(\frac{-Q_d}{RT}\right) \qquad \text{(de Bresser et al., 2000)} \qquad (19)$$

where *A* and *p* are constants, *d* is the recrystallized grain size, and Q_d is the activation energy for lattice or grain boundary diffusion. For lattice diffusion $Q_d=Q_v$, the activation energy for lattice diffusion, and $p=2$, for grain boundary diffusion $Q_d=Q_{gb}$, the activation energy for grain boundary diffusion, and $p=3$. Near the boundary both dislocation creep ε_r and diffusion creep ε_d will contribute to the steady state creep rate ε_{rx}:

$$\dot{\varepsilon}_{rx} = \dot{\varepsilon}_d + \dot{\varepsilon}_r \qquad \text{(de Bresser et al., 2000)} \qquad (20)$$

At the boundary the contribution from both mechanisms is equal, so that $\varepsilon_r=\varepsilon_d$. It is possible that the mean recrystallized grain size *D* will adjust itself to a different relative contribution of dislocation and diffusion creep. We define *C* to correct for this:

$$\dot{\varepsilon}_d / \dot{\varepsilon}_r = C \qquad \text{(de Bresser et al., 2000)} \qquad (21)$$

where C depends on flow stress and temperature. C is considered constant for small ranges of stress and temperature. Assuming a steady state recrystallized grain size, d=D, and combining equations (17), (19), (20), and (21) results in:

$$d = K_2 \sigma^{-(n-1)/p} \exp\left(\frac{Q_r - Q_d}{pRT}\right) \text{ , with } \qquad K_2 = \left(\frac{A}{CB}\right)^{1/p} \qquad \text{(de Bresser et al., 2000)} \qquad (22)$$

where C is 1 for the exact boundary between dislocation and diffusion creep (de Bresser et al., 2000). Equation (22) is rewritten for stress estimates:

$$\sigma = K_3 d^{1/-(n-1)} \exp\left(\frac{Q_r - Q_d}{-(n-1)RT}\right) \text{ , with } \quad K_3 = \left(\frac{B}{A}\right)^{1/-(n-1)} \qquad (23)$$

where σ is the steady state flow stress in MPa, d is the recrystallized grain size in μm, R is the gas constant, T is the temperature in K, Q_r and Q_d are the activation energies for respectively dislocation creep and diffusion creep in J/mol, and n is a constant. For dislocation creep n=3, for diffusion creep n=1 (Rybacki and Dresen, 2004). Values for all constants are given by Rybacki and Dresen (2004), see table 1.

Dislocation creep regime						
Aggregate	n	Q_r (J/mol)	Log B (MPa^{-n} μm^m/s)	m	H_2O wt.%	Reference
An100 (dry)	3	648000	12,7	0	0,004	Rybacki and Dresen, 2000
An100 (wet)	3	356000	2,6	0	0,07	Rybacki and Dresen, 2000
An60	3	235000	-1,5	0	0,3	Dimanov et al., unpublished
Diffusion creep regime						
Aggregate	n	Q_d (J/mol)	Log A (MPa^{-n} μm^m/s)	m	H_2O wt.%	Reference
An100 (dry)	1	467000	12,1	3	0,004	Rybacki and Dresen, 2000
An100 (wet)	1	170000	1,7	3	0,07	Rybacki and Dresen, 2000
An60	1	153000	1,1	3	0,3	Dimanov et al., unpublished

Table 1: Flow law creep parameters for synthetic plagioclase aggregates (modified after Rybacki and Dresen, 2004).

Experiments performed in earlier studies have shown that there is evidence for a modest temperature dependence of stress-recrystallized grain size relations for a few materials, but widespread support is lacking. However most paleopiezometers, like that of Post and Tullis, and Twiss, didn't include temperature as a variable. Because most experiments are performed at higher temperatures than those occurring in naturally deformed rocks, the stresses calculated with paleopiezometer are often over- or underestimated depending on the relative values of the activation ernergy (de Bresser et al., 2000). The field boundary model was tested for olivine and calcite by de Bresser et al. (2000). They found that if grain boundary diffusion controls diffusion (GSS) creep, and dislocation (GSI) creep is controlled by lattice diffusion, than the stress will be underestimated if temperature is not taken into account. For olivine and calcite the error might be as high as an order of magnitude. Therefore temperature might be more important in paleopiezometry than assumed. However the temperaure dependence drops out of equation (22) if dislocation and diffusion creep are both controlled by lattice diffusion (de Bresser et al., 2000). In this study we will test the field boundary model for plagioclase.

Deformation mechanism maps

The stresses inferred from the different piezometers will be used in equation (17), with the constants given above in table 1, to estimate the strain rates. The stresses obtained from the piezometers and the strain rate inferred from the flow law for steady state dislocation creep, equation (17), are the compressional stress σ and the compressional strain rate ε. The steady state flow stress is caused by shearing, instead of the compressional stress σ, the shear stress τ is needed, and instead of the compressional strain rate ε, we need the shear strain rate γ. The relations between the shear stress and the compressional stress, and between the shear strain rate and the compressional strain rate are given in equations (24) and (25):

$$\tau = \frac{\sigma}{\sqrt{3}} \qquad \text{(Frost and Ashby, 1982)} \qquad (24)$$

$$\dot{\gamma} = \sqrt{3}\,\dot{\varepsilon} \qquad \text{(Frost and Ashby, 1982)} \qquad (25)$$

A geological flow stress typically would have a value between 1 and 200 (Drury, personal communication), but higher stresses have been recorded (Kruse and Stünitz, 1999) and geologically correct shear strain rates vary from 10^{-14} to 10^{-10} for the kind of setting we are looking at (Drury,

personal communication). The results obtained from equations (24) and (25) should thus have values within these ranges. The piezometer with results that best fit these values will be used to construct deformation mechanism maps for plagioclase with three different anorthite contents, An100 with 0,004 weight percent water = An100 (dry), An100 with 0,07 weight percent water = An100 (wet), and An60 with 0,3 weight percent water. See figure 15.

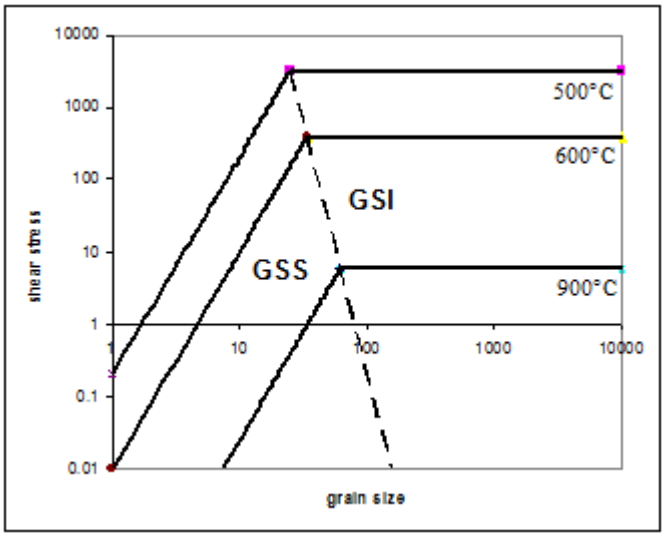

Figure 15: Deformation mechanism map. The horizontal black lines represent certain temperatures, which correspondent with certain metamorphic conditions, 500°C = greenschist facies, 600°C = amphibolite facies, and 900°C = granulite facies. The sloped black lines are constructed with equation (19) the stress-recrystallized grain size relation for diffusion creep, or grain size sensitive (GSS) creep. The interrupted black line is constructed with the piezometer relation, and indicates the border between the diffusion, or GSS, creep regime and the dislocation or GSI, creep regime, where GSI stands for grain size insensitive, for a specific shear strain.

Kruse and Stünitz (1999) found that the deformation during the Caledonian orogeny took place at a maximum confining pressure of 900 MPa, or a shear stress of 520 MPa, and a temperature of 700°C. During the Sveconorwegian orogeny the maximum confining pressure was 900-1000 MPa and temperatures were over 1000°C (Kruse and Stünitz, 1999).

4. Results

The results will be present in four sections, beginning with fieldwork, followed by microstructures, grain size analysis, and paleopiezometry.

4.1 Fieldwork

The fieldwork results will consist of photographs of the sample locations, and composition and water content estimations. Figures with foliations and lineations in the samples from Sognefjord are given in appendix .

Sognefjord

Figure 16: Top left: Fimreite, sample location NFAS08 15.2 Pyroxene with garnet rims. Top right: NFAS08 15.15 Garnet rims around pyroxene on the other end of the road section near Fimreite. Bottom left: NFAS08 15.6 Anorthositic leucogabbro, with mafic minerals occurring in bands. Bottom right: Close-up of NFAS08 15.6 Plagioclase is white or pink to purple. Garnet present in light and dark bands.

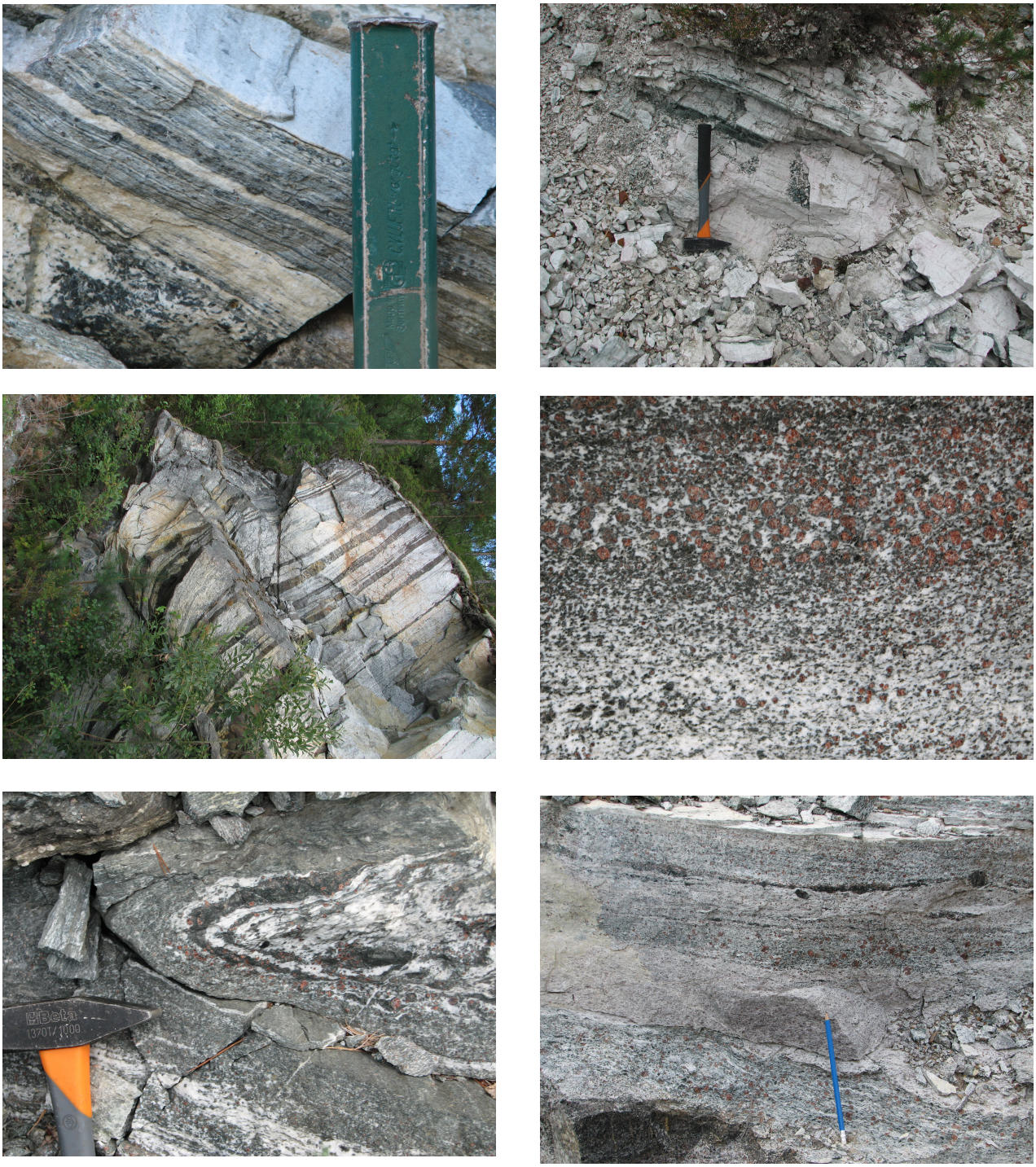

Figure 17: Top left: NFAS08 15.7 Close-up of small scale shear zone. Very fine bands of plagioclase and mafic minerals. Top right: NFAS08 15.10a Local occurrence of proper anorthosite. See also figure 10. Middle left: Overview of mafic bands in anorthositic gabbro at sample location NFAS08 15.11. Middle right: NFAS08 15.12 Close-up of anorthositic gabbro. Larger garnet porphyroclasts in mafic layers. Bottom left: NFAS08 15.13 Small scale fold in anorthositic gabbro, with garnet porphyroclasts. Bottom right: Eide NEAS08 16.1a. Sample from quarry, see figure 2. Anorthositic gabbro, with garnet porphyroclasts.

Figure 18: Top left: Gudvangen NGAS08 18.1a-e Proper anorthosite along a new road near Gudvangen. Top right: Lærdal NLAS08 19.2 Anorthositic gabbro. Plagioclase is white or pink to purple. Bottom left: Amla/ Kaupanger NAAS08 20.1c Block in front is ~20cm. Anorthositic gabbro. Bottom right: Haukasen FHaAS08 20.2 Overview including a fault on the left and two shear zones.

At the outer edges of the Fimreite section, see figure 16 top left and top right, corona structures are found of garnet formed around lenses of pyroxene in anorthositic rock, which are relics of older undeformed structures. The other samples from Fimreite, which are taken more to the centre of the section show bands of plagioclase and mafic minerals, figure 16 bottom, figure 17 middle left, with some isoclinal folds, figure 17 bottom left, and small scale shear zones, figure 17 top left. The largest garnet porpyroblasts are associated with mafic bands, figure 17 middle right. The rocks in Amla/ Kaupanger, figure 18 bottom left, show the same bands of plagioclase and mafic minerals as the rocks in Fimreite. Some locations show proper anorthosite, figure 17 top right, figure 18 top left, with limited amounts of mafic minerals in milky white rocks, however on many locations the plagioclase isn't milky white, but pink to purple, figure 16 bottom right, figure 17 bottom right, and figure 18 top right.

Tafjord

Figure 19: Left: Kallskaret NKAS08 13.1 Shear zone in anorthosite. Rocks are weathered. Right: NKAS08 13.2 Proper anorthosite of white plagioclase. Only 5-10% mafic minerals. Near shear zone.

The rocks in Tafjord are very weathered and appear to be grey, figure 19 left, however underneath the plagioclase is milky white, figure 19 right. The anorthosites found here are proper anorthosites, with only limited amounts of mafic minerals.

Composition

Compositions were acquired from the field and checked with the thin sections and literature. The samples from Sognefjord have variable compositions, whereas the samples from Tafjord have a uniform composition. In Sognefjord the rocks vary from proper anorthosites, with less than 10 percent mafic minerals, to anorthositic gabbro, with up to 35 percent mafic minerals. In some areas the mafic minerals are dominated by pyroxene, while in other areas hornblende is more abundant. Garnet is associated with the pyroxene dominated areas, but can also occur in the hornblende dominated areas. Plagioclase is mostly white, but in some areas it has a pink to purple colour.
In Tafjord all anorthosites are proper anorthosites, with only 5 to 10 percent mafic minerals. The mafic minerals consist of biotite and to a lesser extend hornblende.

Water content

The water content calculated from the atomic weights and the retrograde reaction formulas is the minimum water content needed for the retrograde reactions. See tables 2 and 3. In the Sognefjord pyroxene and hornblende are both common minerals, however in Tafjord we find hornblende and biotite, and no pyroxene is present. All of the pyroxene has been replaced by retrograde reactions, thus the first retrograde reaction (1) has taken place for 100%. The amount of water needed for a certain percentage of the second reaction (2) to occur was calculated by adding the minimum amount of water needed for 100% of the first reaction to occur and the amount of water needed for that certain percentage of the second reaction, because the amount of water needed for the first retrograde reaction (1) is very low, about 0,002 weight percentage of water, it is not shown in the tables. The highlighted areas show a weight percentage of water of about 0,30, which is the weight percentage of water for An60, see table 1. The percentage of mafic minerals in the sample rock is estimated from the thin sections. The percentage of mafic minerals that are affected by the retrograde reactions can also be obtained from the thin sections. A wide variety of affected minerals was used in the calculations to be able to compare with the thin sections better.

Percentage of mafic minerals that are affected by retrograde reaction (1)	Percentage of mafic minerals in the sample rock		
	Sognefjord		
	35%	**30%**	**20%**
100%	0,67	0,56	0,37
90%	0,60	0,50	0,33
80%	0,54	0,45	0,30
70%	0,47	0,39	0,26
60%	0,40	0,34	0,22
50%	0,34	0,28	0,19
40%	0,27	0,22	0,15
30%	0,20	0,17	0,11
20%	0,17	0,11	0,07
10%	0,07	0,06	0,04

Table 2. Weight percentage of water, variable with mafic mineral content, and amount of retrograded grains. For Sognefjord the percentage of mafic minerals in the sample rock is 20-35%, and the percentage of mafic minerals affected by retrograde reaction is referring to reaction (1).

Percentage of mafic minerals that are affected by retrograde reaction (2)	Percentage of mafic minerals in the sample rock	
	Tafjord	
	10%	**5%**
100%	0,72	0,39
90%	0,65	0,35
80%	0,58	0,31
70%	0,50	0,27
60%	0,43	0,23
50%	0,36	0,20
40%	0,29	0,16
30%	0,22	0,12
20%	0,14	0,08
10%	0,07	0,04

Table 3. Weight percentage of water, variable with mafic mineral content, and amount of retrograded grains. For Tafjord the amount of mafic minerals is 5-10%, and the percentage of mafic minerals affected by retrograde reaction is referring to reaction (2), assuming that reaction (1) has taken place for 100%, replacing all pyroxene.

4.2 Microstructures

In this section photographs of thin sections will be presented, first of samples from Sognefjord, and second of samples from Tafjord.

Sognefjord

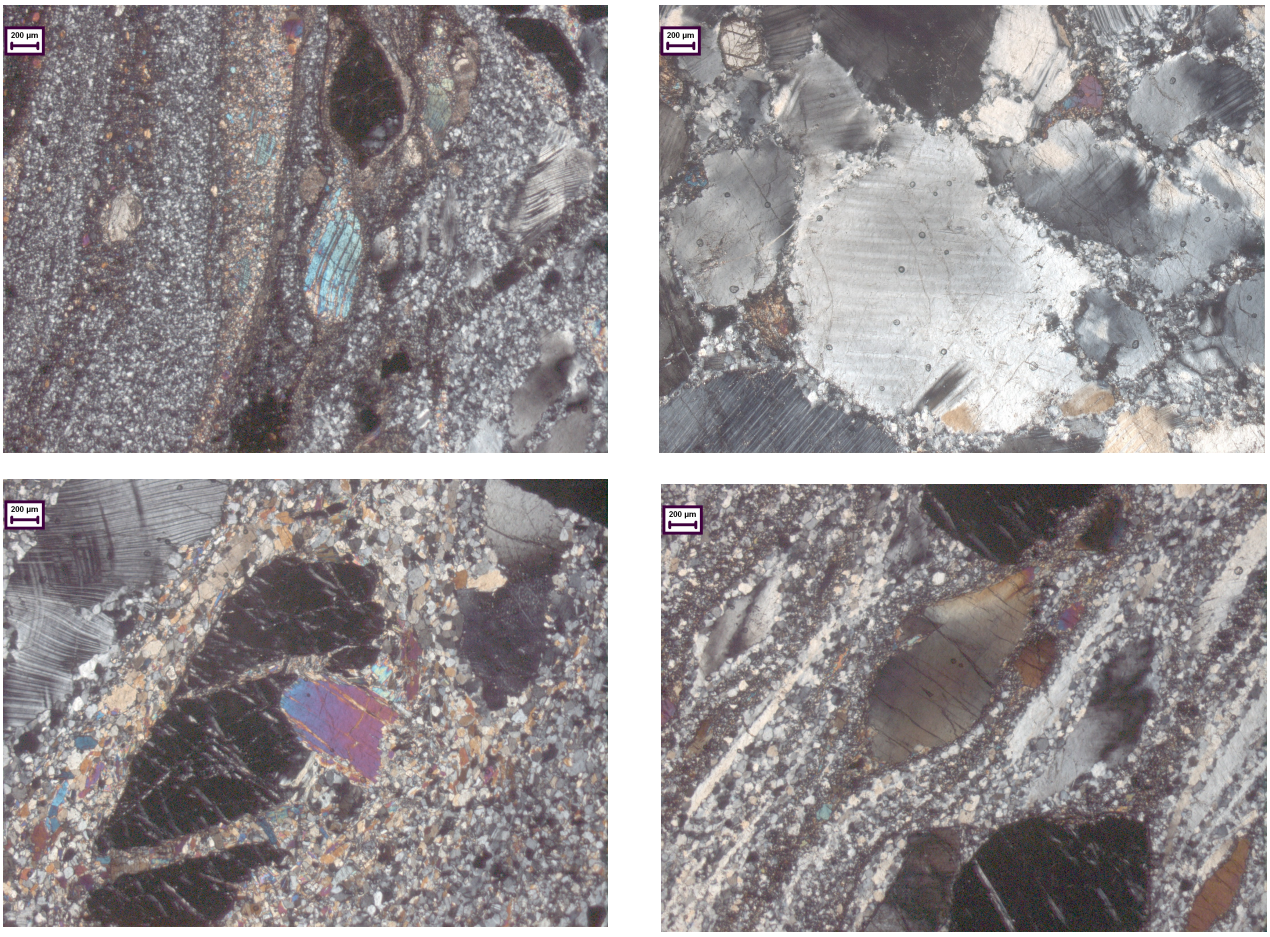

Figure 20: Top left: Thin section 15-1-02 Bands of dark and light small grains, hornblende porphyroclast with tails, and garnet porphyroclast without tails. Top right: 15-5 Large grains of plagioclase with recrystallized grains along grain boundaries. Bottom left: 15-7-02 Porphyroclasts of plagioclase and pyroxene and porhyroblasts of garnet in a matrix of recrystallized grains. Bottom right: 15-8-01 Bands of mafic minerals extend from hornblende porphyroclast. The scalebar in the top left corner indicates a length of 200µm.

The large grains with recrystallized grains along the grain boundaries and at grain intersections, in figure 20: Top right, are an indicator for bulging recrystallization, see figure 12: bottom.

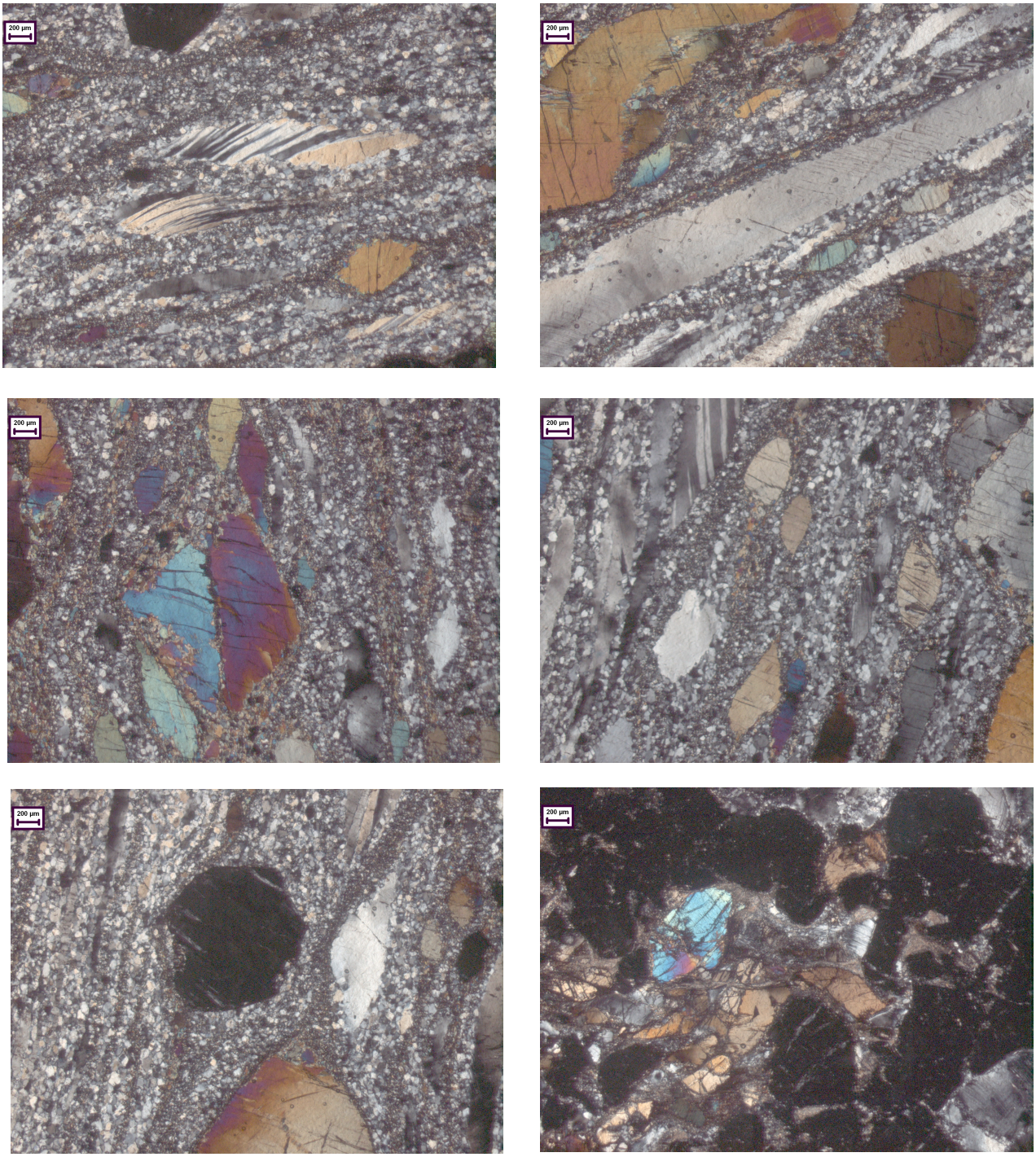

Figure 21: Top left: 15-8-02 Elongated plagioclase grains with twins, hornblende grain is less elongated. Top right: 15-8-04b Very elongated plagioclase grains, pyroxene and hornblende grains are much less elongated. Middle left: 15-8-06 Partly recrystallized pyroxene in matrix of banded recrystallized grains. Middle right: 15-8-08 Recrystallized plagioclase grains in monophase layers are larger than recrystallized plagioclase grains in multiphase layers. Bottom left: 15-8-11 Undeformed garnet. Bands of recrystallized mafic grains extends from pyroxene porphyroclast. Bottom right: 15-1-01 Mafic part of the rock, which contains a large amount of garnet. The scale bar in the top left corner indicates a length of 200µm.

The large plagioclase grains, in figure 20: Bottom right, and figure 21: Top left to bottom left, are much more elongated than the large pyroxene grains in the same figures, indicating that pyroxene is stronger than plagioclase, while garnet grains in these figures are rather undeformed, this means that garnet is the strongest mineral. Garnet porphyroblasts can be very abundant in some parts of the rocks, see figure 21: Bottom right. Some large plagioclase grains, figure 21: Top left, show twins with tapering edges, these are deformation twins, see figure 11b. These deformation twins can be used as indicators for the metamorphic grade of deformation. In figure 20: Top left, and bottom right, and figure 21: Top left to bottom left, bands of very small recrystallized hornblende are found, these bands extend as tails from pyroxene porphyroclasts, see figure 20: Bottom right, and figure 21: Bottom left.

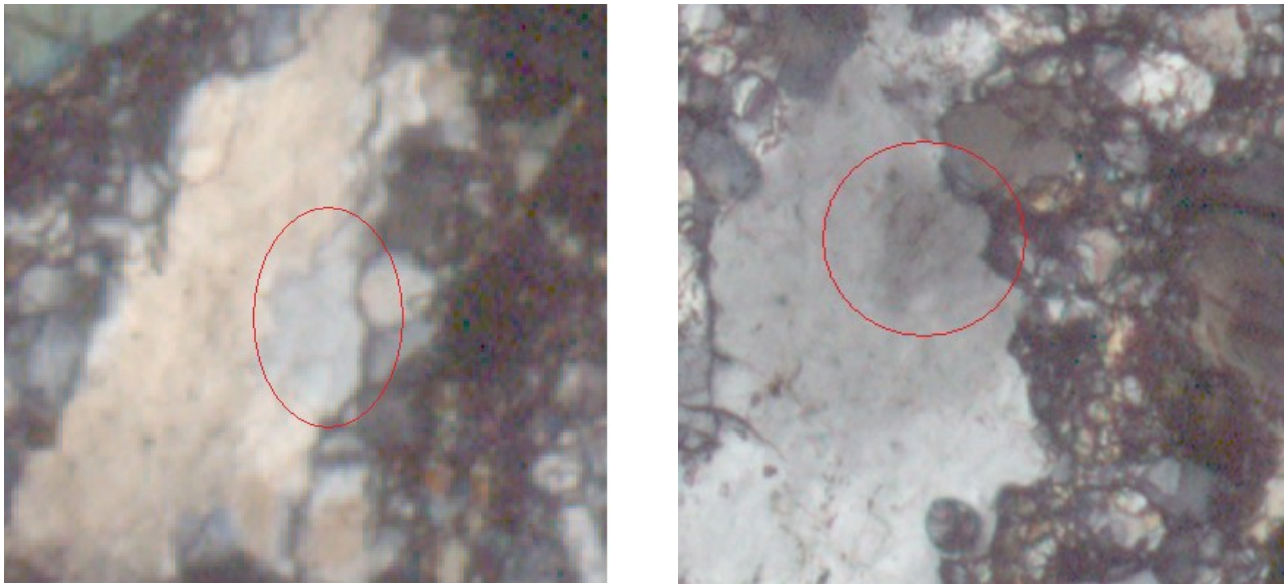

Figure 22: Left: Zoom in of sample 15-8-12, subgrain in plagioclase is shown in red ellipsoid. Right: Zoom in of sample 15-8-09b, subgrain in plagioclase is shown in red ellipsoid.

In figure 22: Left and right, zoom in of samples 15-8-12 and 15-8-09b are given, which show that subgrains are present in the large plagioclase grains, from this it is inferred that subgrain rotation recrystallization is also active on these samples, besides bulging recrystallization, which indicates higher metamorphic grade conditions.

Tafjord

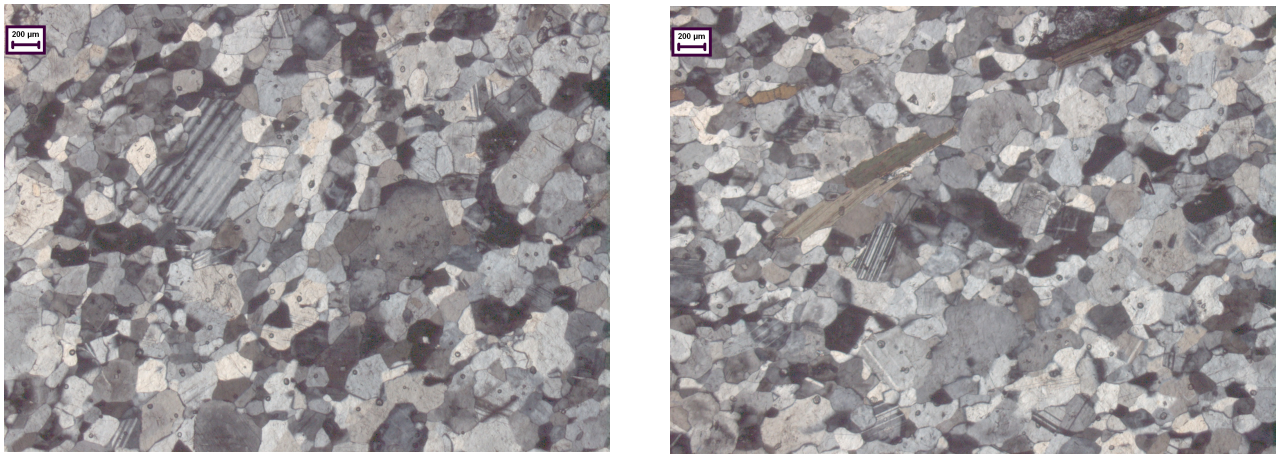

Figure 23: Left: 13-4-01 Variable grain size for plagioclase grains. Large plagioclase grain with twinning. Right: 13-4-02 Grain boundaries are interlobate. Biotite grains are elongated. The scale bar in the top left corner indicates a length of 200µm.

The samples from Tafjord differ from those from Sognefjord, the mafic mineral content is much lower, there are no large older grains present, the recrystallized grains are larger on average, have a larger grain size distribution, and have irregular grain shapes with interlobate grain boundaries, see figure 23: Left and right. Some growth twins can be found, see figure 11a.

Compositions

Two different compositions can be found in the samples from Sognefjord, the first consists of plagioclase, pyroxene, garnet, and some hornblende, the second has a mineral assemblage of plagioclase, hornblende, and some pyroxene, see table 4. In most of the samples plagioclase makes up 65-80% of the mineral assemblage, some zones are very plagioclase rich, see figure 20: Top right, others are mostly composed of pyroxene and garnet, see figure 21: Bottom right. The first composition matches the granulite facies assemblage mentioned by Kruse and Stünitz (1999), while the second composition matches the amphibolite facies assemblage mentioned in the same paper.

Mineral assemblage	**Plagioclase**	**Pyroxene**	**Hornblende**	**Garnet**
Granulite facies	65-80%	15-20%	5-10%	5-10%
Amphibolite facies	70-80%	10-15%	15-20%	0%

Table 4: Mineral assemblages obtained from thin sections of samples from Sognefjord.

If the mineral assemblage contains more plagioclase, than hornblende is often the second most abundant mineral, while if the sample contains only relatively low amounts of plagioclase, than pyroxene is often the second most abundant mineral in the mineral assemblage, and garnet is present here also.

The samples from Tafjord all have the same composition of a proper anorthosite, with 90-95% plagioclase. The other minerals that are present are hornblende and biotite, see table 5. Pyroxene and garnet do not occur in these samples. This is a geenschist facies mineral assemblage.

Mineral assemblage	**Plagioclase**	**Hornblende**	**Biotite**
Greenschist facies	90-95%	2-4%	3-8%

Table 5: Mineral assemblages obtained from thin sections of samples from Tafjord.

4.3 Grain size analysis

First figures containing digital versions of photographs of the thin sections, including layers which contain the drawn grain boundaries, and binaries of these layers, that were used in ImageJ, will be presented. See also figure 14. Later the results from the calculations performed on these grain boundaries will be given, which include grain sizes, grain shapes, grain orientations, and plots of these results. As well as diagrams of the distribution of the grain sizes and grain orientations.

Sognefjord

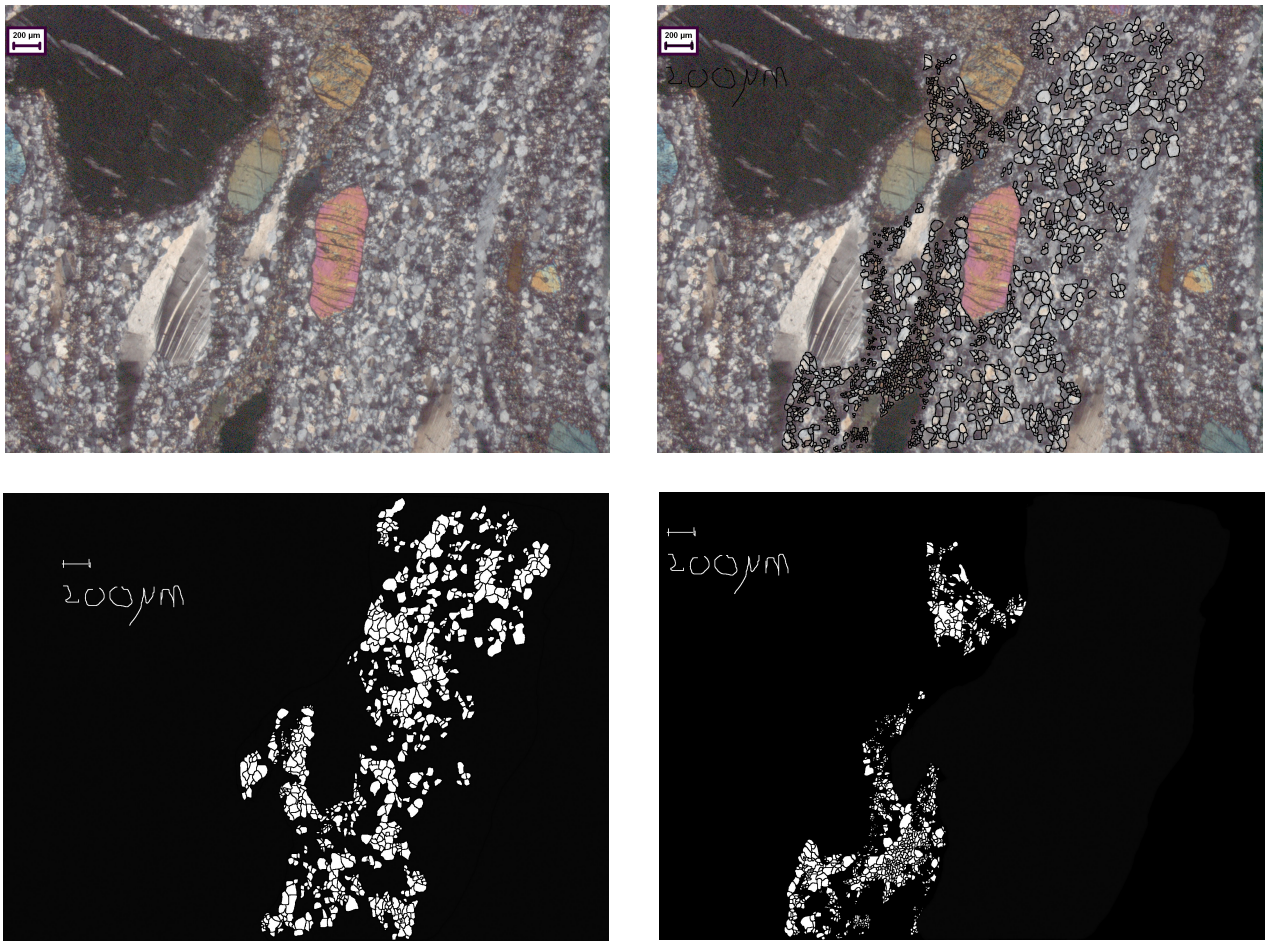

Figure 24: Top left: Digitised photograph of thin section 15-8-12. Top right: Digitised photograph with grain boundaries in a new layer. Bottom left: Binary of layer with grain boundaries for monophase layer of plagioclase. Bottom right: Binary of layer with grain boundaries for multiphase layer, containing plagioclase, and hornblende or pyroxene. The scale bar in the top left corner indicates a length of 200µm.

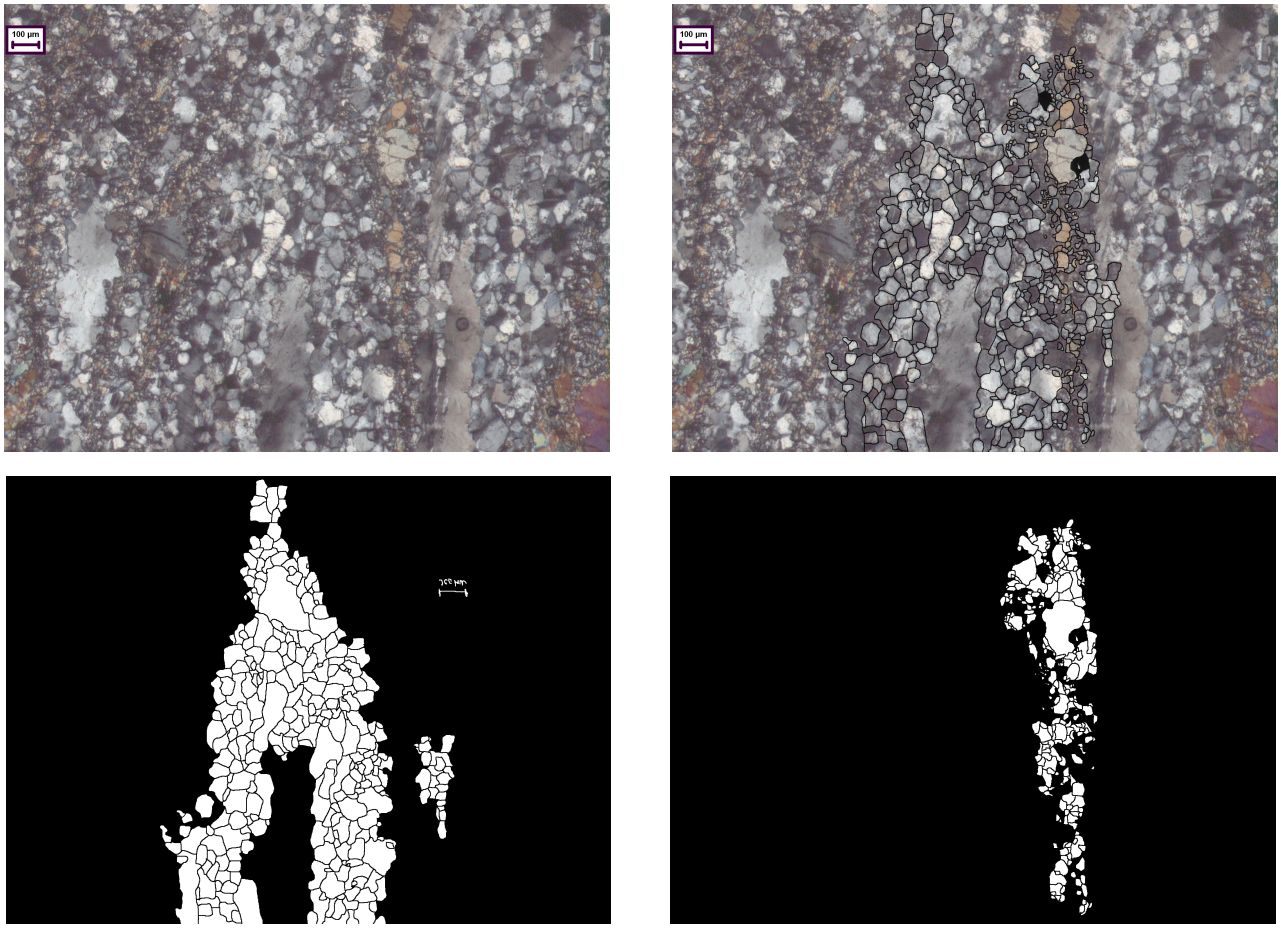

Figure 25: Top left: Digitised photograph of thin section 15-8-09b. Top right: Digitised photograph with grain boundaries in a new layer, with the monophase plagioclase grains being filled. Bottom left: Binary of layer with grain boundaries for monophase layer of plagioclase. Bottom right: Binary of layer with grain boundaries for multiphase layer, containing plagioclase, and hornblende or pyroxene. The scale bar in the top left corner indicates a length of 100µm.

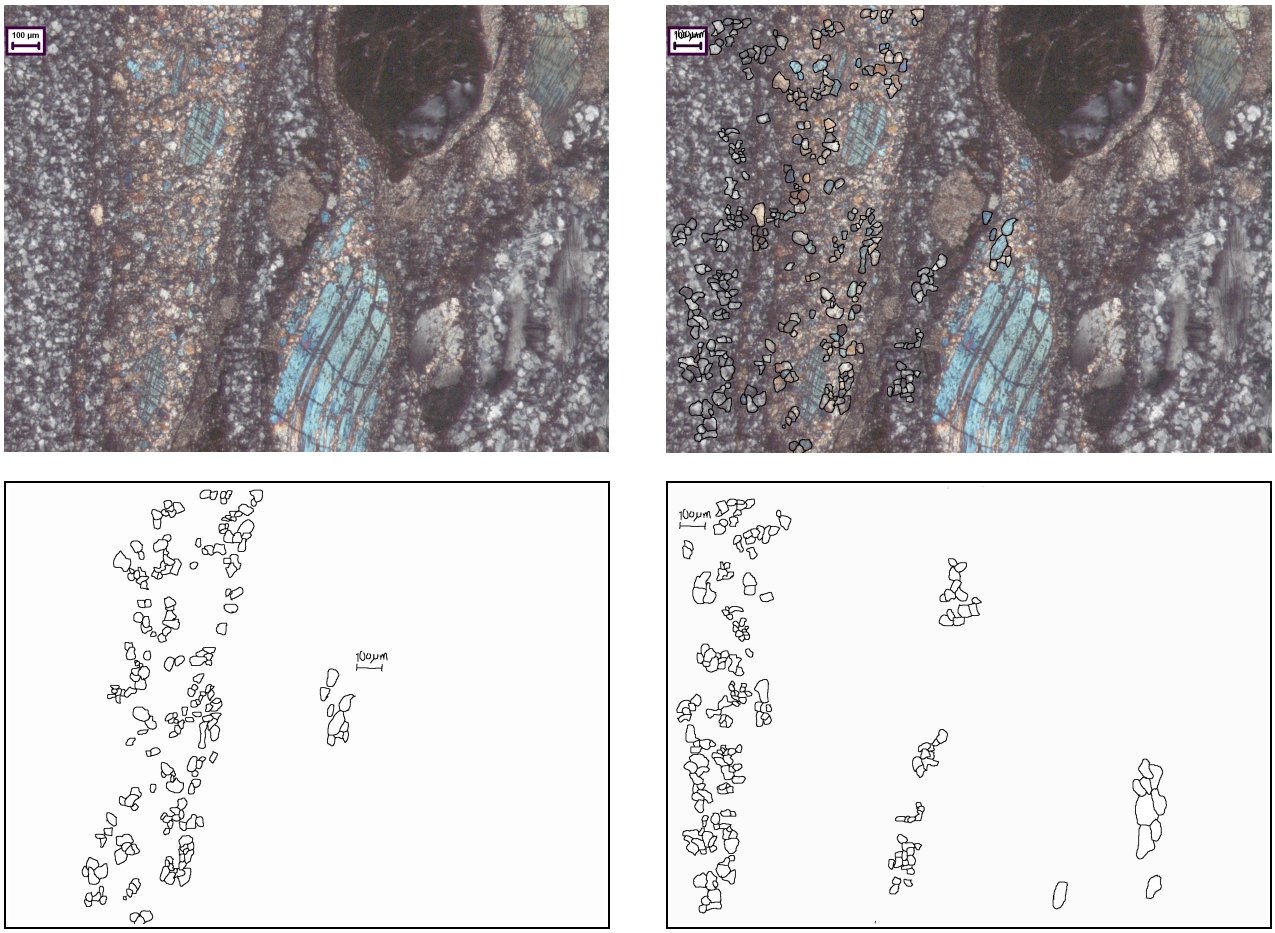

Figure 26: Top left: Digitised photograph of thin section 15-1-02b. Top right: Digitised photograph with grain boundaries in a new layer. Bottom left: Binary of layer with grain boundaries for monophase layer of plagioclase. Bottom right: Binary of layer with grain boundaries for multiphase layer, containing plagioclase, and hornblende or pyroxene. The scale bar in the top left corner indicates a length of 100µm.

The samples from Sognefjord contain a relatively large amount of mafic minerals, as can be seen in the photographs of the thin section, therefore the grain size analysis is divided into two parts. The first measures the grain size in the monophase areas of the thinsection, the second measures the grain size in the multiphase areas of the thin sections.

Sample	Monophase		Multiphase	
	Grain size (µm)	Grain shape	Grain size (µm)	Grain shape
15-1-02b	32,93	1,54	30,41	1,29
15-8-05	48,06	1,39	40,81	1,36
15-8-09b	46,75	1,53	25,71	1,42
15-8-12	41,02	1,33	22,51	1,36

Table 6: Grain size and grain shape for monophase and multiphase layers in samples from Sognefjord. The grain size presented here is the average recrystallized grain size. The grain shape presented is the average grain shape, which is obtained by dividing the major axis of the grains by the minor axis of the grains.

In the table above only averages are presented, complete results for the samples from Sognefjord are given in appendix 6a-9b. Not all plots of major axis versus minor axis, grain shape versus grain size, grain orientation versus grain shape, and grain orientation versus grain size are presented below. The plots for the monophase bands in samples from Sognefjord show the same correlation, therefore one sample was chosen to represented these bands. The plots for the other sample can be found in appendix 6a, 7a, and 8a. The plots for the multiphase bands in samples from Sognefjord also show the same correlation, here too one sample was chosen to represented these bands. The plots for the other sample can be found in appendix 6b, 7b, and 8b.

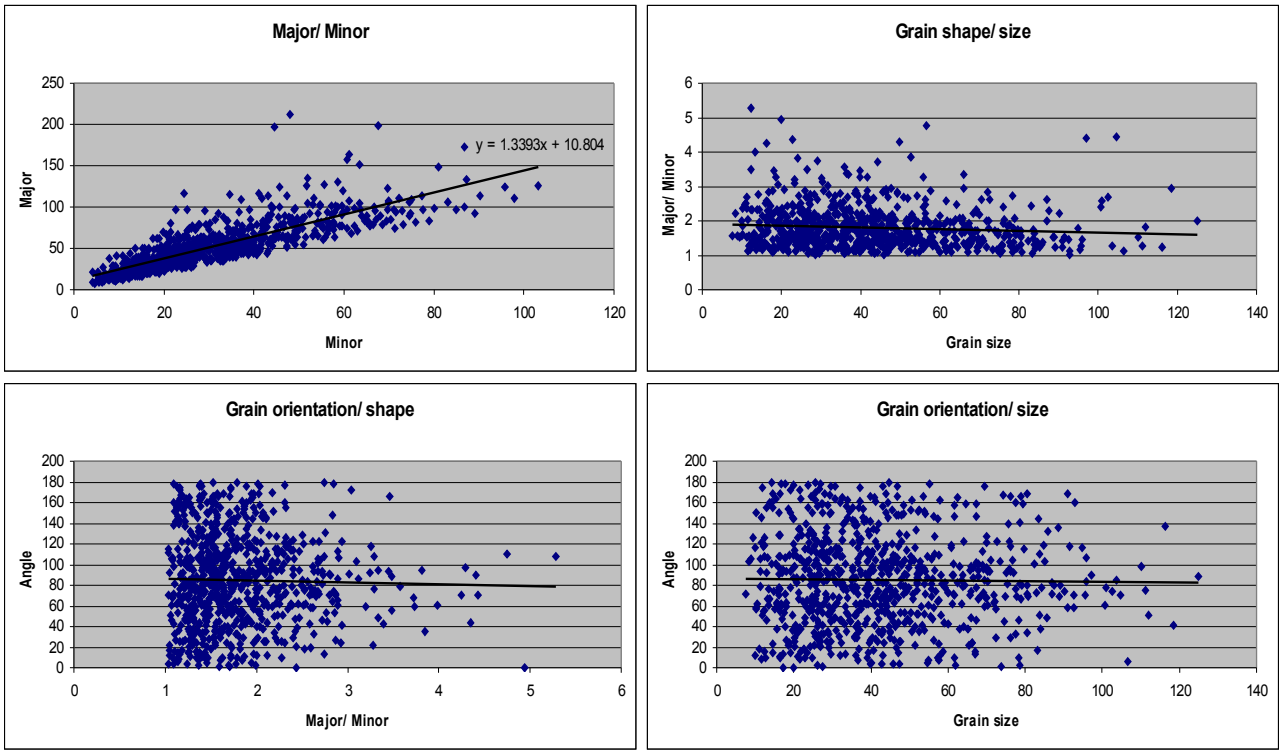

Figure 27: Sample 15-8-12, monophase bands in Sognefjord. Top left: Grain shape, major axis versus minor axis. Top right: Grain shape versus grain size. Bottom right: Grain orientation, angle with north, versus grain shape. Bottom right: Grain orientation versus, grain size.

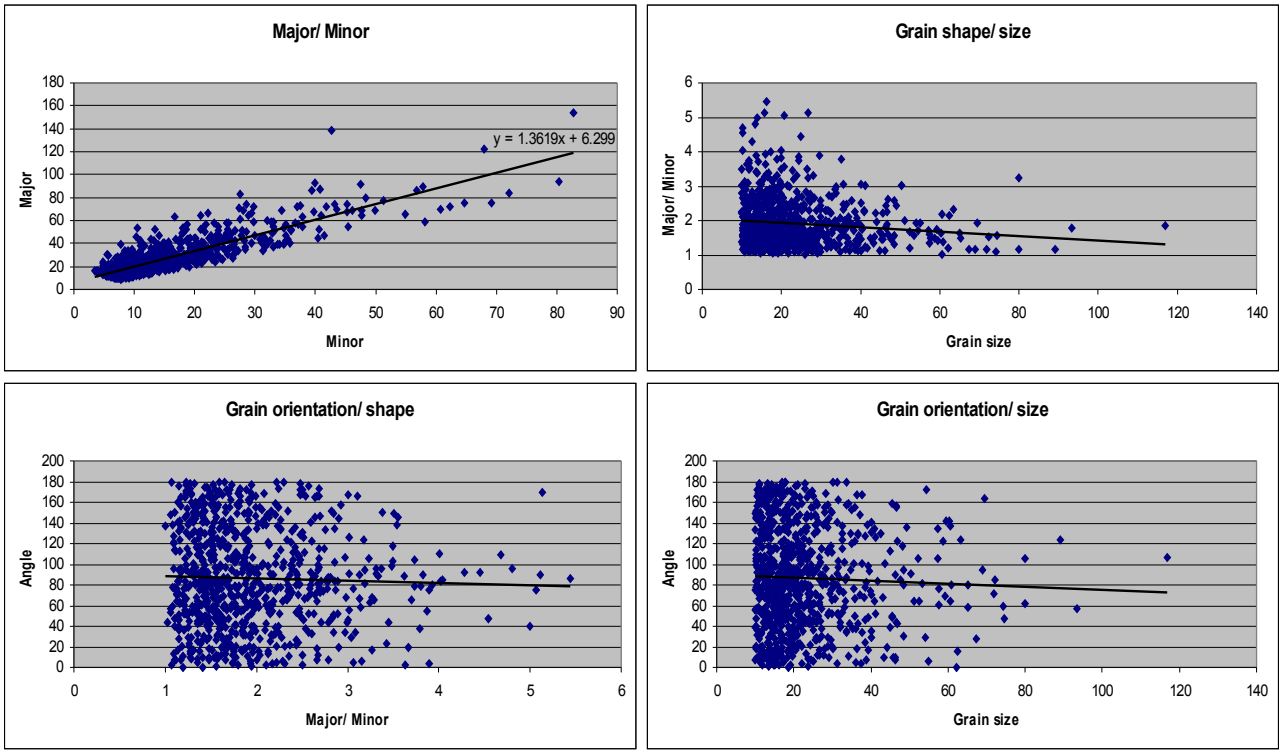

Figure 28: Sample 15-8-12, multiphase bands in Sognefjord. Top left: Grain shape, major axis versus minor axis. Top right: Grain shape versus grain size. Bottom right: Grain orientation, angle with north, versus grain shape. Bottom right: Grain orientation versus, grain size.

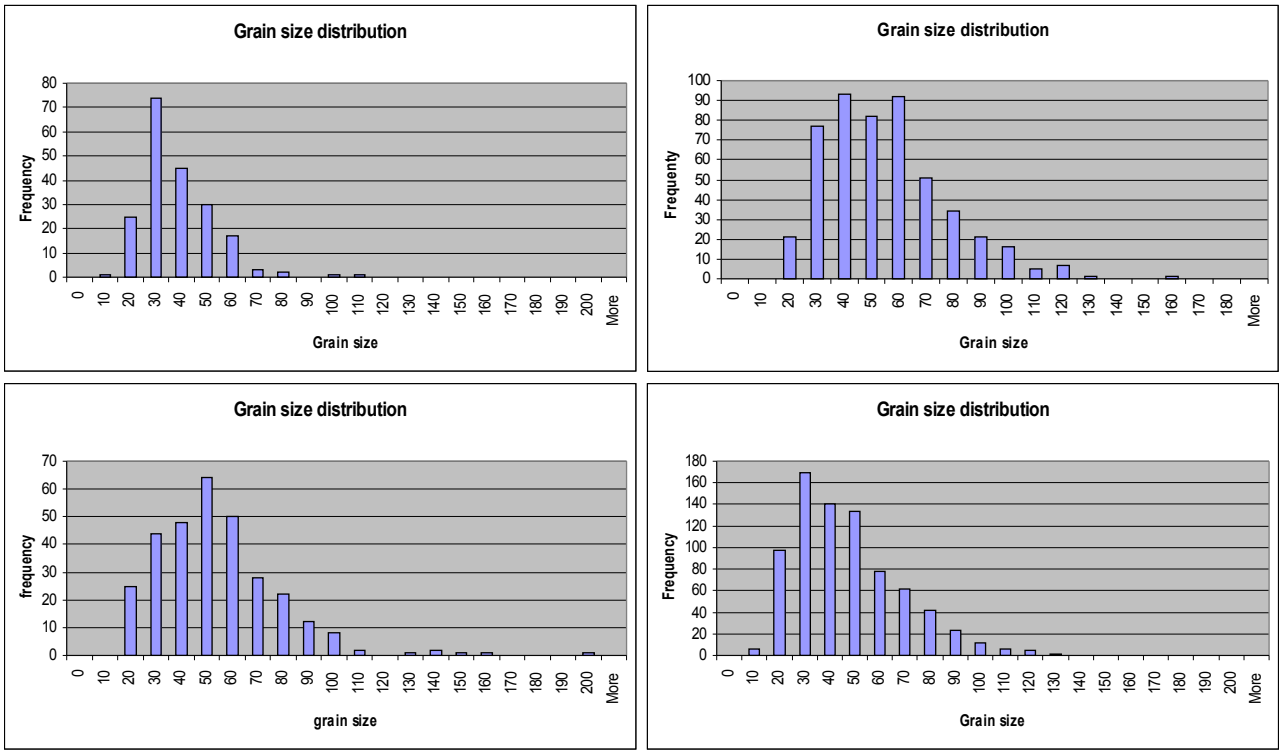

Figure 29: Diagram of grain size distribution for monophase bands in Sognefjord. Top left: Sample 15-1-02b. Top right: Sample 15-8-05. Bottom right: Sample 15-8-09b. Bottom right: Sample 15-8-12.

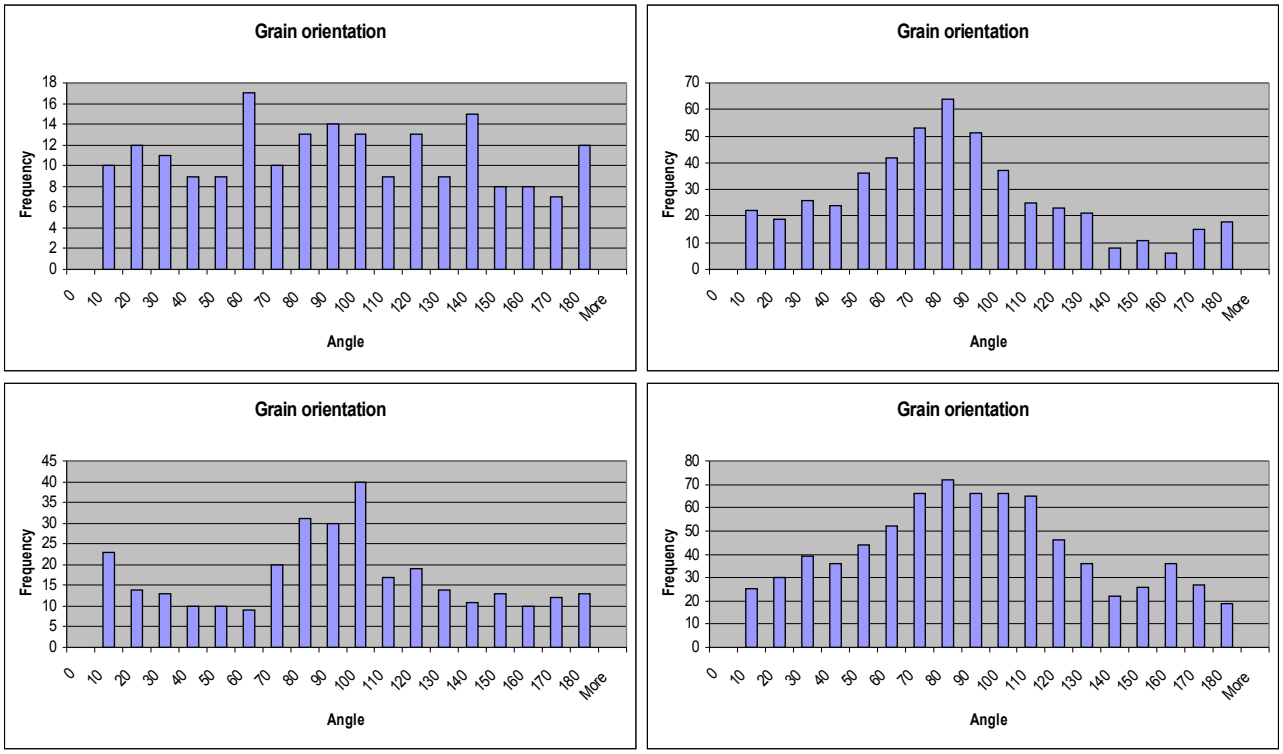

Figure 30: Diagram of grain orientation for monophase bands in Sognefjord. The angle along the x-axis is the angle to the north. Top left: Sample 15-1-02b. Top right: Sample 15-8-05. Bottom right: Sample 15-8-09b. Bottom right: Sample 15-8-12.

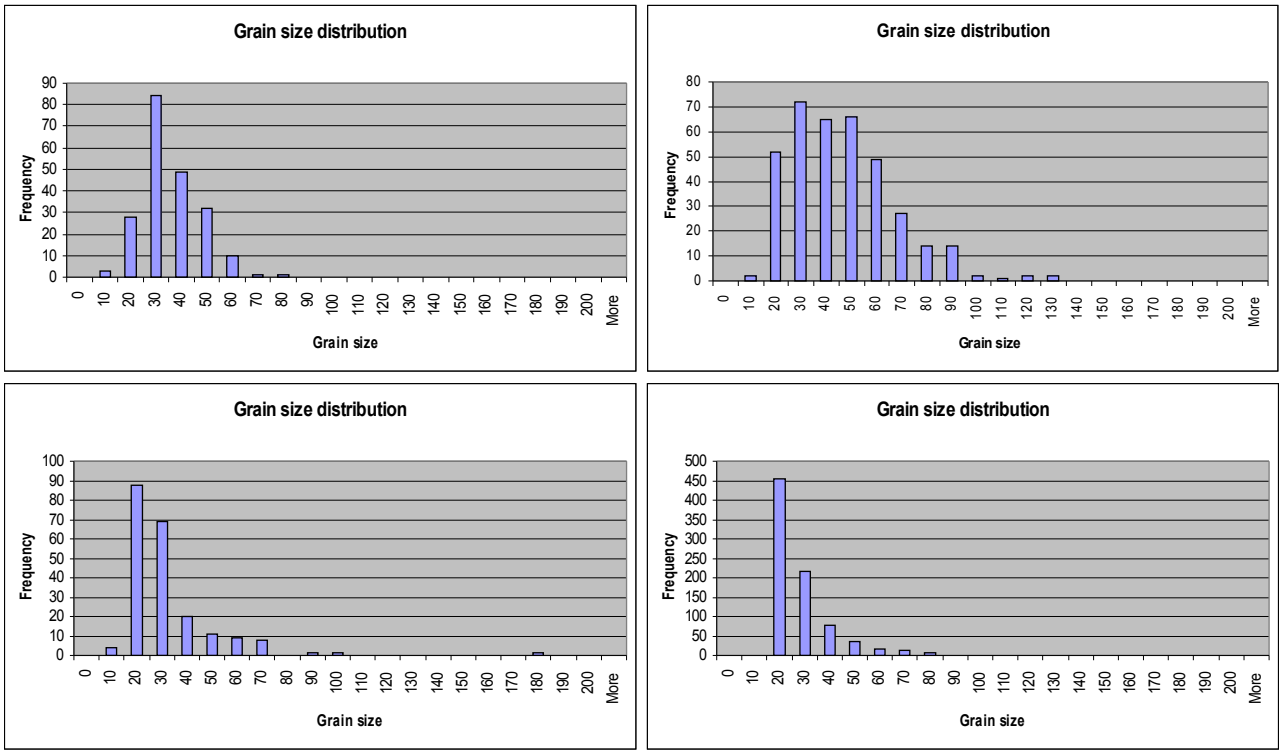

Figure 31: Diagram of grain size distribution for multiphase bands in Sognefjord. Top left: Sample 15-1-02b. Top right: Sample 15-8-05. Bottom right: Sample 15-8-09b. Bottom right: Sample 15-8-12.

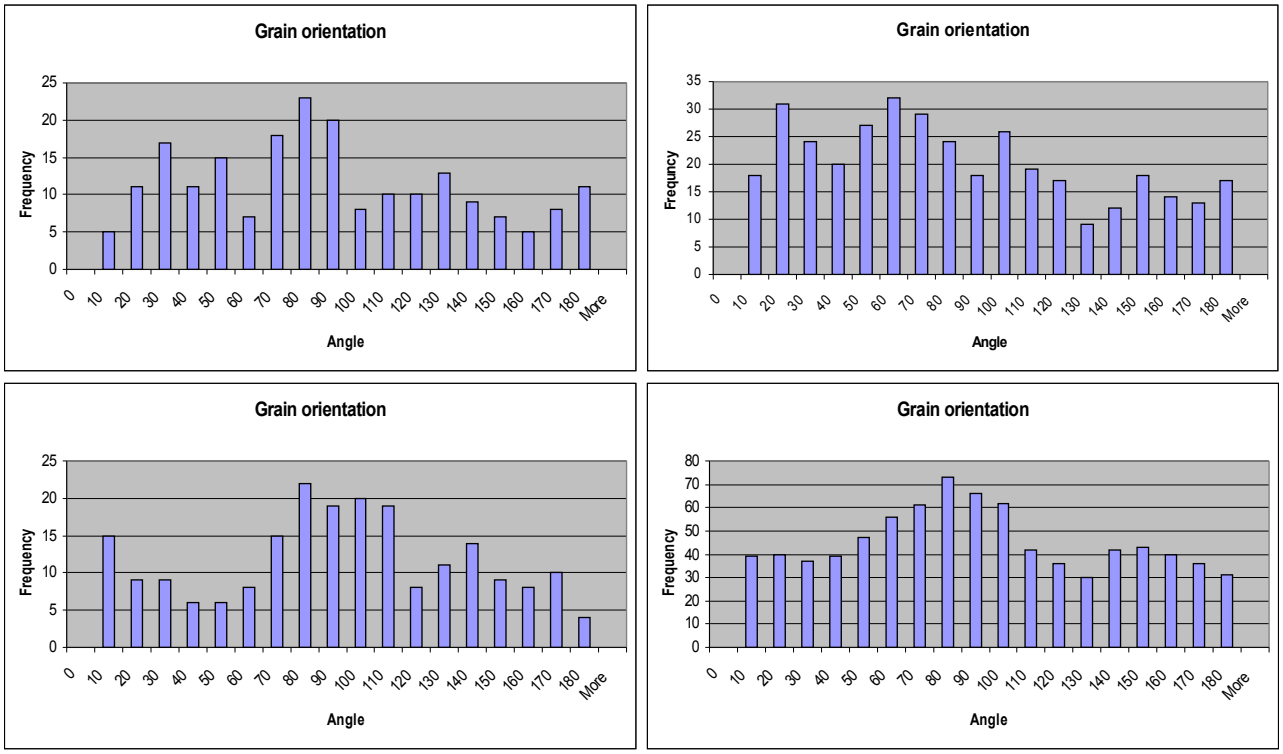

Figure 32: Diagram of grain orientation for multiphase bands in Sognefjord. The angle along the x-axis is the angle to the north. Top left: Sample 15-1-02b. Top right: Sample 15-8-05. Bottom right: Sample 15-8-09b. Bottom right: Sample 15-8-12.

Tafjord

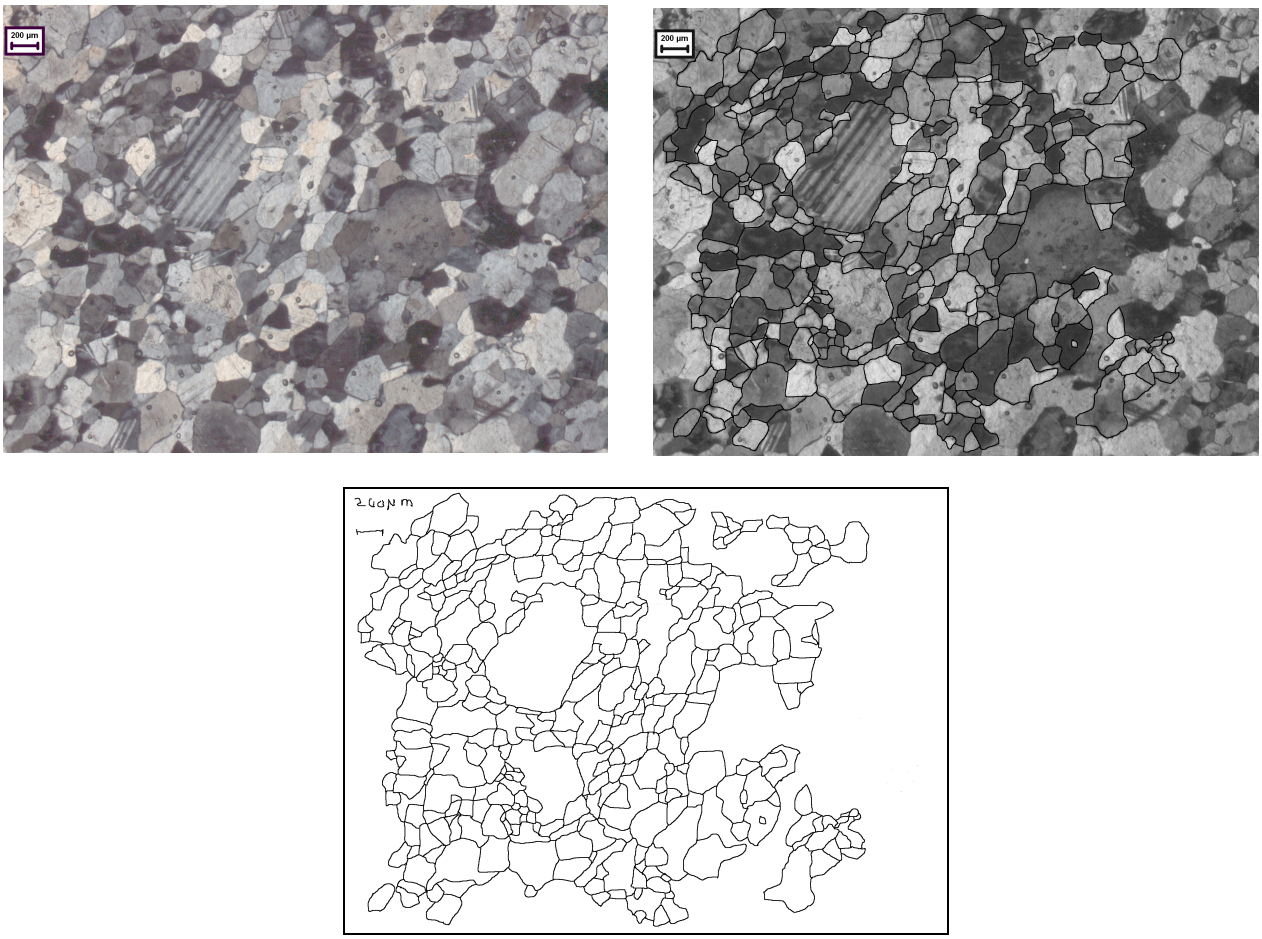

Figure 33: Top left: Digitised photograph of thin section 13-4-01. Top right: Digitised photograph with grain boundaries in a new layer. Bottom: Binary of layer with grain boundaries. The scale bar in the top left corner indicates a length of 200µm.

The samples from Tafjord contain little mafic minerals, as can be seen from the photographs of the thin sections, therefore only a monophase grain size analysis is done for these samples.

Sample	Grain size (µm)	Grain shape
13-4-01	73,17	1,46
13-4-02	74,73	1,43

Table 7: Grain size and grain shape for samples from Tafjord. The grain size presented here is the average recrystallized grain size. The grain shape presented is the average grain shape, which is obtained by dividing the major axis of the grains by the minor axis of the grains.

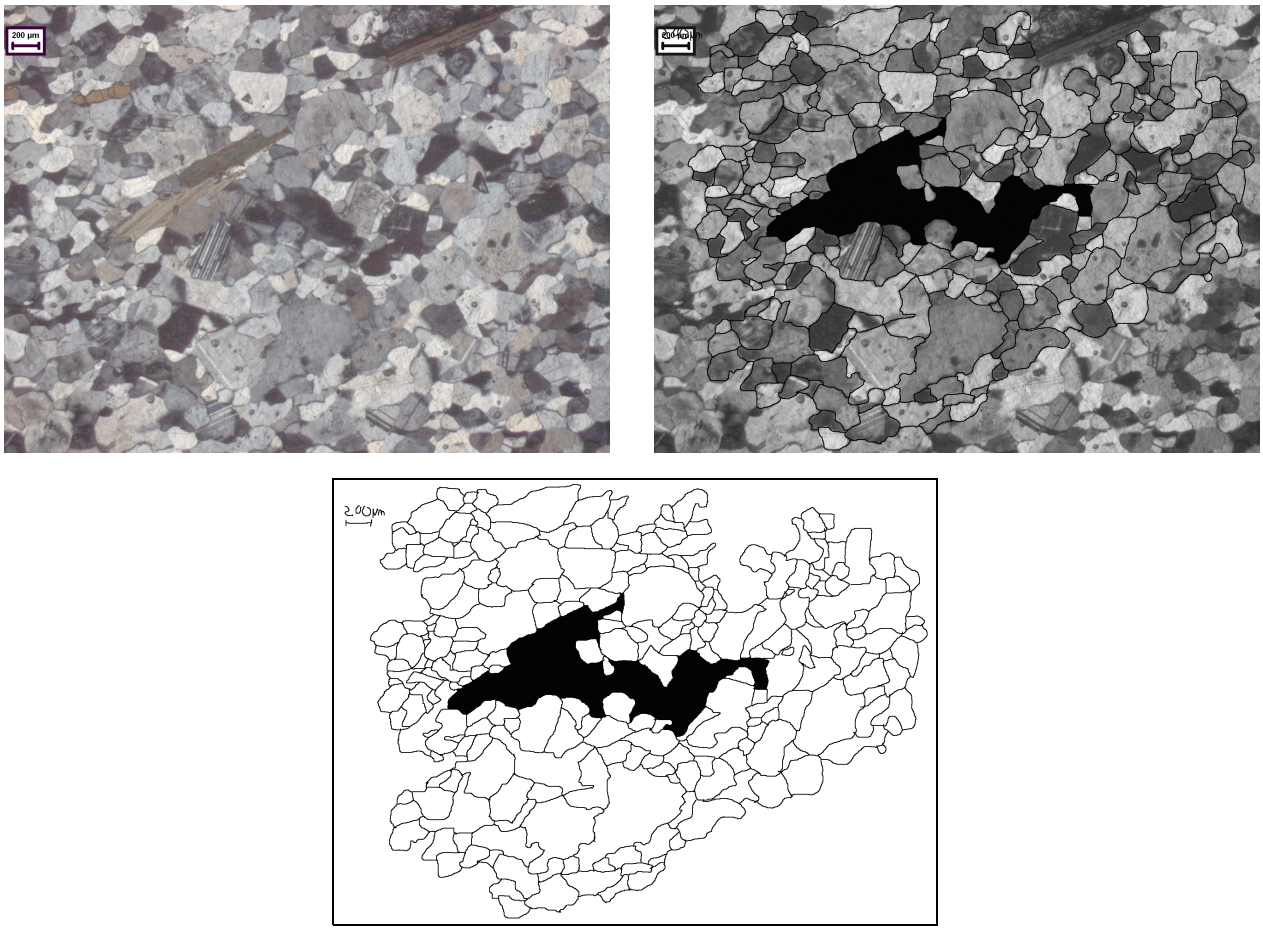

Figure 34: Top left: Digitised photograph of thin section 13-4-02. Top right: Digitised photograph with grain boundaries in a new layer. Bottom: Binary of layer with grain boundaries. The scale bar in the top left corner indicates a length of 200µm.

In the table above only averages are presented, complete results for the samples from Tafjord are given in appendix 10 and 11. Not all plots of major axis versus minor axis, grain shape versus grain size, grain orientation versus grain shape, and grain orientation versus grain size are presented below. The plots for all samples from Tafjord show the same correlation, therefore one sample was chosen to represented this area. The plots for the other sample can be found in appendix 11.

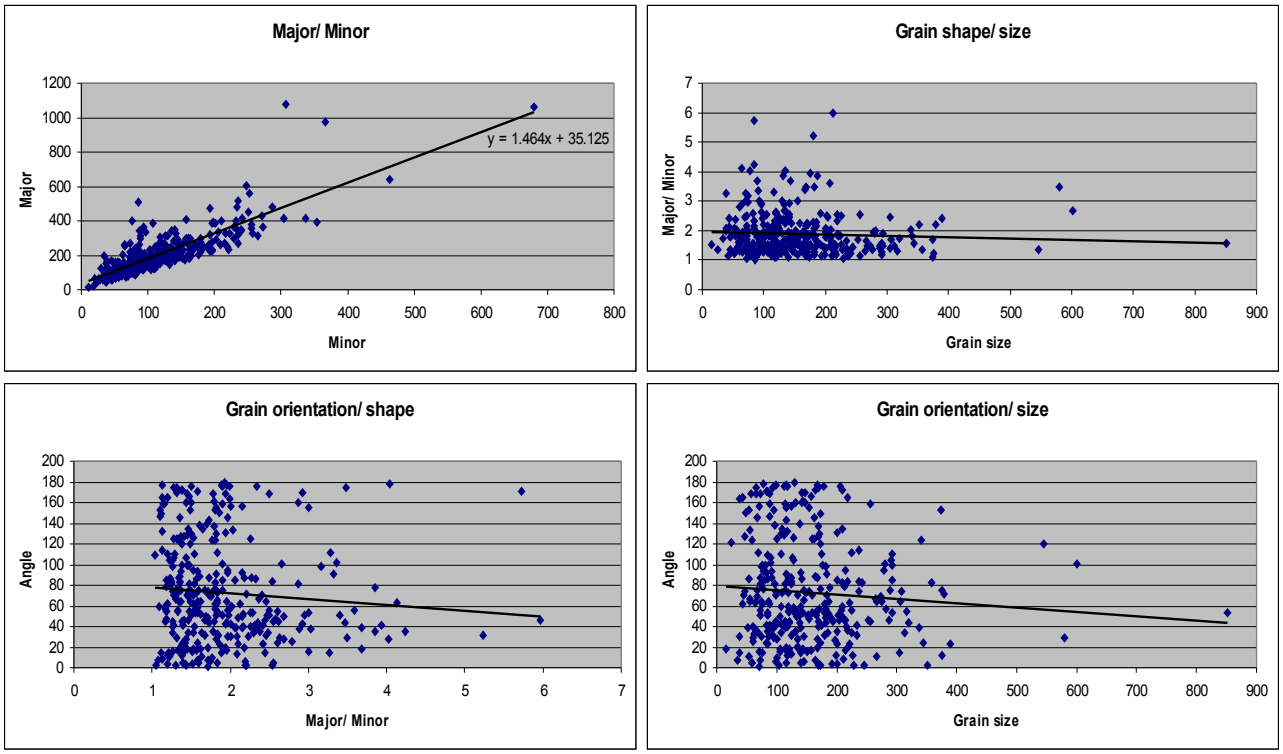

Figure 35: Sample 13-4-01 from Tafjord. Top left: Grain shape, major axis versus minor axis. Top right: Grain shape versus grain size. Bottom right: Grain orientation, angle with north, versus grain shape. Bottom right: Grain orientation versus, grain size.

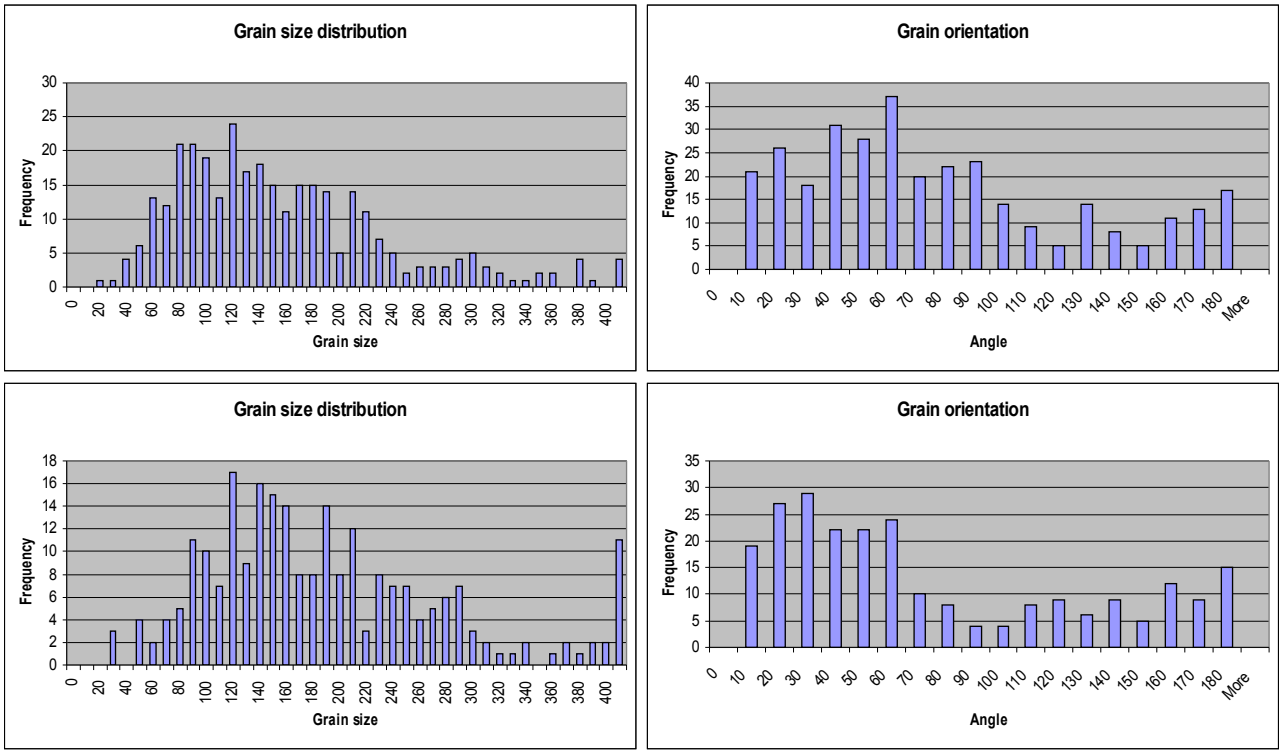

Figure 36: Diagrams of grain size distribution and grain orientation in Tafjord. The angle along the x-axis is the angle to the north. Top left: Diagram of grain size distribution for sample 13-4-01. Top right: Diagram of grain orientation for sample 13-4-01. Bottom right: Diagram of grain size distribution for sample 13-4-02. Bottom right: Diagram of grain orientation for sample 13-4-02.

4.4 Paleopiezometry

In this section plots of shear strain versus recrystallized grain size for the three tested paleopiezometers will be presented. The temperature dependent paleopiezometer of de Bresser et al., is plotted for plagioclase with three different anorthite contents, and for three different temperatures. Deformation mechanism maps will be presented below as well.

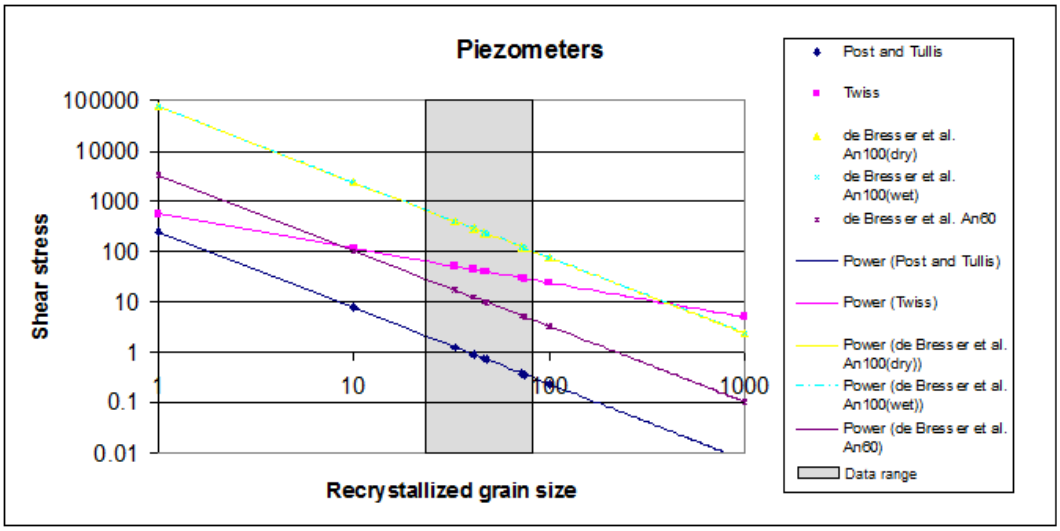

Figure 37: Shear stress versus recrystallized grain size for the three different paleopiezometers, with three different anorthithe contents of plagioclase for the temperature dependent paleopiezometer of de Bresser et al. paleopiezometer, which was plotted for a temperature of 600°C, or 873K.

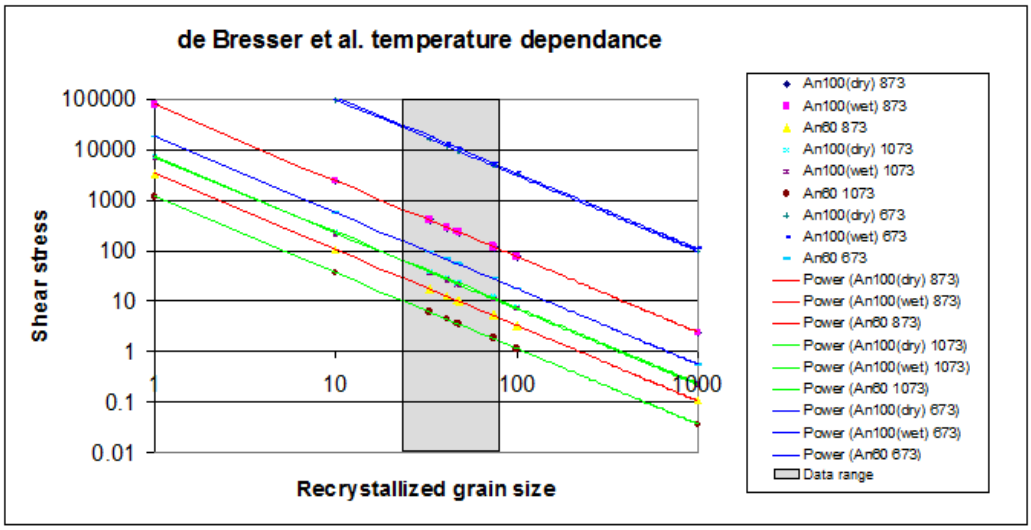

Figure 38: Shear stress versus recrystallized grain size for the temperature dependent paleopiezometer of de Bresser et al. for three different anorthite contents of plagioclase and three different temperatures, of 600°C, or 873K, 900°C, or 1173K, and 500°C, or 773K.

Post and Tullis recrystallized grain size piezometer for feldspar

d (μm)	τ (MPa)	γ An100 (dry)	γ An100 (wet)	γ An60
46,75	0,74	$3{,}06 \cdot 10^{-26}$	$7{,}21 \cdot 10^{-19}$	$9{,}95 \cdot 10^{-16}$
48,06	0,71	$2{,}70 \cdot 10^{-26}$	$6{,}36 \cdot 10^{-19}$	$8{,}78 \cdot 10^{-16}$
41,02	0,90	$5{,}55 \cdot 10^{-26}$	$1{,}31 \cdot 10^{-18}$	$1{,}80 \cdot 10^{-15}$
32,93	1,26	$1{,}51 \cdot 10^{-25}$	$3{,}54 \cdot 10^{-18}$	$4{,}89 \cdot 10^{-15}$
73,17	0,37	$4{,}00 \cdot 10^{-27}$	$9{,}41 \cdot 10^{-20}$	$1{,}30 \cdot 10^{-16}$
74,73	0,36	$3{,}63 \cdot 10^{-27}$	$8{,}55 \cdot 10^{-20}$	$1{,}18 \cdot 10^{-16}$
20	2,67	$1{,}45 \cdot 10^{-24}$	$3{,}42 \cdot 10^{-17}$	$4{,}72 \cdot 10^{-14}$

Table 8: Results for the Post and Tullis recrystallized grain size piezometer for feldspar, with d is the recrystallized grain size for monophase plagioclase, τ is the shear stress and γ is the shear strain for the different anorthite compositions and water contents of plagioclase. A grain size of 20 μm is added, because this is the smallest measured grain size of plagioclase in the monophase layers, therefore it will give the maximum shear stress.

Twiss theoretical paleopiezometer

d (μm)	τ (MPa)	γ An100 (dry)	γ An100 (wet)	γ An60
46,75	39,97	$4{,}85 \cdot 10^{-21}$	$1{,}14 \cdot 10^{-13}$	$1{,}58 \cdot 10^{-10}$
48,06	39,23	$4{,}59 \cdot 10^{-21}$	$1{,}08 \cdot 10^{-13}$	$1{,}49 \cdot 10^{-10}$
41,02	43,69	$6{,}34 \cdot 10^{-21}$	$1{,}49 \cdot 10^{-13}$	$2{,}06 \cdot 10^{-10}$
32,93	50,73	$9{,}92 \cdot 10^{-21}$	$2{,}34 \cdot 10^{-13}$	$3{,}23 \cdot 10^{-10}$
73,17	29,48	$1{,}95 \cdot 10^{-21}$	$4{,}58 \cdot 10^{-14}$	$6{,}33 \cdot 10^{-11}$
74,73	29,06	$1{,}86 \cdot 10^{-21}$	$4{,}39 \cdot 10^{-14}$	$6{,}06 \cdot 10^{-11}$
20	71,21	$2{,}74 \cdot 10^{-20}$	$6{,}46 \cdot 10^{-13}$	$8{,}92 \cdot 10^{-10}$

Table 9: Results for the Twiss theoretical paleopiezometer, with d is the recrystallized grain size for monophase plagioclase, τ is the shear stress and γ is the shear strain for the different anorthite compositions and water contents of plagioclase. A grain size of 20 μm is added, because this is the smallest measured grain size of plagioclase in the monophase layers, therefore it will give the maximum shear stress.

De Bresser et al. temperature dependent paleopiezometer

d (μm)	τ (MPa) An100 (dry)	γ An100 (dry)	τ (MPa) An100 (wet)	γ An100 (wet)	τ (MPa) An60	γ An60
46,75	235,43	$9,92 \cdot 10^{-19}$	235,21	$2,33 \cdot 10^{-11}$	10,23	$2,65 \cdot 10^{-12}$
48,06	225,91	$8,76 \cdot 10^{-19}$	225,69	$2,06 \cdot 10^{-11}$	9,82	$2,34 \cdot 10^{-12}$
41,02	286,51	$1,79 \cdot 10^{-18}$	286,24	$4,20 \cdot 10^{-11}$	12,45	$4,77 \cdot 10^{-12}$
32,93	398,27	$4,80 \cdot 10^{-18}$	397,89	$1,13 \cdot 10^{-10}$	17,31	$1,28 \cdot 10^{-11}$
73,17	120,25	$1,32 \cdot 10^{-19}$	120,13	$3,10 \cdot 10^{-12}$	5,23	$3,53 \cdot 10^{-13}$
74,73	116,50	$1,20 \cdot 10^{-19}$	116,39	$2,82 \cdot 10^{-12}$	5,06	$3,21 \cdot 10^{-13}$
20	841,44	$4,53 \cdot 10^{-17}$	840,64	$1,06 \cdot 10^{-9}$	36,57	$1,21 \cdot 10^{-10}$

Table 10: Results for the de Bresser et al. temperature dependent paleopiezometer, with d is the recrystallized grain size for monophase plagioclase, τ is the shear stress and γ is the shear strain for the different anorthite compositions and water contents of plagioclase, for a temperature of 600°C. A grain size of 20 μm is added, because this is the smallest measured grain size of plagioclase in the monophase layers, therefore it will give the maximum shear stress.

d (μm)	τ (MPa) An100 (dry)	γ An100 (dry)	τ (MPa) An100 (wet)	γ An100 (wet)	τ (MPa) An60	γ An60
46,75	9,70	$5,73 \cdot 10^{-13}$	8,88	$3,51 \cdot 10^{-10}$	2,41	$1,37 \cdot 10^{-10}$
48,06	9,31	$5,06 \cdot 10^{-13}$	8,52	$3,10 \cdot 10^{-10}$	2,32	$1,21 \cdot 10^{-10}$
41,02	11,81	$1,03 \cdot 10^{-12}$	10,80	$6,33 \cdot 10^{-10}$	2,94	$2,47 \cdot 10^{-10}$
32,93	16,41	$2,77 \cdot 10^{-12}$	15,02	$1,70 \cdot 10^{-9}$	4,08	$6,63 \cdot 10^{-10}$
73,17	4,96	$7,63 \cdot 10^{-14}$	4,53	$4,68 \cdot 10^{-11}$	1,23	$1,83 \cdot 10^{-11}$
74,73	4,80	$6,94 \cdot 10^{-14}$	4,39	$4,25 \cdot 10^{-11}$	1,19	$1,66 \cdot 10^{-11}$
20	34,68	$2,61 \cdot 10^{-11}$	31,73	$1,60 \cdot 10^{-8}$	8,62	$6,26 \cdot 10^{-9}$

Table 11: Results for the de Bresser et al. temperature dependent paleopiezometer, with d is the recrystallized grain size for monophase plagioclase, τ is the shear stress and γ is the shear strain for the different anorthite compositions and water contents of plagioclase, for a temperature of 900°C. A grain size of 20 μm is added, because this is the smallest measured grain size of plagioclase in the monophase layers, therefore it will give the maximum shear stress.

d (μm)	τ (MPa) An100 (dry)	γ An100 (dry)	τ (MPa) An100 (wet)	γ An100 (wet)	τ (MPa) An60	γ An60
46,75	1181,39	$1{,}21 \cdot 10^{-21}$	1234,05	$5{,}90 \cdot 10^{-12}$	21,25	$3{,}60 \cdot 10^{-13}$
48,06	1133,61	$1{,}07 \cdot 10^{-21}$	1184,14	$5{,}22 \cdot 10^{-12}$	20,39	$3{,}18 \cdot 10^{-13}$
41,02	1437,71	$2{,}18 \cdot 10^{-21}$	1501,80	$1{,}06 \cdot 10^{-11}$	25,86	$6{,}48 \cdot 10^{-13}$
32,93	1998,53	$5{,}85 \cdot 10^{-21}$	2087,62	$2{,}86 \cdot 10^{-11}$	35,95	$1{,}74 \cdot 10^{-12}$
73,17	603,41	$1{,}61 \cdot 10^{-22}$	630,31	$7{,}87 \cdot 10^{-13}$	10,85	$4{,}79 \cdot 10^{-14}$
74,73	584,60	$1{,}46 \cdot 10^{-22}$	610,67	$7{,}15 \cdot 10^{-13}$	10,52	$4{,}36 \cdot 10^{-14}$
20	4222,36	$5{,}51 \cdot 10^{-20}$	4410,58	$1{,}56 \cdot 10^{-10}$	75,95	$1{,}64 \cdot 10^{-11}$

Table 12: Results for the de Bresser et al. temperature dependent paleopiezometer, with d is the recrystallized grain size for monophase plagioclase, τ is the shear stress and γ is the shear strain for the different anorthite compositions and water contents of plagioclase, for a temperature of 500°C. A grain size of 20 μm is added, because this is the smallest measured grain size, of plagioclase in the monophase layers therefore it will give the maximum shear stress.

All calculations can be found in appendices 12 and 13.

Deformation mechanism maps

The deformation mechanism maps presented here are based on the temperature dependent paleopiezometer of de Bresser et al., because the result from this piezometer fitted best with the calculations. Deformation mechanism maps were made for plagioclase with three different anorthite contents, An100 with 0,004 weight percent water = An100 (dry), An100 with 0,07 weight percent water = An100 (wet), and An60 with 0,3 weight percent water. The temperature dependent paleopiezometer of de Bresser et al. is based on the field boundary model, which suggests that, for materials in which grain size reduction is sufficiently effective, dynamic recrystallization should lead to a steady state balance between grain size reduction and grain growth processes set up in the boundary region between the dislocation, grain size insensitive (GSI), and diffusion, grain size sensitive (GSS), creep field, therefore the results from the paleopiezometer are positioned on this boundary also.

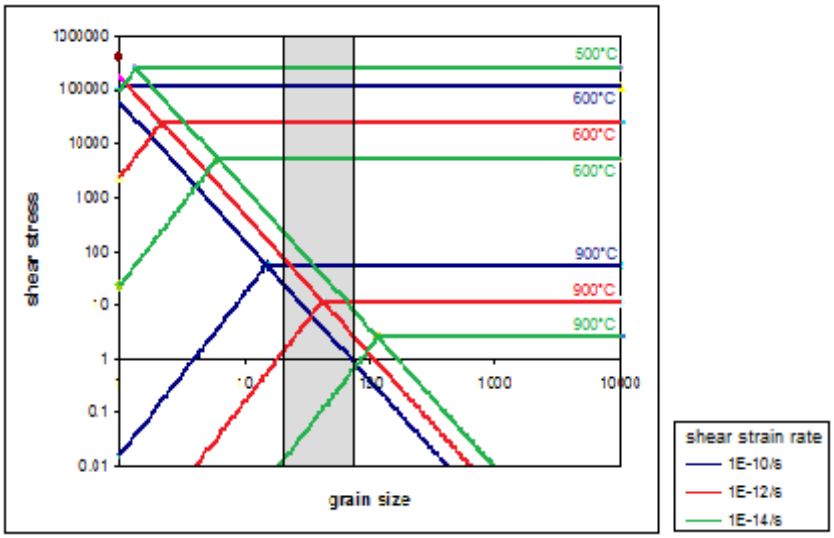

Figure 39: Deformation mechanism map for An100 (dry). The grain size is the recrystallized grain size for plagioclase.

The marked section indicates the recrystallized grain sizes obtained in this study. We assume that all samples plot close to the boundary between GSI and GSS creep. Deformation just above 900°C at a strain rate of $1 \cdot 10^{-10}$ fall within this section, and deformation at a temperature of around 900°C and at a strain rate of $1 \cdot 10^{-12}$ and at a temperature of approximately 800°C and a strain rate of $1 \cdot 10^{-14}$.

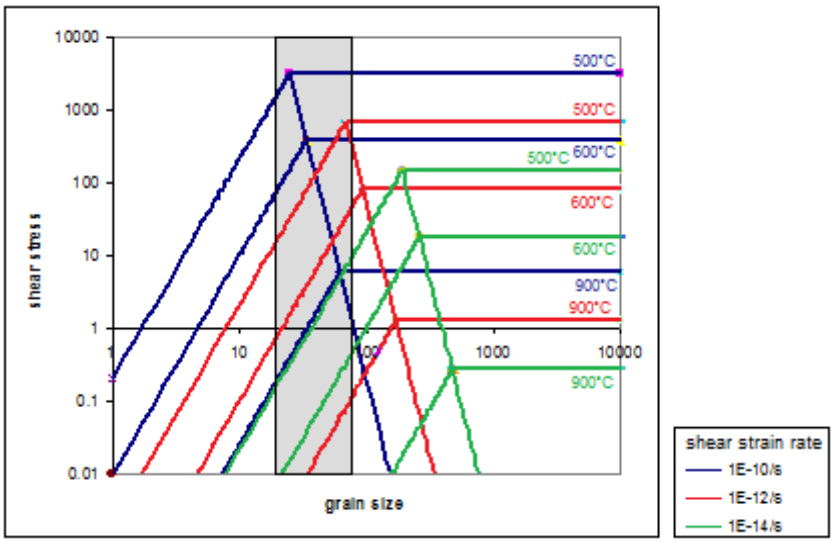

Figure 40: Deformation mechanism map for An100 (wet). The grain size is the recrystallized grain size for plagioclase.

Only deformation at a strain rate of $1 \cdot 10^{-10}$ and a temperature between 500°C and 900°C fall within the marked section.

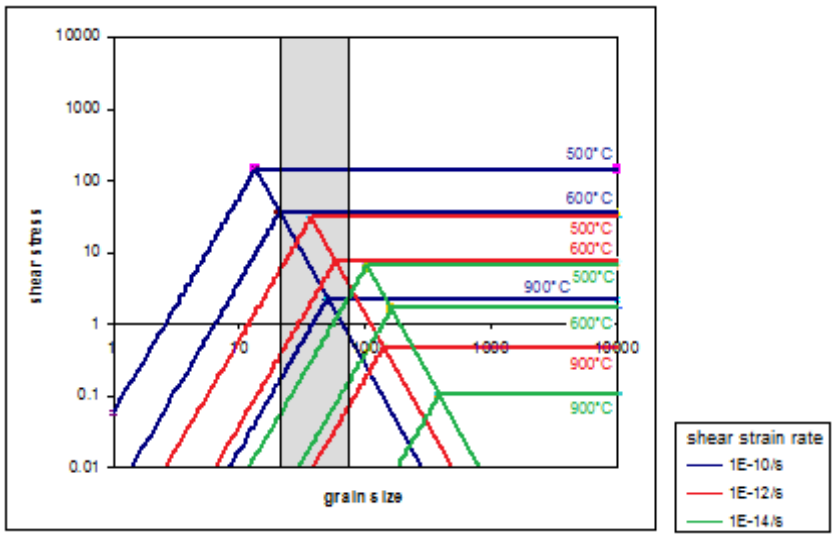

Figure 41: Deformation mechanism map for An60. The grain size is the recrystallized grain size for plagioclase.

Deformation at a strain rate of $1 \cdot 10^{-10}$ and a temperature between 600°C and 900°C fall within the marked section. Also deformation at a strain rate of $1 \cdot 10^{-12}$ and a temperature between 500°C and 600°C fall within this section.

5. Discussion

The discussion of the results will be done in the same four sections as before, beginning with fieldwork, followed by microstructures, grain size analysis, and paleopiezometry.

5.1 Fieldwork

First the photographs will be discussed briefly, after that the composition and the, mostly, retrograde metamorpic facies derived from these composition will be discussed, followed by the water content needed for these retrograde reactions to occur.

Sognefjord

Figure 16: Top left and top right: The rims of garnet around pyroxene are corona structures, which are predeformational structures of granulite facies assemblage. The rocks in Sognefjord in which these structures are found are rather undeformed, these samples were taken at the borders of the massive anorthosite outcrop along the road near Fimreite.
The pink to purple colour found for plagioclase in figure 16: Bottom right, figure 17: Bottom right, and figure 18: Top right is common for anorthite rich plagioclase. In Sognefjord these purple colour can be found at several locations, Fimreite, Eide, and Lærdal.
The small scale shear zone shown in figure 17: Top left, is depleted of garnet and part of the pyroxene has reacted to hornblende, this indicates that the shear zone is related to retrograde amphibolite facies conditions. These small scale shear zones are common in the rocks from Sognefjord. Most rocks in Sognefjord show bands of plagioclase and mafic minerals, figure 17: Middle left, some parts are folded figure 17: Bottom left, the composition within this fault consists of plagioclase, pyroxene, and some hornblende, many garnet porphyroclasts are present, predominantly in the mafic bands.

Tafjord

The rocks in the shear zone found in Tafjord, shown in figure 19: Left, consist of plagioclase, with small amounts of biotite and hornblende, this shear zone is therefore related to retrograde greenschist facies conditions. The rocks are weathered, but underneath the plagioclase is milky white, with only small amounts of mafic minerals.

Composition

The composition of the rocks in Sognefjord is more diverse than that of the rocks in Tafjord. The plagioclase content of the rocks in Sognefjord varies from proper anorthosite, with less than 10 percent mafic minerals, to anorthositic leucogabbro, with 10 to 35 percent mafic minerals, and anorthositic gabbro, with at least 22,5 percent and up to 35 percent mafic minerals, while in Tafjord all anorthosites are proper anorthosites, with only 5 to 10 percent mafic minerals.
Also the mafic mineral content of the rocks differs more in Sognefjord than in Tafjord. In some of the samples from Sognefjord pyroxene, mostly clinopyroxene, is the dominant mafic mineral, with hornblende being the second mineral. Garnet porphyroclasts are abundant in both the mafic bands and the plagioclase bands, with the garnet porphyroclasts in the mafic bands being larger. In other samples from Sognefjord the mafic mineral content is dominated by hornblende, with pyroxene, mostly clinopyroxene, being the second mineral. Here garnet porphyroclast might still be present, mostly in the mafic bands, but are less abundant, and the garnet porphyroclasts are smaller than in the samples mentioned above. The rocks in which pyroxene is the dominant mafic mineral have probably preserved a predeformational granulite facies and are thus rather undeformed, an example of this are the corona structures mentioned above. The hornblende in this rocks is presumably Ti-rich, or brown hornblende. In the rocks with hornblende as the dominant mafic mineral a retrograde amphibolite facies reaction has replaced the pyroxene with hornblende, here the hornblende is green hornblende. The retrograde amphibolite facies reaction consumes water, the water content needed to convert a certain percentage of pyroxene to hornblende by this reaction is discussed below.
In Tafjord the mafic minerals mainly consist of biotite and hornblende. All pyroxene is converted into hornblende by retrograde amphibolite facies reactions, and part of the hornblende is converted into biotite by retrograde greenschist facies reactions. This second reaction also consumes water, the water content needed to convert a certain percentage of hornblende to biotite by this reaction is discussed below. There is no garnet present in the rocks from Tafjord.

Water content

Plagioclases with three different contents of anorthite and water were used in the calculations. The weight percent of water for these plagioclases is given in table 1. The highest water content is that of An60, which is 0,3 weight percent. If we assume that this is a good representation for the rocks in Sognefjord, which have an anorthite content of An55 to An80, or An40 to An60 for the northern massifs were most of the samples are taken, and Tafjord, which have an anorthite content of An45 to An65. If we compare this weight percent with the results presented in table 2, we can obtain the percentage of mafic minerals that were affected by the retrograde reactions. For the most mafic rocks found in Sognefjord, with 35 percent of mafic minerals, between 40 and 50 percent of the minerals could be affected by the retrograde reaction, for 0,3 weight percent of water in the rock. In less mafic rocks, with 20 and 30 percent mafic minerals, respectively between 50 and 60 percent and around 80 percent of the mafic minerals would be affected by the amphibolite facies retrograde reaction, for a rock with a water content of 0,3 weight percent. These results are consistent with the compositions found in the thin sections, thus we can conclude that in rocks with more mafic minerals, less minerals are affected by the retrograde reaction, from this we infer that the water content is the limiting factor of the retrograde reactions.

For the rocks in Tafjord it is assumed in the calculations that the amphibolite facies retrograde reaction has converted 100 percent of the pyroxene to hornblende. The water content needed for this was added to the water content needed for a specific amount of affected minerals by the greenschist facies retrograde reaction, where hornblende is converted to biotite, see table 3. For a rock which consist of 10 percent mafic minerals between 40 and 50 percent of the mafic minerals is affected by the retrograde reaction, for a water content of 0,3 weight percent. For a rock which contains only 5 percent mafic minerals, and has a water content of 0,3 percent, between 70 and 80 percent of the mafic minerals will be affected by the greenschist facies retrograde reaction.

5.2 Microstructures

The photographs of the thin sections will be discussed here. First those from Sognefjord, second those of Tafjord.

Sognefjord

Many different microstructures are found in the thin sections of samples from Sognefjord. The samples show partly recrystallized fabrics. In figure 20: Top left, we see large, old, plagioclase grains with undulose extinction and twins with tappering edges, deformation twins. Along the grain boundaries, and at grain intersections small, new, recrystallized grains are seen. This structure of large grains with small recrystallized grains along the boundaries, in between grains is a good indication for bulging recrystallization. Large grains with undulose extinction and deformation twinning, combined with bulging recrystallization indicates low to medium grade metamorphic conditions, of 400ºC-500ºC. In figure 21: Top left, much more of the fabric is recrystallized into new grains, with the old being smaller and more elongated. About half of the old grains show deformation twins, with tappering edges. These structures indicate medium grade metamorphic conditions, of 450°C-600°C. In figure 21: Top right, the old grains are even more elongated and do not show twinning, subgrains with the size of the recrystallized grains can be found in the zoom in of the thin sections, see figure 22. Bulging recrystallization is still active, and is accompanied by subgrain rotation recrystallization. High metamorphic grade conditions, above 600°C, can be inferred from these microstructures.

Three different types of bands can be distinguished in the thin sections, monophase plagioclase bands, monophase hornblende bands, and multiphase plagioclase-hornblende or plagioclase-pyroxene bands. See figure 20: Top left and bottom right, and figure 21: Top left to bottom left. The monophase plagioclase bands consist of recrystallized plagioclase grains, with some strongly extended larger grains, sometimes with small subgrains the size of the recrystallized grains, while in the multiphase bands these recrystallized plagioclase grains are mixed with recrystallized hornblende grains, and sometimes recrystallized pyroxene grains, here strongly extended porphyroclasts of plagioclase are found too, and less extended porphyroclasts of hornblende and sometimes pyroxene are also present. The monophase hornblende bands start as tails and then extend from the hornblende phorphyroclasts. See figure 20: Top left, and figure 21: Top left and bottom left. The garnet porphyroclasts are rather undeformed, see figure 20: Top left and bottom

right, and figure 21: Bottom left and bottom right, with the garnet in figure 20: Bottom left being slightly deformed. Garnet content varies from being absent to being very abundant, see figure 21: Bottom right.

Tafjord

The microstructures found in the thin sections of samples from Tafjord are very uniform. The samples are completely recrystallized. The recrystallized plagioclase grains are larger than those found in Sognefjord, have many subgrains, and many have interlobate grain boundaries, sometimes with bulges intruding into neighbouring grains. Only a few of the grains show twinning, straight growth twins. See figure 23: Left and right. The completely recrystallized fabric of large grains with subgrains and interlobate grain boundaries are structures associated with subgrain rotation recrystallization, and high temperature grain boundary migration recrystallization, which indicates ultra high grade metamorphic conditions, at 850°C or more, see figure 12. The large amount of subgrains indicate that subgrain rotation was important, thus the peak temperature of deformation must have been close to the onset of 850°C, for high temperature grain boundary migration, and probably this peak temperature didn't last long. These ultra high grade metamorphic conditions at peak conditions of deformation are in contradiction with the growth twins observed in some of the grains, and with the greenschist facies mineral content, which indicates metamorphic conditions of 500°C. Static recrystallization after deformation could have altered the grain structures and mineral assemblage. Static recrystallization by grain boundary area reduction could not have been active very long, since part of the structures formed at high metamorphic grade conditions, the irregular grain shapes and interlobate grain boundaries, are preserved, see figure 13.

5.3 Grain size analysis

First grain size analysis of the samples from Sognefjord are discussed, after that grain size analysis of the samples from Tafjord. In Sognefjord grain size analysis has been done on monophase plagioclase bands, and on multiphase plagioclase-hornblende bands and plagioclase-pyroxene bands. The rocks in Tafjord consist almost entirely of plagioclase, therefore for these samples grain size analysis is done on monophase plagioclase.

Sognefjord

Three different types of bands can be distinguished in the thin sections, monophase plagioclase bands, monophase hornblende bands, and multiphase plagioclase-hornblende or plagioclase-pyroxene bands. All types have different grain sizes, with the monophase plagioclase bands being largest, the multiphase being smaller, and the monophase hornblende bands having a grain size that is to small to measure from the thin sections. The difference in grain size between monophase and multiphase increases if the mafic mineral content of the multiphase bands increases, until the mafic mineral content exceeds the plagioclase content in the multiphase band. This is probably because in this case more grain boundary pinning occurs. In thin section 15-8-05 the difference in grain size between the monophase and multiphase bands is small, because the plagioclase content of the multiphase bands is high, while in thin section 15-1-02b the hornblende content of the multiphase bands is high, also resulting in a small difference in grain size between the multiphase and monophase bands. In thin sections 15-8-09b and 15-8-12 the difference in grain size between the monophase and multiphase bands is much larger, because the multiphase bands content is close to an equal distribution of plagioclase and hornblende. The results of this study are compared to those found by Kruse and Stünitz (1999). It is obvious that the average grain sizes of plagioclase, for both the monophase and the multiphase layers, found in this study are smaller than those obtained by Kruse and Stünitz (1999), see table 13, below. In both studies the grain size of plagioclase is smaller in the multiphase layers than in the monophase layers.

	Kruse and Stünitz (1999)	**This study**
Grain size of plagioclase in monophase layers	50-70 µm, average: 60 µm	20-120 µm, average: ~45 µm, only 15-1-02b smaller: 33 µm
Grain size of plagioclase in multiphase layers	10-70 µm, average: 40 µm	10-90 µm, average: ~25 µm, only 15-8-05 larger: 41 µm

Table 13: Comparison of grain sizes found in Sognefjord between Kruse and Stünitz (1999) and this study.

From figure 27: Top right to bottom right and figure 28: Top right to bottom right we infer that there is little to no correlation, inferred from the horizontal trend lines, between grain shape and grain size, or between grain orientation and grain shape, or between grain orientation and grain size, in both the monophase and the multiphase bands. The grain shape was obtained by dividing the major axis by the minor axis of the grain. See figure 27: Top left, and figure 28: Top left. For a perfectly round grain the result would be equal to one. For the monophase bands the result varies from 1,33

to 1,54. For the multiphase bands the result is between 1,29 and 1,42. All of the grains are subrounded. The grains in the monophase bands are on average a little more subrounded, than the grains in the multiphase bands, with the exception of thin section 15-8-12, see table 3.
From the grain size distribution histograms shown in figure 29 and 31 it is inferred that the recrystallized grain size in the monophase layers is larger and has more variation, than the recrystallized grain size in the multiphase bands. The grains in both the monophase bands and the multiphase bands show no obvious preferred orientation, a mild preferred orientation of an angle of approximately 80° to the north can be inferred from the grain orientation histograms in figure 30 and 32, but it is arguable if the values shown in this diagrams are of sufficient significance to denominate this a preferred orientation.

Tafjord

The recrystallized grain size of the plagioclase grains within the samples from Tafjord varies, however the average grain size of the plagioclase grains in the two samples is uniform. The grains have irregular grain shapes, because of the interlobate grain boundaries. The grain shape, which here is the measured relation between the major and minor axis of the grain, and represents the roundness of the grain, therefore might be less accurate for the grains in Tafjord than for the grains in Sognefjord. It is therefore not surprising that there is no correlation found between grain shape and grain size and between grain orientation and grain shape. See figure 35: Top right and bottom left. For grain orientation versus grain size there is also no correlation seen in figure 35: Bottom right. In the grain size distribution histograms, see figure 36: Top left and bottom left, it is shown that the grain size varies widely, from 20μm to over 400μm. No preferred orientation is shown in the grain orientation histograms, figure 36: Top right and bottom right.

5.4 Paleopiezometry

The monophase plagioclase recrystallized grain sizes were used in the paleopiezometers to obtain the shear stress of deformation. The three different paleopiezometers will be discussed individually below.

Post and Tullis recrystallized grain size piezometer for feldspar

According to Post and Tullis their recrystallized grain size piezometer for alkali feldspar should be applicable to all feldspars, including plagioclase. However the findings of this study are that the shear stresses obtained with this piezometer for recrystallized plagioclase grains are quite low. See table 8. Shear stresses of less than 1 MPa are obtained for the monophase recrystallized plagioclase grain sizes, where shear stresses between 1 and 200 MPa are believed to be geologically correct. For Sognefjord the results are 0,7 to 1,3 MPa, and for Tafjord around 0,4 MPa. The shear strain rates associated with these stresses are dependent on anorthite content of the rocks, for An100 (dry) shear strain rates of around $5{,}5 \cdot 10^{-26}$ are acquired, for An100 (wet) ~$7{,}0 \cdot 10^{-19}$, and for An60 around $2{,}0 \cdot 10^{-15}$. Geologically realistic strain rates are in the order of 10^{-14} to 10^{-10}.
Extrapolation to lower temperatures could correct for the lower stresses, as shown in figure 38 for the temperature dependent paleopiezometer of de Bresser et al., lower temperature indeed gives higher stresses. Another solution is shown in figures 39 to 41, where different compositions and water contents are plotted for the temperature dependent piezometer of de Bresser et al., a difference in the stress-recrystallized grain size relation can be seen for different compositions and different water contents of plagioclase. The relation for An60 is closer to the relation obtained by Post and Tullis, than the relation for An100. This is probably because the composition of An60 is closer to the albite composition feldspar (Ab98An1Or1) used by Post and Tullis. Without extrapolation to lower temperatures it is concluded that the recrystallized grain size piezometer for feldspar of Post and Tullis only works correctly for alkali feldspar, and should not be applied to plagioclase.

Twiss theoretical paleopiezometer

It was already pointed out in the literature that the theoretical paleopiezometer of Twiss has many limitations, furthermore it has been criticized because the theory is based on an assumption of equilibrium, while there is a non-equilibrium, dynamic process taking place.
The slope for the theoretical paleopiezometer from Twiss is shallower than that for the recrystallized grain size piezometer for feldspar from Post and Tullis and the temperature dependant piezometer from de Bresser et al., because the piezometer exponent is different, as pointed out by Post and Tullis (1998). See figure 37. The shear stresses inferred with the theoretical paleopiezometer of Twiss from the monophase plagioclase recrystallized grain sizes are in between

the shear stresses obtained with the temperature dependent paleopiezometer of de Bresser et al. for the monophase plagioclase recrystallized grain sizes for different anorthite contents. Thus for grain sizes with these values the results obtained with theoretical paleopiezometer of Twiss are quite accurate. The results are geologically correct, with values for the shear stress of 39 to 51 MPa for Sognefjord, and around 29 MPa for Tafjord. The shear strain rate associated with these stresses are, for An100 (dry) $7{,}5 \cdot 10^{-21}$, for An100 (wet) $1{,}4 \cdot 10^{-13}$, and for An60 $2{,}1 \cdot 10^{-10}$. Shear strain rates obtained for An100 (wet) and An60 are geologically realistic values. See table 9.

De Bresser et al. temperature dependant paleopiezometer

The results obtained with the temperature dependent paleopiezometer of de Bresser et al. for plagioclase with different anorthite and water contents are plotted in figure 37 for a temperature of 600°C or 873K. In figure 38 the shear stress-recrystallized grain size relations for plagioclase with different anorthite and water contents, obtained with the temperature dependent paleopiezometer, are plotted for different temperatures, of 500°C or 773K, 600°C or 873K, and 900°C or 1173K, representing respectively greenschist, amphibolite, and granulite facies metamorphic conditions. The lines for An100 (dry) and An100 (wet) in figures 37 and 38 overlap for all temperatures. The shear stresses inferred from this paleopiezometer vary with composition and temperature, the shear strain rates inferred from these shear stresses vary with composition, temperature, and also with water content. See tables 10, 11, and 12. Shear stresses obtained for a temperature of 500°C are much to high for plagioclase with anorthite contents of An100, but are geologically realistic for An60, with values of 20 to 36 MPa for Sognefjord, with a maximum of 76 MPa, and almost 11 MPa for Tafjord. Shear strain rates associated with these shear stresses are $3{,}2 \cdot 10^{-13}$ to $1{,}6 \cdot 10^{-11}$ for Sognefjord and $4{,}5 \cdot 10^{-14}$ for Tafjord. For a temperature of 900°C all anorthite compositions for plagioclase show geologically realistic values. Values for Sognefjord of An100 (dry) and An100 (wet) are respectively 9 to 16 MPa, maximum 35 MPa, and 9 to 15 MPa, maximum 32 MPa, the values for An60 are a bit lower, 2 to 4 MPa, maximum 9 MPa. Associated shear strain ratess are $5{,}0 \cdot 10^{-13}$ to $2{,}6 \cdot 10^{-11}$ for An100 (dry), which are geologically correct. For An100 (wet) $3{,}1 \cdot 10^{-10}$ to $1{,}6 \cdot 10^{-8}$, and for An60 $1{,}2 \cdot 10^{-10}$ to $6{,}3 \cdot 10^{-9}$, the strain rates are quire fast. For Tafjord the values for the shear stresses are about 5 MPa, 4 to 5 MPa, and a little over 1 MPa, for respectively An100 (dry), An100 (wet), and An60, with shear strain rates of $7{,}3 \cdot 10^{-14}$ for An100 (dry) and $4{,}5 \cdot 10^{-11}$ for An100 (wet), which are close to that for An60 $1{,}7 \cdot 10^{-11}$, which are also geologically correct. For a temperature of 600°C the values found for Sognefjord of An100 (dry) and An100 (wet) are about

226 to almost 400 MPa for both, with a maximum of over 800 MPa, while values for An60 are 10 to 17 MPa, with a maximum of about 37 MPa, with shear strain rates of up to $4{,}5 \cdot 10^{-17}$ for An100 (dry), $1{,}1 \cdot 10^{-9}$ for An100 (wet), and $2{,}3 \cdot 10^{-12}$ to $1{,}2 \cdot 10^{-10}$ for An60. The shear strain rate for An100 (dry) is thus too slow, while the shear strain rate obtained for An100 (wet) is too fast, but that for An60 is geologically correct. For Tafjord the values of the shear stresses are 116 to 120 MPa for both An100 (dry) and An100 (wet), and a little over 5 MPa for An60. Associated shear strain rates are $1{,}2 \cdot 10^{-19}$, $2{,}9 \cdot 10^{-12}$, and $3{,}4 \cdot 10^{-13}$, for respectively An100 (dry), An100 (wet), and An60. Again the value for An100 (dry) is lower than the geologically realistic values, and values for An100 (wet) and An60 are within this range.

		Post and Tullis felspar	Twiss theoretical	De Bresser et al. temperature dependent		
				500°C	600°C	900°C
Sognefjord	An100 (dry)	no	no	no	no	yes
	An100 (wet)	no	yes	no	no	no
	An60	no	yes	yes	yes	no
Tafjord	An100 (dry)	no	no	no	no	yes
	An100 (wet)	no	yes	no	yes	yes
	An60	no	yes	yes	yes	yes

Table 14: Geologically realistic values of shear stress and strain rate for the samples from Sognefjord and Tafjord obtained with the three different paleopiezometers.

If the results of this study for the samples from Sognefjord are compared with the results of Kruse and Stünitz (1999), see table 15, an obvious difference in the inferred shear stress is seen, while the inferred temperatures are not very different. Further studies should be done to investigate were this difference in shear stress comes from.

	Kruse and Stünitz (1999)	**This study**
Maximum shear stress	520 MPa	37 MPa
Temperature	700°C	600°C

Table 15: Comparison of shear stress and temperature found in Sognefjord between Kruse and Stünitz (1999) and this study.

Without extrapolation to lower temperatures the stresses inferred from the Post and Tullis recrystallized grain size piezometer for feldspar are too low, the assumption of equilibrium for the Twiss theoretical paleopiezometer being wrong, and the values obtained for the shear stress and strain rates with the de Bresser et al. temperature dependent paleopiezometer being geologically realistic, the last mentioned piezometer was used to construct deformation mechanism maps. The field boundary model seems accurate for plagioclase.

Deformation mechanism maps

The lines for An100 (dry) and An100 (wet) in figures 37 and 38 overlap. However the deformation mechanism maps, shown in figure 39 and 40 for these anorthite and water contents are different. It is inferred from this that the shear stress- recrystallized grain size relation is only dependent on the composition, the anorthite content, of the rock samples, while the deformation mechanism maps depend on anorthite composition, and water content as well. With an increase in water content the shear stress decreases and the grain size therefore increases. See figure 42. The lines indicated with An100 (dry) and An100 (wet) in this figure are not overlapping, because these shear stress-recrystallized grain size relations are based on a constant shear strain rate, instead of a constant temperature. The deformation mechanism map for An60, see figure 41, shows a further decrease in shear stress, with an increase in grain size if compared to An100 (dry), but a decrease in grain size if compared to An100 (wet). The grain size is associated with the anorthite composition, which decrease from An100 to An60, therefore other constants need to be used for the shear stress-recrystallized grain size relation, while the increase in water content, from 0,004 weight percent and 0,07 weight percent for respectively An100 (dry) and An100 (wet) to 0,3 weight percent for An60, contributes to the decrease of the shear stress. It was inferred from figure 42 that the water content of a rock has a rather significant influence on the conditions of deformation.

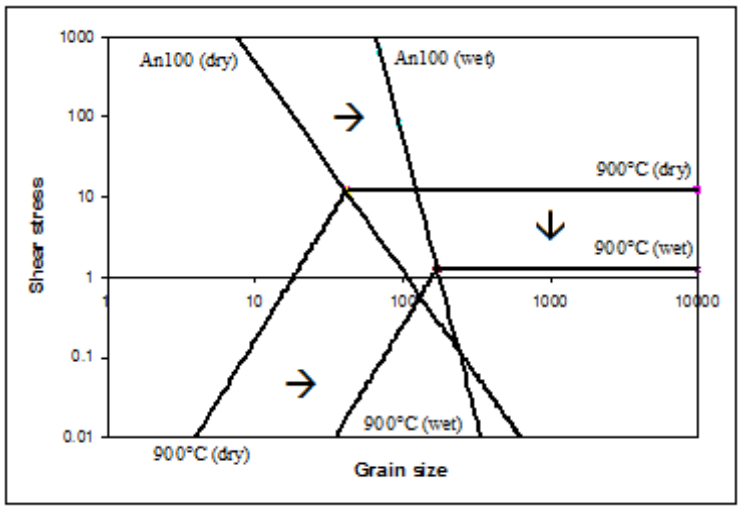

Figure 42: Deformation mechanism map for An100 (dry) and An100 (wet). The arrows show the displacement with increasing water content.

5.5 Deformation history

The deformation history will be based on observations from the field and from microstructures, and on the results from the grain size analysis and paleopiezometry. The deformation histories for Sognefjord and Tafjord will be discussed below.

Sognefjord

The samples from the rocks in Sognefjord show two different compositions, a predeformational granulite facies composition, which consists of plagioclase, pyroxene, brown hornblende and garnet, and a retrograde ampibolite facies composition, which contains plagioclase, green hornblende, pyroxene and in some places relics of garnet. The corona structures of pyroxene with garnet rims are predeformational structures of granulite facies composition, probably of Sveconorwegian age, which indicate that the rocks are only partly overprinted by retrograde amphbolite facies reactions during the Caledoinian orogeny. The shear zones are related to these retrograde ampibolite facies conditions. Microstructures obtained from these rocks indicate a gradual increase in deformation from the undeformed granulite facies structures to partly recrystallized fabrics, and with increasing deformation to almost completely recrystallized fabrics, which are formed by retrograde deformation during the Caledonian orogeny, temperatures of 400°C

to over 600°C are inferred from these microstructures, which agree with amphibolite facies metamorphic conditions of 600°C. Water is needed for this retrograde amphibolite facies reaction to occur, for a water content of 0,3 weight percent the amount of mafic minerals affected by the retrograde reaction seems coherent with the observations from the field and from optical microscopy. Shear stresses and shear strain rates inferred from the recrystallized monophase plagioclase grains, at amphibolite facies metamorphic conditions, are geologically realistic, with a maximum shear stress of 37 MPa and strain rates of 10^{-10}. There is no evidence found for static recrystallization after deformation, which is coherent with the temperature of deformation not being very high, and no excess water being present, since most of the water is consumed by the retrograde amphibolite facies reaction, see table 16.

Different grain sizes are found in monophase layers of plagioclase, multiphase layers of plagioclase and hornblende or plagioclase and pyroxene, and monophase layers of hornblende. All of these layers are associated with the shear zones of Caledonian age. There is no evidence found for the relative timing of these different layers, only for these layers and larger, older grains of plagioclase and pyroxene and garnet porphyroblasts. Further research should be done to determine the relative or absolute timing of these layers.

Event	**Age**	**Large scale structures**	**Microstructures**	**Recrystallization mechanism**	**Metamorphic grade**
Formation of anorthosites	1700 Ma	Not preserved	Not preserved	Not preserved	Not preserved
Sveconorwegian orogeny	1140-900 Ma	Corona structures around lenses of mafic minerals in anorthosite	Large plagioclase grains with twins, large grains of pyroxene and garnet	Not preserved	Granulite facies: plagioclase, pyroxene, garnet as main minerals
Caledonian orogeny	520-400 Ma	Meter scale shear zones in banded rocks with isoclinal folds	Bands of recrystallized plagioclase and hornblende	Bulging and subgrain rotation	Amphibolite facies: plagioclase and hornblende as main minerals
Post-Caledonian	<400 Ma	Not present	Not present	Not present	Not present

Table 16: Overview of results found for Sognefjord and link with deformation characteristics of geological events.

Tafjord

The samples from the rocks from Tafjord show a retrograde greenschist facies composition, which consist of plagioclase, biotite and hornblende, however microstructures indicate ultra high grade metamorphic conditions. The rocks show a completely recrystallized fabric, which was formed during the Caledonian orogeny. A water content of 0,3 weight percent would be sufficient to convert most of the amphibolite to biotite by the retrograde greenschist facies reaction, and is coherent with the mineral composition of the rock.
Earlier studies show that the metamorphic conditions during the Caledonian orogeny where highest in the Western Gneiss Region (WGR) in the west, and decreased eastward, see figure 5. Tafjord lies closer to the WGR than Sognefjord, therefore the metamorphic conditions in Tafjord must have been higher than in Sognefjord. The shear stress inferred from the recrystallized plagioclase grains, at ultra high grade conditions, are quite low, a little over 1 MPa. The associated shear strain rate is $1{,}2 \cdot 10^{-11}$. The ultra high grade metamorphic conditions inferred from the microstructures are in contradiction with the greenschist facies mineral composition. If the temperature of deformation was high or if excess water was present in the grain boundaries static recrystallization can occur, both of these conditions could have occurred for the rocks in Tafjord, where microstructures indicate the onset of ultra high grade metamorphic conditions, and some water might not have been used by the retrograde greenschist reaction in the most plagioclase-rich rocks. The grain size would have been altered, increased, by static recrystallization, that could have taken place during cooling to greenschist facies metamorphic conditions, therefore the shear stresses inferred with the paleopiezometer would be an underestimate of the actual shear stress during deformation. Cooling can not have been gradual after deformation, but must have been fast, because the fabric is not completely statically recrystallized, deformation structures, like interlobate grain boundaries, are still present. Deformation at initially ultra high grade metamorphic conditions during the Caledonian orogeny followed by static recrystallization during cooling to greenschist facies metamorphic conditions is a likely deformation history for the rocks in Tafjord, and is in agreement with the overall deformation history during the Caledonian orogeny, with metamorphic condition in Tafjord being higher than those in Sognefjord, see table 17.

An alternative deformation history for Tafjord would be one were biotite growth was not static, but formed during dynamic recrystallization under low metamorphic grade, greenschist facies, conditions, during cooling from peak temperature. At these conditions bulging recrystallization would be the active recrystallization mechanism. However the irregular grain shapes found in the

thin sections are not consistent with bulging recrystallization, but with grain boundary migration recrystallization, so the recrystallization by bulging recrystallization during cooling can only have been partial. Furthermore if recrystallization was not static, then the inferred shear stresses and strain rates should be correct. For greenschist facies conditions a shear stress of approximately 11 MPa is found and an associated shear strain rate of $4{,}5 \cdot 10^{-14}$. These values fall within the geologically correct values. The author favours the deformation history mentioned earlier above this alternative history, however further research should be done to exclude one of these deformation histories with more certainty.

Event	**Age**	**Large scale structures**	**Microstructures**	**Recrystallization mechanism**	**Metamorphic grade**
Formation of anorthosites	1700 Ma	Not preserved	Not preserved	Not preserved	Not preserved
Sveconorwegian orogeny	1140-900 Ma	Not preserved	Not preserved	Not preserved	Not preserved
Caledonian orogeny	520-400 Ma	Large scale shear zone	Plagioclase grains of various sizes, with interlobate grain boundaries	Grain boundary migration	Amphibolite facies: plagioclase and hornblende as main minerals
Post-Caledonian	<400 Ma	Not present	Subrounded grains with less interlobate grain boundaries	Static trough grain boundary area reduction	Greenschist facies: plagioclase and biotite as main minerals

Table 17: Overview of results found for Tafjord and link with deformation characteristics of geological events.

6. Conclusions

- Two different types of compositions can be distinguished in the samples from the rocks in Sognefjord, a predeformational granulite facies composition, which consists of plagioclase, pyroxene, brown hornblende and garnet, and a retrograde amphibolite facies composition, containing plagioclase, green hornblende, pyroxene and relics of garnet.
- The samples from the rocks in Tafjord show a greenschist facies composition of plagioclase, biotite and hornblende.
- It was inferred from calculations that a water content of 0,3 weight percent is accurate for the rocks in both Sognefjord and Tafjord, which is consistent with a plagioclase composition of An60. Water content was the limiting factor for the retrograde reactions.
- Evidence for bulging recrystallization and subgrain rotation recrystallization is found in thin sections of samples from Sognefjord. With gradual increase in deformation the microstructures change from undeformed structures, to partly recrystallized fabrics with bulging recrystallization along grain boundaries in between grains, and further into almost completely recrystallized fabrics with bulging and subgrain rotation recrystallization.
- Irregular shaped grains with subgrains and interlobate grain boundaries, found in thin sections of samples from Tafjord, are evidence for high temperature grain boundary migration recrystallization and subgrain rotation recrystallization. A completely recrystallized fabric is shown by these samples.
- Three different types of bands of recrystallized grains can be distinguished in the thin sections of samples from Sognefjord, monophase plagioclase bands, with an average recrystallized grain size of 33 to 48 μm, multiphase plagioclase-pyroxene and plagioclase-hornblende bands with an average recrystallized grain size of 23 to 41 μm, and monophase hornblende bands, which extend from hornblende porphroclasts, with a grain size that is too small to measure with optical microscopy. The recrystallized grain size in the multiphase bands is smaller due to grain boundary pinning. The difference in recrystallized grain size between monophase and multiphase bands increases if the composition of the multiphase bands has a more equal amount of plagioclase and mafic minerals.
- The average recrystallized grain size of the plagioclase in Tafjord is 73 to 75 μm, however the grain size might have increased due to static recrystallization after deformation.
- The Post and Tullis recrystallized grain size piezometer for feldspar should not be applied to plagioclase, without correction for lower temperatures or higher anorthite content.

- The values for the shear stress obtained with the Twiss theoretical paleopiezometer are geologically realistic, however it has many limitations and more important it is based on a false assumption of equilibrium.
- The results for the shear stress inferred with the de Bresser et al. temperature dependent paleopiezometer are geologically correct. The field boundary model seems accurate for plagioclase. The deformation mechanism maps constructed with this paleopiezometer show that the influence of water on deformation conditions is significant. See figure 42.
- Deformation during the Caledonian orogeny on the rocks in Sognefjord involved retrograde amphibolite facies conditions. Obtained shear stresses are 10-17 MPa, with a maximum shear stress of 37 MPa, and associated shear strain rates of $2{,}3 \cdot 10^{-12}$ to $1{,}2 \cdot 10^{-10}$ for a plagioclase composition of An60. Structures that are related to this deformation are relatively small scale shear zones. The deformation was followed by fast cooling, not enabling static recrystallization. Some parts of the rocks in Sognefjord are not altered during the Caledonian orogeny and show predeformational, probably post Sveconorwegian, structures, like corona structures, and banded rocks with isoclinal folds, which are relics of the Sveconorwegian orogeny.
- The conditions of deformation during the Caledonian orogeny in Tafjord where ultra high grade metamorphic conditions. After deformation some static recrystallization occurred during relatively fast cooling to greenschist facies metamorphic conditions. The grain size of the recrystallized grains was increased, therefore the inferred shear stresses are an underestimate of the actual shear stress during deformation. The large shear zone is associated with the Caledonian orogeny.
- Metamorphic conditions during the Caledonian orogeny were higher in Tafjord than in Sognefjord. Cooling after deformation was relatively fast at both locations.
- The rocks from Sognefjord and Tafjord have both undergone at least two deformation events after formation of the anorthosite massifs. First during the Sveconorwegian orogeny and later during the Caledonian orogeny. In Sognefjord relics of the Sveconorwegian orogeny are preserved, but in Tafjord the rocks have a completely recrystalized fabric, formed during the Caledonian orogeny.

Acknowledgements

First I would like to thank Dr. Auke Barnhoorn for his company and help during the fieldwork in Norway, and for the instructions during the research in Utrecht. Second my thanks goes to Prof. Dr. Martyn Drury for his guidance and instructions during the research and writing of this master-thesis. Last but not least I thank my family, girlfriend and friends for their support over the years, it has been hard at times, and I could not have done it without them.

References

Barnichon, J.D., Havenith, H., Hoffer, B., Charlier, R., Jongmans, D., Duchesne, J.C., 1999. *The deformation of the Egersund-Ogna anorthosite massif, south Norway: finite-element modelling of diapirism.* Tectonophysics 303, 109-130.

Bédard, J.H., 2001. *Parental magmas of the Nain Plutonic Suite anorthosites and mafic cumulates: a trace element modelling approach.* Contributions to mineralogy and petrology, Vol. 141, 747-771.

Bingen, B., Nordgulen, Ø., Viola, G., 2008. *A four-phase model for the Sveconorwegian orogeny, SW Scandinavia.* Norwegian Journal of Geology, Vol. 88, 43-72.

Bruckner, H. K., 1968. *Relations of anorthosite, eclogite and ultramafic rock to the countryrock, Tafjord area, Norway.* Yale University, Ph.D., Geology. University Microfilms.

De Bresser, J.H.P., Ter Heege, J.H., Spiers, C.J., 2000. *Grain size reduction by dynamicrecrystallization: can it result in major rheological weakening?* Published online; Springer-Verslag 2000, International Journal Earth Sciences (2001) 90, 28-45.

De Meer, S., Drury, M.R., de Bresser, J.H.P., Pennock, G.M., (eds) 2002. *Deformation Mechanisms, Rheology and Tectonics: Current status and Future Perspectives.* Geological Society, Londen, Special Publications, 200.

Dimanov, A., Wirth, R., Dresen, G., 2000. *The effect of melt distribution on the rheology of plagioclase rocks.* Tectonophysics 328, 307–327.

Drury, M.R., Urai, J.L., 1990. *Deformation-related recrystallization processes.* Tectonophysics 172, 235-253.

Evans, B., Renner, J., Hirth, G., 2001. A *few remarks on the kinetics of static grain growth in rocks.* Published online; Springer-Verslag 2001, International Journal Earth Sciences 90. 88-103.

Frost, H.J., Ashby, M.F., 1982. *Deformation mechanism maps: the plasticity and creep of metals and ceramics.* Oxford, Pergamon.

Hirth, Tullis, J., 1992. *Dislocation creep regimes in quartz aggregates.* Journal of Structural Geology 14, 145-159.

Kellerman Slotemaker, A., 2006. *Dynamic recrystallization and grain growth in olivine rocks.* Universiteit Utrecht, Ph.D. Geolgica Ultraiectina, 268.

Kruse, R., Stünitz, H., 1999. *Deformation mechanisms and phase distribution in mafic high temperature mylonites from the Jotun Nappe, southern Norway.* Tectonophysics 303, 223–249.

Lafrance, B., John, B.E., Scoates, J.S., 1996. *Syn-emplacement recrystallization and deformation microstructures in the Poe Mountain anorthosite, Wyoming.* Contributions to Mineralogy and Petrology, 122, 431-440.

Lafrance, B., John, B.E., Frost, J.S., 1998. *Ultra high-temperature and subsolidus shear zones: examples from the Poe Mountain anorthosite, Wyoming.* Journal of Structural Geology, Vol. 20, 945-955.

Lundmark, A.M., Corfu, F., 2007. *Late-orogenic Sveconorwegian massif anorthosite in the Jotun Nappe Complex, SW Norway, and causes of repeated AMCG magmatism along the Baltoscandian margin.* Published online; Springer-Verslag 2007, Contributions to Mineralogy and Petrology (2008) 155, 147–163.

Lundmark, A.M., Corfu, F., Spürgin, S., Selbekk, R.S., 2007. *Proterozoic evolution and provenance of the high-grade Jotun Nappe Complex, SW Norway: U–Pb geochronology.* Precambrian Research 159, 133–154.

MacKenzie, W.S., Adams, A.E., 1994. *A Colour Atlas of Rocks and Minerals in Thin Section.* Manson Publishing Ltd.

McLaren, A.C., Pryer, L.L., 2001. *Microstructural investigation of the interaction and interdependence of cataclastic and plastic mechanisms in feldspar crystals deformed in the semi-brittle field.* Tectonophysics 335, 1-15.

Passchier, C.W., Trouw, R.A.J., 2005. *Microtectonics.* 2nd, Revised and Enlarged Edition. Springer Berlin Heidelberg New York.

Post, A., Tullis, J., 1998. *A recrystallized grain size piezometer for experimentally deformed feldspar aggregates.* Tectonophysics 303, 159-173.

Pryer, L.L., 1993. *Microstructures in feldspars from a major crustal thrust zone: the Grenville Front, Ontario, Canada.* Journal of Structural Geology15, 21-36.

Roberts, D., 2003. *The Scandinavian Caledonides: event chronology, palaeogeographic settings and likely modern analogues.* Tectonophysics 365, 283– 299.

Rybacki, E., Dresen, G., 2000. *Dislocation and diffusion creep of synthetic anorthite aggregates.* Journal of Geophysical Research 105, 17-36.

Rybacki, E., Dresen, G., 2004. *Deformation mechanism maps for feldspar rocks.* Tectonophysics 382, 173-187.

Svahnberg, H., 2010. *Deformation behaviour and chemical signatures of anorthosites: Examples from southern West Greenland and south-central Sweden.* Stockholms Universitets Institution, Ph.D. Geologiska Vetenskaper, 340.

Stipp, M., Stünitz, H., Heilbronner, R., Schmid, S.M., 2002. *The eastern Tonale fault zone: a "natural laboratory" for crystal plastic deformation of quartz over a temperature range from 250 to 700°C.* Journal of Structural Geology 24, 1861-1884.

Stipp, M., Kunze, K., 2007. *Dynamic recrystallization near the brittle-plastic transition in naturally and experimentally deformed quartz aggregates.* Available online; ScienceDirect 2007, Tectonophysics 448, 77–97.

Stünitz, H., Tullis, J., 2000. *Weakening and strain localization produced by syn-deformational reaction of plagioclase.* Published online; Springer-Verslag, 2000. International Journal Earth Sciences (2001) 90, 136-148.

Tullis, J., Yund, R.A., 1987. *Transition from cataclastic flow to dislocation creep of feldspar: mechanisms and microstructures.* Geology 15, 606-609.

Tullis, J., Yund, R.A., 1991. *Diffusion creep in feldspar aggregates: experimental evidence.* Journal of Structural Geology 13, 987-1000.

Tullis, J., Dell' Angelo, L., Yund, R.A., 1990. *Ductile shear zones from brittle precursors in feldspathic rocks: the role of dynamic recrystallization.* In: Hobbs, B.E., Heard, H.E. (eds) Mineral and rock deformation: laboratory studies. AGU, Geophysical Monograph 56, 67-81.

Twiss, R.J., 1977. T*heory and Applicability of a Recrystallized Grain Size Piezometer.* Pure and Applied Geophysics, Vol. 115, Birkhäuser Verslag, Basel.

Walsh, E.O., Hacker, B.R., 2004. *The fate of subducted continental margins: Two-stage exhumation of the high-pressure to ultrahigh-pressure Western Gneiss Region, Norway.* Journal of metamorphic Geology 22, 671–687.

Wanvik, J.E., 2000. *Norwegian anorthosites and their industrial uses, with emphasis on the massifs of the Inner Sogn-Voss area in western Norway.* Norges geologiske undersøkelse Bulletin 436, 103-112.

Wheeler, J., 1992. *Importance of pressure solution and Coble creep in the deformation of polymineralic rocks.* Journal of Geophysical Research 97, 4579-4586.

Appendices

Fieldwork

Appendix 1: List of samples, with GPS, numbers of associated photographs, foliation, and lineation.

2: Photographs of sample locations

3: Figures of foliations and lineations in Sognefjord

Microstructures

Appendix 4: Photographs of thin sections

Grain size analysis

Appendix 5: Photographs with layer including drawn grain boundaries, and binaries

6a: Thin section 15-1-02b, monophase

6b: Thin section 15-1-02b, multiphase

7a: Thin section 15-8-05, monophase

7b: Thin section 15-8-05, multiphase

8a: Thin section 15-8-09b, monophase

8b: Thin section 15-8-09b, multiphase

9a: Thin section 15-8-12, monophase

9b: Thin section 15-8-12, multiphase

10: Thin section 13-4-01

11: Thin section 13-4-02

Paleopiezometry

Appendix 12: Paleopiezometry

13: Deformation mechanism maps